UNIVERSIDADE ESTADUAL DE CAMPINAS
Faculdade de Engenharia Mecânica

LIDY MARCELA ANAYA JAIMES

Thermo-elastic topology optimization using a multi-scale approach

Otimização topológica termoelástica usando uma abordagem multiescala

CAMPINAS
2018

LIDY MARCELA ANAYA JAIMES

Thermo-elastic topology optimization using a multi-scale approach

Otimização topológica termoelástica usando uma abordagem multiescala

Thesis presented to the School of Mechanical Engineering of the University of Campinas in partial fulfillment of the requirements for the degree of Master in Mechanical Engineering in the area of Solid Mechanics and Mechanical Design.

Tese de Mestrado apresentada à Faculdade de Engenharia Mecânica da Universidade Estadual de Campinas como parte dos requisitos exigidos para a obtenção do título de Mestra em Engenharia Mecânica, na área de Mecânica dos Sólidos e Projeto Mecânico.

Orientador: Prof. Dr. Renato Pavanello

ESTE EXEMPLAR CORRESPONDE À VERSÃO FINAL DA DISERTAÇÃO DEFENDIDA PELA ALUNA LIDY MARCELA ANAYA JAIMES E ORIENTADA PELO PROF. DR. RENATO PAVANELLO.

.....
ASSINATURA DO ORIENTADOR

CAMPINAS
2018

Agência(s) de fomento e nº(s) de processo(s): CAPES, 33003017

Ficha catalográfica
Universidade Estadual de Campinas
Biblioteca da Área de Engenharia e Arquitetura
Luciana Pietrosanto Milla - CRB 8/8129

An18t

Anaya Jaimes, Lidy Marcela, 1993-
Thermo-elastic topology optimization using a multi-scale approach / Lidy Marcela Anaya Jaimes. – Campinas, SP : [s.n.], 2018.

Orientador: Renato Pavanello.
Dissertação (mestrado) – Universidade Estadual de Campinas, Faculdade de Engenharia Mecânica.

1. Otimização topológica. 2. Multiescala. 3. Homogeneização (Equações diferenciais). 4. Métodos dos elementos finitos. I. Pavanello, Renato, 1958-. II. Universidade Estadual de Campinas. Faculdade de Engenharia Mecânica. III. Título.

Informações para Biblioteca Digital

Título em outro idioma: Otimização topológica termoelástica usando uma abordagem multiescala
Palavras-chave em inglês:
Topological optimization
Multiescala
Homogenization (Differential equations)
Finite element methods
Área de concentração: Mecânica dos Sólidos e Projeto Mecânico
Titulação: Mestra em Engenharia Mecânica
Banca examinadora:
Renato Pavanello [Orientador]
Paulo Sollero
Eduardo Lenz Cardoso
Data de defesa: 28-02-2018
Programa de Pós-Graduação: Engenharia Mecânica

UNIVERSIDADE ESTADUAL DE CAMPINAS

FACULDADE DE ENGENHARIA MECÂNICA

COMISSÃO DE PÓS-GRADUAÇÃO EM ENGENHARIA MECÂNICA

DEPARTAMENTO DE MECÂNICA COMPUTACIONAL

DISSERTAÇÃO DE MESTRADO ACADEMICO

Thermo-elastic topology optimization using a multi-scale approach

Otimização topológica termoelástica usando uma abordagem multiescala

Autora: Lidy Marcela Anaya Jaimes
Orientador: Prof. Dr. Renato Pavanello

A Banca Examinadora composta pelos membros abaixo aprovou esta Tese:

Prof. Dr. Renato Pavanello, Presidente
DMC/FEM/UNICAMP

Prof. Dr. Paulo Sollero
DMC/FEM/UNICAMP

Prof. Dr. Eduardo Lenz Cardoso
DEM/CCT/UDESC

A Ata da defesa com as respectivas assinaturas dos membros encontra-se no processo de vida acadêmica do aluno.

Campinas, 28 de Fevereiro de 2018.

Dedicatória

A mi amada familia Juana, Ramiro, Karina, Jeison y Thiago.

Agradecimentos

À meus pais, Juana e Ramiro por sempre acreditar em mim e me brindar seu apoio incondicional.

À minha irmã, Karina, porque sem ela nada teria sido possível.

Ao meu irmão que me fez acreditar que nunca é tarde para realizar os sonhos.

Ao meu melhor amigo, Gerson, pelas palavras de apoio nos momentos difíceis.

À Nayla, pelos sorrisos, cuidados, palavras de apoio, a amizade diária, e por fazer que a vida em Barão Geraldo fosse toda uma aventura.

Ao Omar, pelo apoio, paciência e colaboração recebidas.

Aos amigos da universidade, dos quais espero levar a amizade para toda a vida.

Ao professor Renato Pavanello, pela oportunidade de estudar na Unicamp. Por sua amizade, dedicação e confiança durante todo o mestrado.

À Faculdade de Engenharia Mecânica da UNICAMP pela oportunidade de realizar este trabalho e à CAPES pelo suporte financeiro.

Acknowledgements

To my parents, Juana and Ramiro for always believing in me and giving me their unconditional support.

To my sister, Karina, because without her nothing would have been possible.

To my brother who made me believe that it's never too late to realize the dreams.

To my best friend, Gerson, for the words of support in difficult times.

To Nayla, for the smiles, the care, the words of support, the daily friendship, the coexistence, and for making life in Barão Geraldo an adventure.

To Omar, for the support, patience and collaboration received.

To the friends of the university , of which I hope to carry the friendship for the rest of my life.

To Professor Renato Pavanello, for the opportunity to study at Unicamp. For his friendship, dedication and trust throughout the Masters.

To the Faculty of Mechanical Engineering of UNICAMP for the opportunity to carry out this work and to CAPES for the financial support.

"Concentra los afanes de tu voluntad en el gran objetivo de la vida, que es la superación, el perfeccionamiento. Ese objetivo es el aliciente que debe impulsarla en todos los momentos de su existir. Pero no te conformes con ser mejor en esto o en aquello; ser mejor significa serlo en todo.."

Raumsol, *Bases para tu conducta*

Resumo

ANAYA, L. M. Otimização topológica termoelástica usando uma abordagem multiescala. 2018. 94p. Dissertação (Mestrado). Faculdade de Engenharia Mecânica, Universidade Estadual de Campinas, Campinas, Brasil.

A otimização topológica evolucionária é uma ferramenta versatil para o projeto de estruturas, sendo amplamente usada na solução de muitos problemas de engenharia. Quando uma estrutura está sujeita à carregamentos térmicos e mecânicos simultâneos, o procedimento de projeto topológico torna-se complexo e às vezes não intuitivo.

Este trabalho apresenta o estudo do método BESO (Bidirectional Evolutionary Structural Optimization) aplicado à sistemas multiescala bidimensionais, com o intuito de desenvolver uma metodologia para projetar estruturas termomecânicas. O algoritmo implementado pode ser usado para projetar uma estrutura na macroescala, na microescala ou em ambas escalas simultaneamente. São apresentados dois problemas, o primeiro para estudar a influência da mudança de temperatura e dos carregamentos mecânicos na estrutura projetada e o segundo para minimizar o coeficiente de expansão térmica. Com o intuito de resolver os dois problemas apresentados é feita a otimização topológica de uma estrutura termoelástica usando multiplos materiais considerando apenas a macroescala e a microescala, respectivamente. O método de homogeneização é usado para obter as propriedades equivalentes do material projetado na macroescala em função da sua topologia na microescala.

Palavras-chave: Otimização Topológica Estrutural, Termoelástico, Modelo Multiescala, Método da Homogeneização, Método BESO.

Abstract

ANAYA, L. M. Thermo-elastic topology optimization using a multi-scale approach. 2018. 94p. Thesis (Mestrado). School of Mechanical Engineering, University of Campinas, Campinas, Brazil.

The evolutionary topology optimization is a versatile tool for the design, that is widely used in the solution of many engineering problems. When thermal and mechanical loads occur simultaneously in a structure, its shape and topological design become complex and sometimes non-intuitive.

This work presents the study of the Bi-directional Evolutionary Structural Optimization method (BESO) applied to multi-scale systems, in order to develop a methodology to design thermo-mechanical structures. The implemented algorithm can be used to design two dimensional structures in the macro-scale or in the micro-scale separately or to do a concurrent design. Two problems are presented, the first one to study the influence of the temperature change and the mechanical loads on the designed structure and the second one to minimize the thermal expansion coefficient, in order to do that, it is made a topology optimization of a thermoelastic structure using multiple materials considering only the macro-scale and using a multi-scale approach, respectively. The homogenization method is used to obtain the equivalents properties of the designed material.

Keywords: Structural Topology Optimization, Thermo-elastic, Multi-scale Model, Homogenization Method, BESO method.

List of Figures

List of Tables

Table of Contents

1 INTRODUCTION

The objective of this chapter is present the general scope of this research. It is widely discussed the motivation for modeling and optimization of thermo-mechanical structures and design new materials with a desired thermal expansion coefficient. It is presented a brief literature review of the thermoelastic topological design. General and specific objectives are included in this chapter and the description of each chapter goals is presented.

1.1 Motivation and general scope

Numerical modeling and topological design methods for thermo-elasticity continuum problems has been applied successfully to solve a large class of engineering problems for more than two decades (Rodrigues and Fernandes, 1995) The topological design methods can be used to change the topologies inside the predefined design domains and to find optimal layouts without the need for an initial given topology. For the particular case of thermo-elasticity problems, two kinds of mechanical loads are considered in the analysis: mechanical and thermal loads. In this work, the mechanical loads are considered constant along the optimization procedure and thermal loads are considered as a design dependent load that varies along the optimization procedure; due to this, the optimized structures are complex and the design is non-intuitive. For this class of problems, the development of reliable, efficient and inexpensive methods is relevant. Thermo-elastic topology optimization seeks to achieve the best performance for a structure while satisfying various constraints such as a thermo-mechanical equilibrium state and a given final volume.

Several engineering problems deal with compound thermo-mechanical loads such as the structures used in the solar power plants. It can be exemplified by the following problem: the rise in energy demand increases the need for developing technologies to generate renewable energy. The solar energy is an important source of renewable energy, where the concentrated solar power plants(CSP) are gaining interest (Zhang *et al.*, 2013). Concentrated solar power is an electricity generation technology, that uses mirrors to concentrate the solar radiation in a small area to produce steam. This steam switches a turbine on and generates electricity. In order to maximize the efficiency of the CSP, it is proposed the use of magnetic bearing, which supports moving parts without contact, wear and lubrication (Maslen and Schweitzer, 2009). However, due to the high temperatures reached by the solar concentration, the magnetic bearing expands losing the clearance between it and the movings parts. Due to this fact, it is important to find a material that allows the control of the thermal expansion of the magnetic bearing, in order to maintain a constant clearance or a variation of it, less than 10% of its initial value.

The topology optimization has been prominent in academic and practical environments, proving to be a versatile computational tool for application in various types of engineering analyzes. In general, the topology optimization pretends to find the material distribution of a structure, in order to optimize an objective function. This objective function could be the mean compliance or an error function in order to maximize the stiffness and to obtain a desired property, respectively. Some authors have been used the topology optimization to design materials with desired properties. Sigmund and Torquato (1997) used the SIMP method to design materials with extreme thermal expansion coefficient; Wang *et al.* (2016a) used the level set method to design meta materials with exotic thermo-mechanical properties. In this work, it is proposed a methodology to design thermo-mechanical structures using the Bi-directional Evolutionary Structural Optimization method (BESO), and the material interpolation scheme with penalization. First, it is proposed a topology optimization of a thermo-elastic structure using multiple materials, in order to study the influence of the temperature change and the mechanical loads on the structure. Then, it is proposed a multi-scale approach to design a material with a thermal expansion coefficient less than the 10% of the value of the thermal expansion coefficient of the considered materials, where the homogenization method is used to obtain the equivalents properties of the designed material.

1.2 Literature Review

The topology optimization has experimented a huge development since its introduction, becoming a very important tool in the industry and research. Topology optimization methods based on sensitivity analysis, such as homogenization method, topological derivative method, SIMP method, level-set method and BESO method have been developed. These methods have been applied to the design of continuum structures, in order to find a proper distribution of material in a given design domain that minimize an objective function taking into account a certain number of constraints.

Bendsøe and Kikuchi (1988) used for the first time the homogenization method to solve topology optimization problems. The topology optimization problem is posed as optimizing the material distribution in a perforated structure with infinite microscale voids. In the optimization process the part of the structure that is made of a material is considered as structure, while, the portion with only voids is considered no structure (NISHIWAKI *et al.*, 1998).The topology optimization of thermo-elastic structures has become more intense over the last few years. Rodrigues and Fernandes (1995) studied for the first time the topology optimization of 2D linear-elastic solid subjected to thermal loads using the homogenization method and Jog (1996) extended this study to the non-linear thermo-elasticity problems.

Using the Evolutionary Structural Optimization method (ESO), Li *et al.* (1999) proposed a procedure for topology design involving thermo-elasticity, and considering the thickness of the elements as the design variables in problems with varying fields of temperature. The ESO method was proposed by Xie and Steven (1993) and use discrete design variable (solid and void) to define the topology, in order avoid the intermediate materials on the final topology.

Subsequently, Li *et al.* (2001a) proposed an smoothing algorithm to avoid the presence of checkerboard patterns on the topology optimization of coupled thermo-mechanical problems under von Misses's stress criterion. Afterwards, Li *et al.* (2001b) proposed an evolutionary optimization procedure for topology design involving thermo-elasticity, considering elastic structures that experiment steady-state or transient heat conduction.

The mechanisms that control the amount and direction of thermal expansion in specific regions was studied using the topology optimization. Sigmund (2001), design multi-physics actuators using the SIMP method, for applications in the design of thermally and electro-thermally driven micro actuator for use in micro-electro-mechanical systems (MEMS). The SIMP method considers a continuous design variable, which represents a pseudo-density of the material, hence, intermediate materials (gray-scale) may be present in the final topology. A complete approach to the method, containing studies carried out in this area and possible applications, is presented by Bendsøe and Sigmund (2003). Actually, the SIMP method became the most popular topology optimization procedure.

The thermo-mechanical actuators have been studied in others works. Du *et al.* (2009) made a thermo-mechanical multi-physics modeling and geometrically nonlinear analysis in compliant actuators using a mesh-free method. Minimizing the output displacement, Luo *et al.* (2009) made a shape and topology optimization for electro-thermo-mechanical micro-actuators using the level set method.

In the level set method, the design variable is the free boundary of the structure and the objective function is defined as a function of the shape of a structure (Wang *et al.*, 2003). This method has been used also to minimize the mean compliance in thermoelastic structures (Xia and Wang, 2008).

An important issue in the thermo-elastic structure design is the treatment of the load. The structural and thermal loads can be considered design-dependent or design independent. Xia and Wang (2008) used the level set method to minimize the mean compliance subject to a material volume constraint considering a design independent temperature distribution, while Pedersen and Pedersen (2010) studied the topology optimization problems of a structure subject to thermo-mechanical design-depended loads.

In the work of Pedersen and Pedersen (2010), it is stated that the compliance is a questionable objective for the thermoelastic design problems. Pedersen and Pedersen (2010) proposed the stress distribution as a practical important objective and justified their work affirming that the stress can reach higher values than desirable in cases where volume reduction is large. Some works were developed using the von Mises stress as a constraint on the topology optimization of thermo-elastic structures (Neto, 2011; Deaton and Grandhi, 2013; Hou *et al.*, 2016; Deaton and Grandhi, 2016).

Considering an initial stress field due to a uniform temperature variations, Desmorat (2013) presented a compliance optimization methodology. The obtained numerical procedure is composed of stress calculations by the finite element method associated with the SIMP material model, assuming a dependence of the initial stress field on the distributed optimization parameters.

Using the mean compliance as objective function, Li *et al.* (2010) analyzed the equivalent nodal thermal load based on thermo-elastic finite element theory. Considering the effect of the design-dependent thermal loads, Rodriguez and Pavanello (2014) used the Bi-evolutionary Structural Optimization method (BESO) to develop a methodology for the sensitivity calculation. Xu *et al.* (2016) used the BESO method to made a concurrent topological design of composite thermo-elastic micro-structure and macro-structure using multiple materials.

The difference between the work developed in this study and the work of Xu *et al.* (2016) is the interpolation scheme used. While this work uses the same material interpolation, based on the material interpolation scheme of the solid isotropic material with penalization (SIMP), for the thermo-mechanical properties in the macro-scale and micro-scale. Xu *et al.* (2016) used differents interpolation for the macro-scale and micro-scale; for the micro-scale a different interpolation to the presented in this work, also based in the SIMP material interpolation scheme, and for the macroscale an alternative interpolation scheme proposed by Stolpe and Svanberg (2001).

The topology optimization using a thermo-elastic approach has been also used to design materials with desired properties. Sigmund and Torquato (1996), Sigmund and Torquato (1997) and Sigmund and Torquato (1999) used the solid isotropic material with penalization method (SIMP) to design a composite with extremal thermal expansion coefficients, and the homogenization method to find the effective properties of the designed composite material. In these works, the homogenization method was used to model the heterogeneous materials when a micro-structure has periodic heterogeneities. The origin of the word Homogenization is related to the fact that it is made a replacement of the heterogeneous material by an equivalent homogeneous one (Babuska, 1976).

The homogenization method has been used to calculate the effective properties of the designed thermo-elastic materials. Wang *et al.* (2016b) made a topological shape optimization for the design of mechanical meta-materials of thermoelastic micro-structured composite using the multi-phase level set method (MPLSM). Numerical examples to demonstrate the effectiveness of the MPLSM in the design of meta-materials with an expected and, an extreme thermal expansion coefficients, are presented. Using level-set, Wang *et al.* (2016a) designed multi-materials meta-materials with exotic thermo-mechanical properties, as a desired thermal expansion. In this work, the proposed algorithm allows the design of a material using the Bi-directional Evolutionary Structural Optimization method, in order to minimize the thermal expansion coefficient.

The studies presented thus far provide evidence that it is possible to develop an algorithm using the BESO method and the homogenization method, in order to do a topological design and to find the effective properties of a material, respectively. In this work, it is proposed an algorithm using these methods to solve thermo-elastic topology optimization problems using multiple materials, where the thermo-elastic topology optimization problem can be a macro-scale problem, micro-scale problem or a concurrent problem. The main advantage of this algorithm is that it allows the use of the same formulation to solve any of the three types of problems mentioned above, being a flexible tool for the thermo-mechanical design.

In the group of applied mechanics and topological optimization (GMO) of the department of computational mechanics (DMC,by its initials in Portuguese) of the University of Campinas, works in topology optimization were developed using the homogenization method (Porto, 2006; Porto and Pavanello, 2007; Silva, 2007; Silva and Pavanello, 2010b,a) and the Bi-Evolutionary Structural Optimization method (BESO) (Picelli, 2011; Vicente, 2013; Vicente *et al.*, 2015; Picelli *et al.*, 2015; MADRID, 2016; Azevedo, 2017), considering design-dependent thermo-mechanical loads (Rodriguez and Pavanello, 2014, 2015; Rodríguez, 2015) and considering a concurrent design (Calixto, 2015; Vicente *et al.*, 2016).

It can be noticed the existence of a consolidated research field in topology optimization. In view of all that has been mentioned so far, an analysis which considers more than two materials on the design domain and an algorithm to design thermo-elastic structures and materials in the macro-scale, the micro-scale or both scales(concurrent design) is an important contribution. Due to these facts, this work seeks to deepen the studies of multi-scale topological optimization introducing a multi-material approach.

1.3 Objectives

The main purpose of this work is to develop and implement a topology optimization algorithm, using the Bi-directional Evolutionary Structural Optimization method (BESO), in order to design a thermo-elastic structure and a material with a specific thermal expansion for a given temperature change. The specific objectives are summarized in the list below:

- Implement and validate the micro-structural model using the homogenization theory.
- Implement and validate an algorithm using the Bi-directional Evolutionary Structural Optimization method (BESO) for one or multiple materials.
- Validate the calculation of the derivatives of the homogenized properties.
- Implement the multi-scale and multi-material BESO algorithm.
- Design a thermo-elastic structure using multiple-materials.
- Design a material with a thermal expansion less than the 10%.
- Analyze the influence of some parameters of the BESO method over the final topologies, and its importance in the overall optimization process.

1.4 Work description

This work is divided into five chapters. The present chapter introduces a general scope of the studied problem in this work and the literature review of the thermo-elastic topology optimization. The main and specific objectives followed during the development of this study are also presented.

Chapter two provided details of the thermo-elastic multi-scale modeling on macro and micro-scale. The homogenization method used to calculate the equivalent properties of the micro-scale, the considered periodic boundary conditions, the numerical calculation of the homogenized tensor, and the solution of the thermo-elasticity problem are also covered in this chapter.

The optimization problem, the material interpolation schemes, and the implemented topology optimization method are described in chapter three.

Chapter four shows the numerical validation of the BESO, multi-material BESO, and the multi-scale and multi-material BESO procedure. The chapter also includes the numerical results of a compliance minimization of a thermo-elastic beam using multiples materials and the numerical results of a minimization of the thermal expansion coefficient.

Finally, Chapter 5 presents the conclusions from the results obtained in previous sections, as well as the suggested future works.

2 THERMO-ELASTIC MULTI-SCALE MODELING

Structures made of a homogeneous or heterogeneous material, subjected to thermal loads, due to a change in temperature (ΔT), and mechanical loads, are simultaneously considered in this work. This chapter presents the model of thermo-elasticity used to describe the thermo-elastic problem and the homogenization method; this method allows the calculation of the equivalent properties of the material, when it is heterogeneous and its heterogeneities are periodic.

2.1 Model of the thermo-elasticity problem

Figure 2.1(a) shows a schematic representation of the macroscopic model which can be represented by a linear thermo-elasticity boundary value problem. The macro-structural domain is represented by Ω. Figure 2.1(c), represent the periodic micro-structure domain, where Y_s is the volume filled with material and Y_v is void. The thermo-elastic macro-structural problem could be represented by equation 2.1 subject to the Dirichlet boundary conditions in Γ_d shown in the equation 2.2.

$$\frac{\partial \sigma_{ij}}{\partial x_j} = -f_i \quad in \quad \Omega, \tag{2.1}$$

$$\boldsymbol{u} = 0 \qquad in \quad \Gamma_d, \tag{2.2}$$

where f_i is the body force applied on Ω, $\boldsymbol{u}$ is the displacement constraints of the problem applied on the boundary Γ_d and σ_{ij} is the Cauchy stress tensor. For the linear elastic, isotropic materials, the constitutive equation can be written as

$$\sigma_{ij} = D_{ijkl}\varepsilon_{kl} - \beta_{ij}\Delta T. \tag{2.3}$$

Assuming the multi-material case with, perfect bonding between phases, uniform distribution of the temperature, and constant properties of each phases materials; thus, the equation 2.3 is the constitutive relation that described the thermoelastic behavior of the materials phases (Sigmund and Torquato, 1997), where D_{ijkl} is the elasticity 4^{th} order tensor, ΔT is the temperature change, ε_{kl} is the strain tensor, and β_{ij} is the thermal stress tensor given by the equations 2.4 and 2.5, respectively.

$$\varepsilon_{kl} = \frac{1}{2}\left(\frac{\partial u_k}{\partial x_l} + \frac{\partial u_l}{\partial x_k}\right), \tag{2.4}$$

$$\beta_{ij}^M = D_{ijkl}^M \alpha_{kl}^M, \tag{2.5}$$

where α_{kl} is the tensor of the thermal expansion coefficients and u_k represents a component displacement field.

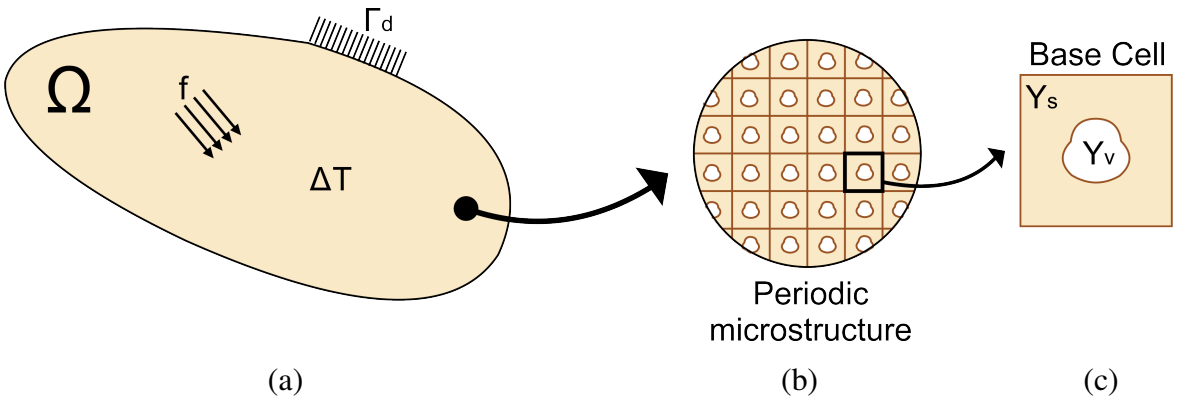

Figure 2.1: Thermo-elastic multi-scale modeling: (a) Macroscopic solid model; (b) Periodic conditions and (c) Base cell for homogenization.

For the bi-dimensional case the equation 2.1 can be written as:

$$\begin{aligned} \frac{\partial \sigma_{11}}{\partial x_1} + \frac{\partial \sigma_{12}}{\partial x_2} &= -f_1 \\ \frac{\partial \sigma_{21}}{\partial x_1} + \frac{\partial \sigma_{22}}{\partial x_2} &= -f_2. \end{aligned} \tag{2.6}$$

Equation 2.6 can be stated in a matrix operator form as follow:

$$\begin{bmatrix} \frac{\partial}{\partial x_1} & 0 & \frac{\partial}{\partial x_2} \\ 0 & \frac{\partial}{\partial x_2} & \frac{\partial}{\partial x_1} \end{bmatrix} \begin{Bmatrix} \sigma_{11} \\ \sigma_{22} \\ \sigma_{12} \end{Bmatrix} = \begin{Bmatrix} -f_1 \\ -f_2 \end{Bmatrix}, \tag{2.7}$$

where $\sigma_{21} = \sigma_{12}$, and f_1 and f_2 are the body forces in the x_1 and x_2 directions, respectively.

The operator $\boldsymbol{\partial}$, and the vectors $\boldsymbol{\sigma}$ and $\boldsymbol{f}$ are given by the equation 2.8, 2.9 and 2.10, respectively.

$$\boldsymbol{\partial} = \begin{bmatrix} \frac{\partial}{\partial x_1} & 0 \\ 0 & \frac{\partial}{\partial x_2} \\ \frac{\partial}{\partial x_2} & \frac{\partial}{\partial x_1} \end{bmatrix}, \tag{2.8}$$

$$\boldsymbol{\sigma} = \begin{Bmatrix} \sigma_{11} \\ \sigma_{22} \\ \sigma_{12} \end{Bmatrix}, \tag{2.9}$$

and

$$\boldsymbol{f} = \left\{ \begin{array}{c} f_1 \\ f_2 \end{array} \right\}. \tag{2.10}$$

Using the equations 2.8, 2.9 and 2.10 it is possible to rewrite the equation 2.7 as follow:

$$\boldsymbol{\partial}^T \boldsymbol{\sigma} = -\boldsymbol{f}. \tag{2.11}$$

From the equations 2.3 and 2.9, it is possible to state the following relation:

$$\boldsymbol{\sigma} = \boldsymbol{D}\boldsymbol{\varepsilon} + \boldsymbol{\beta}\Delta T, \tag{2.12}$$

where $\boldsymbol{D}$ is the elasticity matrix, given by the equation 2.13 for the plane stress condition considering in this work, $\boldsymbol{\varepsilon}$ the strain vector and $\boldsymbol{\beta}$ the thermal stress vector, given by the equations 2.14 and 2.15 for the bi-dimensional case, and ΔT the temperature change.

$$\boldsymbol{D} = E * \left[\begin{array}{ccc} \frac{1}{1-\nu^2} & \frac{\nu}{1-\nu^2} & 0 \\ \frac{\nu}{1-\nu^2} & \frac{1}{1-\nu^2} & 0 \\ 0 & 0 & \frac{1}{2(1+(\nu))} \end{array} \right]. \tag{2.13}$$

$$\boldsymbol{\varepsilon} = \left\{ \begin{array}{c} \varepsilon_{11} \\ \varepsilon_{22} \\ \gamma_{12} \end{array} \right\}. \tag{2.14}$$

$$\boldsymbol{\beta} = \left\{ \begin{array}{c} \beta_{11} \\ \beta_{22} \\ \beta_{12} \end{array} \right\}. \tag{2.15}$$

Using the matrix form and the operator given by the equation 2.8, it possible to rewrite the equation 2.4 as follow:

$$\boldsymbol{\varepsilon} = \boldsymbol{\partial}\boldsymbol{u}. \tag{2.16}$$

2.2 Numerical solution of thermo-elasticity problem on the macro-scale

The solution of the thermo-elastic problem on the macro-scale, is obtained using the finite element method and the weak form of equation 2.1.

Applying the weighted residual method on the equation 2.1, where ω is an arbitrary function, it is possible to obtain the weak form of the problem (Hughes, 2000), expressed as

$$\int_\Omega \omega_i \frac{\partial \sigma_{ij}}{\partial x_j} d\Omega = -\int_\Omega \omega_i f_i d\Omega. \tag{2.17}$$

Substituting the equations 2.4 and 2.5 into 2.3, and the equation 2.3 into 2.1, the equation 2.17 can be written as

$$\int_{\Omega} \omega_i \frac{\partial}{\partial x_j} \left(D_{ijkl} \frac{1}{2} \left(\frac{\partial u_k}{\partial x_l} + \frac{\partial u_l}{\partial x_k} \right) - \beta_{ij} \Delta T \right) d\Omega = - \int_{\Omega} \omega_i f_i d\Omega, \tag{2.18}$$

and, due to the symmetry of the strain tensor ($\varepsilon_{kl} = \varepsilon_{lk}$), the equation 2.18 can be written as

$$\int_{\Omega} \omega_i \frac{\partial}{\partial x_j} \left(D_{ijkl} \frac{\partial u_k}{\partial x_l} - \beta_{ij} \Delta T \right) d\Omega = - \int_{\Omega} \omega_i f_i d\Omega. \tag{2.19}$$

Integrating by parts the terms on the left-hand side of the equation 2.19, it is obtained the equation 2.20.

$$\int_{\Omega} \frac{\partial \omega_i}{\partial x_j} D_{ijkl} \frac{\partial u_k}{\partial x_l} d\Omega = \int_{\Omega} \frac{\partial \omega_i}{\partial x_j} \beta_{ij} \Delta T d\Omega + \int_{\Omega} \omega_i f_i d\Omega. \tag{2.20}$$

For the bi-dimensional case and using the matrix formulation with $f_i = \boldsymbol{f}$ from the equation 2.10, $D_{ijkl} = \boldsymbol{D}^M$ from de equation 2.13, $\beta_{ij} = \boldsymbol{\beta}^M$ from the equation 2.15, and $u_k = \boldsymbol{u}^M$, it is possible to rewrite the equation 2.20 as

$$\begin{gathered} \int_{\Omega} \left(\begin{bmatrix} \frac{\partial}{\partial x_1} & 0 \\ 0 & \frac{\partial}{\partial x_2} \\ \frac{\partial}{\partial x_2} & \frac{\partial}{\partial x_1} \end{bmatrix} \begin{Bmatrix} \omega_1 \\ \omega_2 \end{Bmatrix} \right)^T \boldsymbol{D}^M \begin{bmatrix} \frac{\partial}{\partial x_1} & 0 \\ 0 & \frac{\partial}{\partial x_2} \\ \frac{\partial}{\partial x_2} & \frac{\partial}{\partial x_1} \end{bmatrix} \boldsymbol{u}^M d\Omega = \\ \int_{\Omega} \left(\begin{bmatrix} \frac{\partial}{\partial x_1} & 0 \\ 0 & \frac{\partial}{\partial x_2} \\ \frac{\partial}{\partial x_2} & \frac{\partial}{\partial x_1} \end{bmatrix} \begin{Bmatrix} \omega_1 \\ \omega_2 \end{Bmatrix} \right)^T \boldsymbol{\beta}^M \Delta T d\Omega + \int_{\Omega} \begin{Bmatrix} \omega_1 \\ \omega_2 \end{Bmatrix}^T \boldsymbol{f} d\Omega. \end{gathered} \tag{2.21}$$

Dividing the domain into N element. Each element has the following interpolated displacement field:

$$\boldsymbol{u}^M = \boldsymbol{N}_s \boldsymbol{u}_d^M, \tag{2.22}$$

where $\boldsymbol{N}_s$ are the matrix that contain shape functions (Cook *et al.*, 2001), and $\boldsymbol{u}_d^M$ is the vector of the nodal displacement. Using the Galergin Method, the weights functions are equal to the shape function,

$$\boldsymbol{\omega} = \boldsymbol{N}_s \boldsymbol{\omega}_d, \tag{2.23}$$

due to this fact and using the equations 2.8 and 2.22, it is possible to rewrite the equation 2.21 as

$$\int_{\Omega} \boldsymbol{\partial}^T \boldsymbol{N}_s^T \boldsymbol{\omega}_d \boldsymbol{D}^M \boldsymbol{\partial} \boldsymbol{N}_s \boldsymbol{u}_d^M d\Omega = \int_{\Omega} \boldsymbol{\partial}^T \boldsymbol{N}_s^T \boldsymbol{\omega}_d \boldsymbol{\beta}^M \Delta T d\Omega + \int_{\Omega} \boldsymbol{N}_s \boldsymbol{\omega}_d \boldsymbol{f} d\Omega, \tag{2.24}$$

where the terms $\boldsymbol{\omega_d}$ are presented in the left-hand and in the right-hand of the equation, making possible to write the equation 2.24 as

$$\int_{\Omega} \boldsymbol{\partial}^T \boldsymbol{N}_s^T \boldsymbol{D}^M \boldsymbol{\partial} \boldsymbol{N}_s \boldsymbol{u}_d^M d\Omega = \int_{\Omega} \boldsymbol{\partial}^T \boldsymbol{N}_s^T \boldsymbol{\beta}^M \Delta T d\Omega + \int_{\Omega} \boldsymbol{N}_s \boldsymbol{f} d\Omega. \tag{2.25}$$

Defining the strain/displacement matrix $\boldsymbol{B}$ as

$$\boldsymbol{B} = \boldsymbol{\partial} \boldsymbol{N}_s, \tag{2.26}$$

the equation 2.21 can be written in a matrix formulation as

$$\int_{\Omega} \boldsymbol{B}^T \boldsymbol{D}^M \boldsymbol{B} d\Omega \boldsymbol{u}_d^M = \int_{\Omega} \boldsymbol{B}^T \boldsymbol{\beta}^M \Delta T d\Omega + \boldsymbol{f}^{M,mec}, \tag{2.27}$$

where the superscript M indicates that the properties are related to the macro-scale and $\boldsymbol{f}^{mec}$ is the nodal mechanical force applied on the structure, given by the equation:

$$\boldsymbol{f}^{M,mec} = \int_{\Omega} \boldsymbol{N}_s \boldsymbol{f} d\Omega. \tag{2.28}$$

Equation 2.27 can be rewritten as

$$\boldsymbol{K}^M \boldsymbol{u}_d^M = \boldsymbol{f}^{M,ter} + \boldsymbol{f}^{M,mec}, \tag{2.29}$$

where $\boldsymbol{K}^M$ is the global stiffness matrix and $\boldsymbol{f}^{M,ter}$ is the global thermal force, calculated using

$$\boldsymbol{K}^M = \underset{e=1}{\overset{Nel}{\mathop{A}}} \boldsymbol{K}_e^M = \underset{e=1}{\overset{Nel}{\mathop{A}}} \int_{\Omega_e} \boldsymbol{B}_e^T \boldsymbol{D}_e^M \boldsymbol{B}_e d\Omega, \tag{2.30}$$

and

$$\boldsymbol{f}^{M,ter} = \underset{e=1}{\overset{Nel}{\mathop{A}}} \boldsymbol{f}_e^{M,ter} = \underset{e=1}{\overset{Nel}{\mathop{A}}} \int_{\Omega_e} \boldsymbol{B}_e^T \boldsymbol{\beta}_e^M \Delta T d\Omega, \tag{2.31}$$

where the operator A indicates the assembly of the e elements on the global system, the subscript e indicates that the matrix and vectors are associated to the element e and Nel is the number of macro-structural elements.

Applying the boundary conditions and solving the linear systems presented on the equations 2.27, the numerical solution, $\boldsymbol{u}_d^M$, of a thermo-elastic problem on a macro-scale is determined.

2.3 Multi-scale analysis of the thermal-elasticity problem

On the previous section the macro-scale thermo-elasticity model was presented. This model is valid when the material of the structure is homogeneous or heterogeneous, if the heterogeneities are periodic and if the perfect bonding between phases is valid. When the material is heterogeneous, it is necessary obtain its equivalent properties. If the heterogeneities are periodic, the equivalent properties can be calculated using the homogenization method. In this section are presented the homogenization method by asymptotic expansion, the calculation of the homogenized elasticity matrix, the homogenized thermal stress tensor and the boundary condition used to solve the micro-scale problems.

2.3.1 Multi-scale analysis using the homogenization theory

The multi-scale analysis of a structure made of a composite periodic material, can be done using the homogenization method. When the composite material has enough regular heterogeneities, it could be assumed that its micro-structure is periodic as ilustrated in figure 2.1. Thus, the homogenization method is used to find the effective properties of the equivalent homogenized material (Hassani and Hinton, 1998a) and to perform a consistent micro-scale analysis.

Defining F as a function that represent any physical quantity of the heterogeneous medium with a regular periodicity; it must satisfy the following property on the micro-scale:

$$F(\boldsymbol{x} + \boldsymbol{NY}) = F(\boldsymbol{x}), \tag{2.32}$$

where $\boldsymbol{x} = \{x_1, x_2, x_3\}^T$ is the position vector of the point; $\boldsymbol{N}$ is a 3 x 3 diagonal matrix of arbitrary integers n_1, n_2 and n_3:

$$\boldsymbol{N} = \begin{bmatrix} n_1 & 0 & 0 \\ 0 & n_2 & 0 \\ 0 & 0 & n_3 \end{bmatrix}, \tag{2.33}$$

and $\boldsymbol{Y} = \{Y_1, Y_2, Y_3\}^T$ is a constant vector which determines the period of the structure. This means that the physical quantities described by $F(\boldsymbol{x})$ on a micro-scale domain, must be repeated in every base cell with Y dimensions.

For example, considering the heterogeneous micro-structure as a regular periodic medium, it is possible to define base cells with Y dimensions, where the $F(\boldsymbol{x})$ function have

the same value as shown in equation 2.34 and figure 2.2.

$$F(P_1) = F(P_2) = F(P_3) = F(P_4) = F(P_5) = F(P_6). \tag{2.34}$$

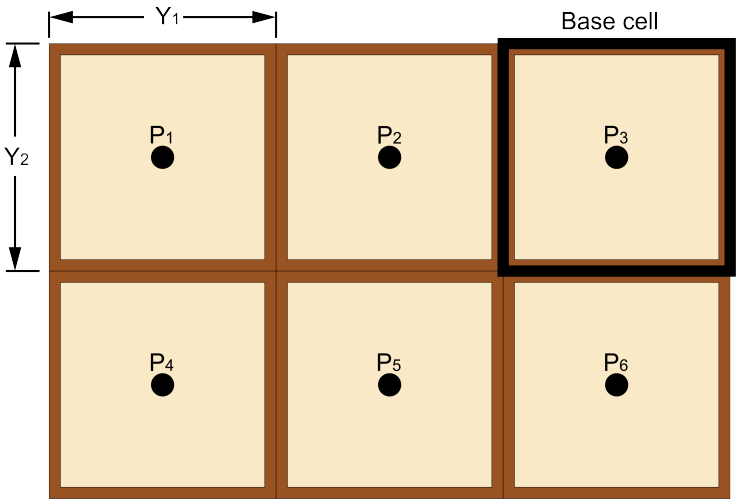

Figure 2.2: Bi-dimensional model of a micro-structural periodic medium.

The homogenization theory assumed a very small period Y compared to the dimensions of the structure. For this reason, the characteristic functions $F(\boldsymbol{x})$ vary significantly and rapidly within its neighborhood. Hence, it is reasonable to considerate that the quantities have two dependencies (Hassani and Hinton, 1998a): one in the macroscopic or global level $\boldsymbol{x}$, which indicates slow variations; and the other in the microscopic or local level $\boldsymbol{y}$, which describes rapid oscillations as illustrated in the figure 2.3.

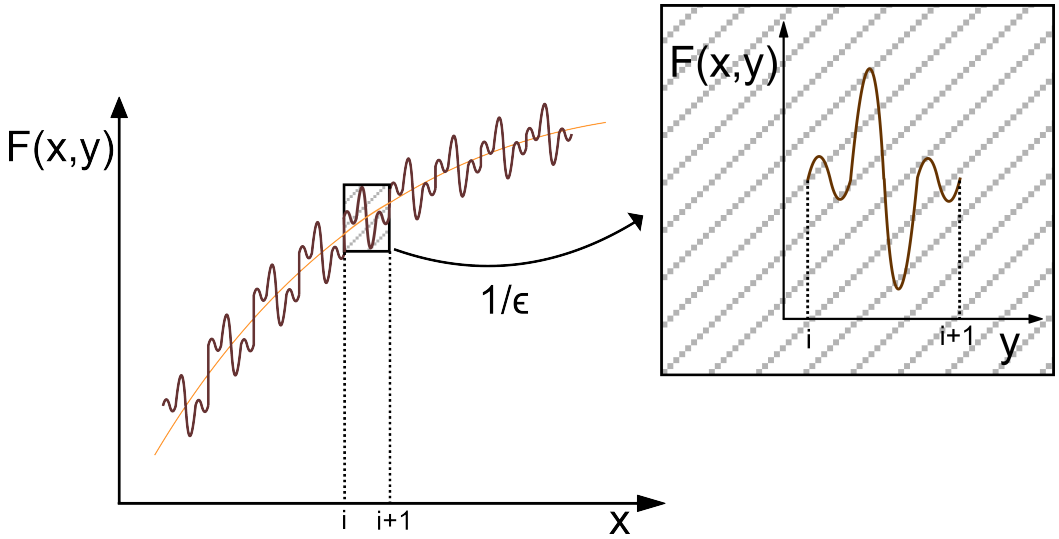

Figure 2.3: Function $F(\boldsymbol{x}, \boldsymbol{y})$ in the macroscopic and microscopic levels

This double-scale expansion is used to describe $F(\boldsymbol{x}, \boldsymbol{y})$ oscillations. Being ϵ the proportion between the base cell and the whole structure, and $F(\boldsymbol{x}, \boldsymbol{y})$ a general function of the structure, it is possible to state the following relation

$$F(\boldsymbol{x}) = F\left(\boldsymbol{x}, \frac{\boldsymbol{x}}{\epsilon}\right) = F(\boldsymbol{x}, \boldsymbol{y}), \tag{2.35}$$

where ϵ is a very small positive number (Guedes and Kikuchi, 1990). ϵ is known as the characteristic inhomogeneity dimension and it gives an estimate of the size of the base cell dimension compared with the size of the whole domain (Hassani and Hinton, 1998a).

The function $F(\boldsymbol{x})$ of a composite material can be expanded using an asymptotic expansion as

$$F(\boldsymbol{x}) = F^0(\boldsymbol{x}, \boldsymbol{y}) + \epsilon F^1(\boldsymbol{x}, \boldsymbol{y}) + \epsilon^2 F^2(\boldsymbol{x}, \boldsymbol{y}) + ..., \tag{2.36}$$

where $\epsilon \to 0$ and the functions $F^0(\boldsymbol{x}, \boldsymbol{y})$, $F^1(\boldsymbol{x}, \boldsymbol{y})$, $F^2(\boldsymbol{x}, \boldsymbol{y})$,... are smooth in the macroscopic level and Y-periodic in the microscopic level.

The equation 2.36 is obtained using the concept of asymptotic expansion developed by Poincaré, which says that if a sequence of continuous functions on some domain $\{g_k(\boldsymbol{x})\}_{K \geq 0}$ is given with $g_{k+1}(\boldsymbol{x}) = O(g_k(\boldsymbol{x}))$ for $k \geq 0$,

$$F(\boldsymbol{x}) = c_0 g_0(\boldsymbol{x}) + c_1 g_1(\boldsymbol{x}) + c_2 g_2(\boldsymbol{x}) + ... \tag{2.37}$$

It is called an asymptotic series for $F(\boldsymbol{x})$, or an asymptotic expansion of $F(\boldsymbol{x})$ where the O notation is used to bound error terms that have smaller values than the main value. For instance, it can be said that $f(\boldsymbol{x}) = g(\boldsymbol{x}) + O(h(\boldsymbol{x}))$ to indicate that the function $f(\boldsymbol{x})$ can be approximated by the calculation of $g(\boldsymbol{x})$ and the error will be within a constant factor of $h(\boldsymbol{x})$ (Sedgewick and Flajolet, 2013).

2.3.2 Homogenization of the thermo-elasticity problem

The solution of the thermo-elastic problem, represented by the equation 2.1 subject to the Dirichlet boundary condition, showed in the equation 2.2 when the material has periodic heterogeneities, can be written using the asymptotic expansion as

$$\boldsymbol{u}^\epsilon(\boldsymbol{x}, \boldsymbol{y}) = \boldsymbol{u}^0(\boldsymbol{x}, \boldsymbol{y}) + \epsilon \boldsymbol{u}^1(\boldsymbol{x}, \boldsymbol{y}) + \epsilon^2 \boldsymbol{u}^2(\boldsymbol{x}, \boldsymbol{y}) + ..., \tag{2.38}$$

where the superscript ϵ indicates that the function is approximated using a asymptotic expansion and depends on the characteristic inhomogeneity dimension.

Due to the symmetry of the strain tensor ($\varepsilon_{kl} = \varepsilon_{lk}$), the equation 2.4 can be written as

$$\varepsilon_{kl} = \frac{\partial u_k^\epsilon(\boldsymbol{x}, \boldsymbol{y})}{\partial x_l}. \tag{2.39}$$

Substituting equations 2.39 and 2.3 into 2.1 yields

$$\frac{\partial}{\partial x_j}\left(D_{ijkl}(\boldsymbol{x}, \boldsymbol{y})\frac{\partial u_k^\epsilon(\boldsymbol{x}, \boldsymbol{y})}{\partial x_l} - \beta_{ij}(\boldsymbol{x}, \boldsymbol{y})\Delta T\right) = -f_i, \tag{2.40}$$

where $D_{ijkl}(\boldsymbol{x}, \boldsymbol{y})$ is the elasticity tensor and $\beta_{ij}(\boldsymbol{x}, \boldsymbol{y})$ the thermal stress tensor. For the theory of homogenization, the elasticity tensor and the thermal stress tensor are uniform on the macroscopic scale ($D_{ijkl}(\boldsymbol{x}, \boldsymbol{y}) = D_{ijkl}(\boldsymbol{y})$ and $\beta_{ij}(\boldsymbol{x}, \boldsymbol{y}) = \beta_{ij}(\boldsymbol{y})$).

Defining the elliptic operator Υ^ϵ as

$$\Upsilon^\epsilon = \frac{\partial}{\partial x_j}\left(D_{ijkl}(\boldsymbol{y})\frac{\partial}{\partial x_l}\right), \tag{2.41}$$

the equation 2.40 can be written as

$$\Upsilon^\epsilon u_k^\epsilon(\boldsymbol{x}, \boldsymbol{y}) = \frac{\partial}{\partial x_j}\left(\beta_{ij}(\boldsymbol{y})\Delta T\right) - f_i, \tag{2.42}$$

applying the chain rule of differentiation, given by the equation 2.43, to the elliptic operator,

$$\frac{\partial}{\partial x} = \frac{\partial}{\partial x} + \frac{\partial}{\partial y}\frac{\partial y}{\partial x} = \frac{\partial}{\partial x} + \frac{1}{\epsilon}\frac{\partial}{\partial y}, \tag{2.43}$$

$$\Upsilon^\epsilon = \frac{\partial}{\partial x_j}\left(D_{ijkl}(\boldsymbol{y})\frac{\partial}{\partial x_l}\right) + \frac{1}{\epsilon}\frac{\partial}{\partial y_j}\left(D_{ijkl}(\boldsymbol{y})\frac{\partial}{\partial x_l}\right), \tag{2.44}$$

and, applying a second time the chain rule of differentiation to the elliptic operator it is obtained the following

$$\Upsilon^\epsilon = \frac{\partial}{\partial x_j}\left[D_{ijkl}(\boldsymbol{y})\left(\frac{\partial}{\partial x_l} + \frac{1}{\epsilon}\frac{\partial}{\partial y_l}\right)\right] + \frac{1}{\epsilon}\frac{\partial}{\partial y_j}\left[D_{ijkl}(\boldsymbol{y})\left(\frac{\partial}{\partial x_l} + \frac{1}{\epsilon}\frac{\partial}{\partial y_l}\right)\right]. \tag{2.45}$$

Multiplying and assembling the terms with the same power of ϵ yields

$$\Upsilon^{\epsilon} = \underbrace{\frac{\partial}{\partial x_j}\left(D_{ijkl}(\boldsymbol{y})\frac{\partial}{\partial x_l}\right)}_{A^3} + \frac{1}{\epsilon}\underbrace{\left[\frac{\partial}{\partial x_j}\left(D_{ijkl}(\boldsymbol{y})\frac{\partial}{\partial y_l}\right) + \frac{\partial}{\partial y_j}\left(D_{ijkl}(\boldsymbol{y})\frac{\partial}{\partial x_l}\right)\right]}_{A^2} + \frac{1}{\epsilon^2}\underbrace{\frac{\partial}{\partial y_j}\left(D_{ijkl}(\boldsymbol{y})\frac{\partial}{\partial y_l}\right)}_{A^1}. \quad (2.46)$$

The equation 2.41 can be rewritten as

$$\Upsilon^{\epsilon} = \epsilon^{-2}A^1 + \epsilon^{-1}A^2 + A^3, \quad (2.47)$$

where

$$A^1 = \frac{\partial}{\partial y_j}\left(D_{ijkl}(\boldsymbol{y})\frac{\partial}{\partial y_l}\right), \quad (2.48)$$

$$A^2 = \frac{\partial}{\partial x_j}\left(D_{ijkl}(\boldsymbol{y})\frac{\partial}{\partial y_l}\right) + \frac{\partial}{\partial y_j}\left(D_{ijkl}(\boldsymbol{y})\frac{\partial}{\partial x_l}\right) \quad (2.49)$$

and

$$A^3 = \frac{\partial}{\partial x_j}\left(D_{ijkl}(\boldsymbol{y})\frac{\partial}{\partial x_l}\right) \quad (2.50)$$

Applying the chain rule of differentiation to the term related to the thermal stress of the equation 2.42 and substituting the equations 2.38 and 2.47 into 2.1 yields

$$\left(\epsilon^{-2}A^1 + \epsilon^{-1}A^2 + A^3\right)\left(u_k^0(\boldsymbol{x},\boldsymbol{y}) + \epsilon u_k^1(\boldsymbol{x},\boldsymbol{y}) + \epsilon^2 u_k^2(\boldsymbol{x},\boldsymbol{y}) + ...\right) = \frac{\partial}{\partial x_j}\left(\beta_{ij}(\boldsymbol{y})\Delta T\right) + \frac{1}{\epsilon}\frac{\partial}{\partial y_j}\left(\beta_{ij}(\boldsymbol{y})\Delta T\right) - f_i \quad (2.51)$$

and by equating the terms with the same power of ϵ on equation 2.51, the following equations can be written

$$A^1 u_k^0(\boldsymbol{x},\boldsymbol{y}) = 0, \quad (2.52)$$

$$A^2 u_k^0(\boldsymbol{x},\boldsymbol{y}) + A^1 u_k^1(\boldsymbol{x},\boldsymbol{y}) = \frac{\partial}{\partial y_j}\left(\beta_{ij}(\boldsymbol{y})\Delta T\right), \quad (2.53)$$

and

$$A^3 u_k^0(\boldsymbol{x},\boldsymbol{y}) + A^2 u_k^1(\boldsymbol{x},\boldsymbol{y}) + A^1 u_k^2(\boldsymbol{x},\boldsymbol{y}) = \frac{\partial}{\partial x_j}\left(\beta_{ij}(\boldsymbol{y})\Delta T\right) - f_i. \quad (2.54)$$

Before solving this system is important to notice the following facts (Hassani and Hinton, 1998a):

Fact 1: given an equilibrium equation for a generic Y-periodic function $\boldsymbol{u}^i$

$$A^1\boldsymbol{u}^i = \boldsymbol{f} \qquad in \quad \boldsymbol{Y}, \tag{2.55}$$

the equation 2.55 has a unique solution if the integral of the force $\boldsymbol{f}$ over the period divided by the volume of the base cell $|\boldsymbol{Y}|$ is zero (see equation 2.56)

$$\overline{\boldsymbol{f}} = \frac{1}{|\boldsymbol{Y}|}\int_Y \boldsymbol{f} dy = 0, \tag{2.56}$$

where the volume of the base cell is given by the equation 2.57.

$$|\boldsymbol{Y}| = \int_Y dy. \tag{2.57}$$

Fact 2: The integral of the derivative of the periodic function over the period is zero (see equation 2.58)

$$\frac{1}{|\boldsymbol{Y}|}\int_Y \frac{\partial \boldsymbol{f}}{\partial y} dy = 0. \tag{2.58}$$

Using the Fact 1 and from the equations 2.48 and 2.52, it could be concluded that $\boldsymbol{u}^0(\boldsymbol{x}, \boldsymbol{y})$ only depends on $\boldsymbol{x}$, in other words the function $\boldsymbol{u}^0(\boldsymbol{x}, \boldsymbol{y})$ only depends on the macroscopic level

$$\boldsymbol{u}^0(\boldsymbol{x}, \boldsymbol{y}) = \boldsymbol{u}^0(\boldsymbol{x}). \tag{2.59}$$

Substituting the equation 2.49 into the equation 2.53 yields

$$A^1 u_k^1(\boldsymbol{x}, \boldsymbol{y}) = -\frac{\partial}{\partial x_j}\left(D_{ijkl}(\boldsymbol{y})\frac{\partial u_k^0(\boldsymbol{x})}{\partial y_l}\right) - \frac{\partial}{\partial y_j}\left(D_{ijkl}(\boldsymbol{y})\frac{\partial u_k^0(\boldsymbol{x})}{\partial x_l}\right) + \frac{\partial}{\partial y_j}\left(\beta_{ij}(\boldsymbol{y})\Delta T\right), \tag{2.60}$$

where $\frac{\partial}{\partial x_j}\left(D_{ijkl}(\boldsymbol{y})\frac{\partial u_k^0(\boldsymbol{x})}{\partial y_l}\right) = 0$ since $\boldsymbol{u}^0(\boldsymbol{x})$ is an independent variable of $\boldsymbol{y}$. The solution of the equation 2.60 can be written as

$$u_p^1(\boldsymbol{x}, \boldsymbol{y}) = -\chi_p^{kl}(\boldsymbol{y})\frac{\partial u_k^0(\boldsymbol{x})}{\partial x_l} + \psi_p(\boldsymbol{y}) + \xi_p(\boldsymbol{x}), \tag{2.61}$$

where $\boldsymbol{\xi}(\boldsymbol{x})$ is the constant of the integration due to $\boldsymbol{y}$, whereby it only depends on $\boldsymbol{x}$. Multiplying the equation 2.61 for the operator A^1 yields

$$A^1 u_p^1(\boldsymbol{x}, \boldsymbol{y}) = -A^1\chi_p^{kl}(\boldsymbol{y})\frac{\partial u_k^0(\boldsymbol{x})}{\partial x_l} + A^1\psi_p(\boldsymbol{y}) + A^1\xi_p(\boldsymbol{x}). \tag{2.62}$$

Comparing the equations 2.60 and 2.62 it can be obtained the micro-scale equations 2.63 and 2.64

$$\frac{\partial}{\partial y_j}\left(D_{ijpq}(\boldsymbol{y})\frac{\partial \chi_p^{kl}(\boldsymbol{y})}{\partial y_q}\right) = \frac{\partial D_{ijkl}(\boldsymbol{y})}{\partial y_j} \tag{2.63}$$

and

$$\frac{\partial}{\partial y_j}\left(D_{ijpq}(\boldsymbol{y})\frac{\partial \psi_p(\boldsymbol{y})}{\partial y_q}\right) = \frac{\partial \beta_{ij}(\boldsymbol{y})\Delta T}{\partial y_j}, \tag{2.64}$$

where $\chi_p^{kl}(\boldsymbol{y})$ is the characteristic tensor in micro-structure and $\psi_p(\boldsymbol{y})$, the characteristic displacement vector due to the thermal expansion effect (Cheng, 1992).

The equation 2.54 can be written as

$$A^1 u_k^2(\boldsymbol{x},\boldsymbol{y}) = -A^2 u_k^1(\boldsymbol{x},\boldsymbol{y}) - A^3 u_k^0(\boldsymbol{x}) + \frac{\partial \beta_{ij}(\boldsymbol{y})\Delta T}{\partial x_j} - f_i. \tag{2.65}$$

Considering the Fact 1, the equation 2.65 has a unique solution if the following equation is satisfied

$$\frac{1}{|\boldsymbol{Y}|}\int_Y \left(-A^2 u_k^1(\boldsymbol{x},\boldsymbol{y}) - A^3 u_k^0(\boldsymbol{x}) + \frac{\partial \beta_{ij}(\boldsymbol{y})\Delta T}{\partial x_j} - f_i\right) dy = 0. \tag{2.66}$$

Substituting the operators A^2 and A^3 on the equation 2.66 yields

$$\begin{aligned}&\frac{1}{|\boldsymbol{Y}|}\int_Y \frac{\partial}{\partial x_j}\left(D_{ijkl}(\boldsymbol{y})\frac{\partial u_k^1(\boldsymbol{x},\boldsymbol{y})}{\partial y_l}\right) dy + \frac{1}{|\boldsymbol{Y}|}\int_Y \frac{\partial}{\partial y_j}\left(D_{ijkl}(\boldsymbol{y})\frac{\partial u_k^1(\boldsymbol{x},\boldsymbol{y})}{\partial x_l}\right) dy \\ &+\frac{1}{|\boldsymbol{Y}|}\int_Y \frac{\partial}{\partial x_j}\left(D_{ijkl}(\boldsymbol{y})\frac{\partial u_k^0(\boldsymbol{x})}{\partial x_l}\right) dy = \frac{1}{|\boldsymbol{Y}|}\int_Y \frac{\partial \beta_{ij}(\boldsymbol{y})\Delta T}{\partial x_j} dy - \frac{1}{|\boldsymbol{Y}|}\int_Y f_i dy,\end{aligned} \tag{2.67}$$

and, for the Fact 2 the second term of the equation 2.67 is zero.

$$\frac{1}{|\boldsymbol{Y}|}\int_Y \frac{\partial}{\partial y_j}\left(D_{ijkl}(\boldsymbol{y})\frac{\partial \boldsymbol{u}_k^1(\boldsymbol{x},\boldsymbol{y})}{\partial x_l}\right) dy = 0. \tag{2.68}$$

Substituting the equation 2.61 into the equation 2.67 yields

$$\begin{aligned}&\frac{1}{|\boldsymbol{Y}|}\int_Y \frac{\partial}{\partial x_j}\left\{D_{ijpq}(\boldsymbol{y})\frac{\partial}{\partial y_q}\left(-\chi_p^{kl}(\boldsymbol{y})\frac{\partial u_k^0(\boldsymbol{x})}{\partial x_l} + \psi_p(\boldsymbol{y}) + \xi_p(\boldsymbol{x})\right)\right\} dy \\ &+\frac{1}{|\boldsymbol{Y}|}\int_Y \frac{\partial}{\partial x_j}\left(D_{ijkl}(\boldsymbol{y})\frac{\partial u_k^0(\boldsymbol{x})}{\partial x_l}\right) dy = \frac{1}{|\boldsymbol{Y}|}\int_Y \frac{\partial \beta_{ij}(\boldsymbol{y})\Delta T}{\partial x_j} dy - \frac{1}{|\boldsymbol{Y}|}\int_Y f_i dy.\end{aligned} \tag{2.69}$$

Reorganizing the terms, the equation 2.69 can be written as

$$\frac{1}{|\boldsymbol{Y}|}\int_Y \left(D_{ijkl}(\boldsymbol{y}) - D_{ijpq}(\boldsymbol{y})\frac{\partial \chi_p^{kl}(\boldsymbol{y})}{\partial y_q} \right) dy \frac{\partial^2 u_k^0(\boldsymbol{x})}{\partial x_j \partial x_l} = \frac{1}{|\boldsymbol{Y}|}\int_Y \frac{\partial}{\partial x_j}\left(\beta_{ij}(\boldsymbol{y})\Delta T - D_{ijpq}(\boldsymbol{y})\frac{\partial \psi_p(\boldsymbol{y})}{\partial y_q} \right) dy - \frac{1}{|\boldsymbol{Y}|}\int_Y f_i dy. \tag{2.70}$$

The equation 2.70 can be written as

$$D_{ijkl}^H(\boldsymbol{y})\frac{\partial^2 u_k^0(\boldsymbol{x})}{\partial x_j \partial x_l} = \frac{\partial}{\partial x_j}\beta_{ij}^H(\boldsymbol{y})\Delta T - f_i^H, \tag{2.71}$$

where the homogenized elasticity tensor, D_{ijkl}^H; the homogenized thermal stress tensor, β_{ij}^H; and the homogenized force f_i^H are given by

$$D_{ijkl}^H(\boldsymbol{y}) = \frac{1}{|\boldsymbol{Y}|}\int_Y \left(D_{ijkl}(\boldsymbol{y}) - D_{ijpq}(\boldsymbol{y})\frac{\partial \chi_p^{kl}(\boldsymbol{y})}{\partial y_q} \right) dy, \tag{2.72}$$

$$\beta_{ij}^H(\boldsymbol{y}) = \frac{1}{|\boldsymbol{Y}|}\int_Y \left(\beta_{ij}(\boldsymbol{y}) - D_{ijpq}(\boldsymbol{y})\frac{\partial \varphi_p(\boldsymbol{y})}{\partial y_q} \right) dy, \tag{2.73}$$

and

$$f_i^H = \frac{1}{|\boldsymbol{Y}|}\int_{Y_s} f_i dy, \tag{2.74}$$

respectively, where $\varphi_p(\boldsymbol{y})$ is the solution of

$$\frac{\partial}{\partial y_j}\left(D_{ijpq}(\boldsymbol{y})\frac{\partial \varphi_p(\boldsymbol{y})}{\partial y_q} \right) = \frac{\partial \beta_{ij}(\boldsymbol{y})}{\partial y_j} \tag{2.75}$$

on the micro-scale

2.3.3 Numerical calculation of the homogenized tensors

It is necessary to obtain the displacement $\chi_p^{kl}(\boldsymbol{y})$ and $\varphi_p(\boldsymbol{y})$ on the micro-scale level y, in order to calculate the homogenized elasticity matrix (D_{ijkl}^H)and the homogenized thermal stress tensor(β_{ij}^H). The calculation of $\chi_p^{kl}(\boldsymbol{y})$ and $\varphi_p(\boldsymbol{y})$ is made using the finite element method and the weak form of the equations 2.63 and 2.75.

Integrating the two sides of the equations 2.63 and 2.75, where v_i and w_i are an arbitrary

functions, it is obtained

$$\int_Y v_i \frac{\partial}{\partial y_i}\left(D_{ijpq}(\boldsymbol{y})\frac{\partial \chi_p^{kl}(\boldsymbol{y})}{\partial y_q}\right)dy = \int_Y v_i \frac{\partial D_{ijkl}(\boldsymbol{y})}{\partial y_i}dy, \tag{2.76}$$

and

$$\int_Y w_i \frac{\partial}{\partial y_i}\left(D_{ijpq}(\boldsymbol{y})\frac{\partial \varphi_p(\boldsymbol{y})}{\partial y_q}\right)dy = \int_Y w_i \frac{\partial \beta_{ij}(\boldsymbol{y})}{\partial y_i}dy, \tag{2.77}$$

then integrating by parts on the two sides of the equations 2.76 and 2.77, and reorganizing the terms, it is obtained

$$\int_Y \frac{\partial v_i}{\partial y_j}D_{ijkl}(\boldsymbol{y})dy - \int_Y \left(\frac{\partial v_i}{\partial y_j}D_{ijpq}(\boldsymbol{y})\frac{\partial \chi_p^{kl}(\boldsymbol{y})}{\partial y_q}\right)dy = \left[v_i D_{ijkl}(\boldsymbol{y})\right]_{\partial Y} - \left[v_i D_{ijpq}(\boldsymbol{y})\frac{\partial \chi_p^{kl}(\boldsymbol{y})}{\partial y_q}\right]_{\partial Y}, \tag{2.78}$$

and

$$\int_Y \frac{\partial w_i}{\partial y_j}\beta_{ij}(\boldsymbol{y})dy - \int_Y \left(\frac{\partial w_i}{\partial y_j}D_{ijpq}(\boldsymbol{y})\frac{\partial \varphi_p(\boldsymbol{y})}{\partial y_q}\right)dy = \left[w_i \beta_{ij}(\boldsymbol{y})\right]_{\partial Y} - \left[w_i D_{ijpq}(\boldsymbol{y})\frac{\partial \varphi_p(\boldsymbol{y})}{\partial y_q}\right]_{\partial Y}, \tag{2.79}$$

respectively, where excluding the terms on the right side of the equations 2.78 and 2.79, which are the natural boundary conditions, it is obtained

$$\int_Y \left(\frac{\partial v_i}{\partial y_i}D_{ijpq}(\boldsymbol{y})\frac{\partial \chi_p^{kl}(\boldsymbol{y})}{\partial y_q}\right)dy = \int_Y \frac{\partial v_i}{\partial y_j}D_{ijkl}(\boldsymbol{y})dy \tag{2.80}$$

and

$$\int_Y \left(\frac{\partial w_i}{\partial y_i}D_{ijpq}(\boldsymbol{y})\frac{\partial \varphi_p(\boldsymbol{y})}{\partial y_q}\right)dy = \int_Y \frac{\partial w_i}{\partial y_j}\beta_{ij}(\boldsymbol{y})dy, \tag{2.81}$$

which are the weak form of the equations 2.63 and 2.75, respectively.

Adopting the Galerkin method and the matrix formulation, it is possible to rewrite the equations 2.80 and 2.81 on the form

$$\int_Y (\boldsymbol{B}^m)^T \boldsymbol{D}^m \boldsymbol{B}^m dy \boldsymbol{U}^m = \int_Y (\boldsymbol{B}^m)^T \boldsymbol{D}^m dy \tag{2.82}$$

and

$$\int_Y (\boldsymbol{B}^m)^T \boldsymbol{D}^m \boldsymbol{B} dy \boldsymbol{\varphi}^m = \int_Y (\boldsymbol{B}^m)^T \boldsymbol{\beta}^m dy, \tag{2.83}$$

where $\boldsymbol{B}$ is the strain/displacement matrix, $\boldsymbol{D}$ the elasticity matrix, $\boldsymbol{\beta}$ is the thermal stress vector of local material, and the superscript m indicates that the matrices and vectors are associated to the micro-scale.

The solution $\boldsymbol{U}^m$ is a three-column matrix where the values of the first, second and third

column correspond to the deformation induced by a unit initial strain in horizontal and vertical direction and an initial shear strain, respectively. The solution $\boldsymbol{\varphi}^m$ is a vector that correspond to the deformation induced by a unit initial thermal stress.

Considering an isotropic material inside the base cell and two dimensional problem, the elasticity matrix of micro-scale material is

$$\boldsymbol{D}^m = \begin{bmatrix} D_{1111} & D_{1122} & 0 \\ D_{1122} & D_{2222} & 0 \\ 0 & 0 & D_{1212} \end{bmatrix}, \tag{2.84}$$

and the thermal stress tensor is

$$\boldsymbol{\beta}^m = \begin{Bmatrix} \beta_{11} \\ \beta_{22} \\ 0 \end{Bmatrix}, \tag{2.85}$$

the equations 2.82 and 2.81 can be rewritten as

$$\boldsymbol{K}^m \boldsymbol{U}^m = \boldsymbol{F}^m \tag{2.86}$$

and

$$\boldsymbol{K}^m \boldsymbol{\varphi}^m = \boldsymbol{f}_t^m, \tag{2.87}$$

where $\boldsymbol{K}^m$ is the stiffness matrix in the local level y, given by

$$\boldsymbol{K}^m = \mathop{\mathbin{\mathop{\mathrm{A}}}}_{e=1}^{nel} \boldsymbol{K}_e^m = \mathop{\mathbin{\mathop{\mathrm{A}}}}_{e=1}^{nel} \int_{\Omega_e} (\boldsymbol{B}_e^m)^T \boldsymbol{D}_e^m \boldsymbol{B}_e^m d\Omega, \tag{2.88}$$

$\boldsymbol{F}^m$ the force due to the initial strain as follow:

$$\boldsymbol{F}^m = \mathop{\mathbin{\mathop{\mathrm{A}}}}_{e=1}^{nel} \boldsymbol{f}_e^m = \mathop{\mathbin{\mathop{\mathrm{A}}}}_{e=1}^{nel} \int_{\Omega_e} (\boldsymbol{B}_e^m)^T \boldsymbol{D}_e^m d\Omega, \tag{2.89}$$

and $\boldsymbol{f}_t^m$ is the force due to the thermal expansion due to a unitary temperature change ($\Delta T = 1$) as follow:

$$\boldsymbol{f}_t^m = \mathop{\mathbin{\mathop{\mathrm{A}}}}_{e=1}^{nel} \boldsymbol{f}_{t,e}^m = \mathop{\mathbin{\mathop{\mathrm{A}}}}_{e=1}^{nel} \int_{\Omega_e} (\boldsymbol{B}_e^m)^T \boldsymbol{\beta}_e^m d\Omega. \tag{2.90}$$

Applying the boundary conditions and solving the linear systems presented on the equations 2.86 ans 2.87, the vectors $\boldsymbol{U}^m$ and $\boldsymbol{\varphi}^m$ on the local level are determined.

Since no constraint on topology is imposed on the base cell, the homogenized elasticity

matrix can be anisotropic

$$\boldsymbol{D}^H = \begin{bmatrix} D^H_{1111} & D^H_{1122} & D^H_{1112} \\ D^H_{1122} & D^H_{2222} & D^H_{2212} \\ D^H_{1112} & D^H_{2212} & D^H_{1212} \end{bmatrix}, \tag{2.91}$$

or orthotropic in the case $D^H_{1112} = D^H_{2212} = 0$, and the homogenized thermal stress vector could be represented as

$$\boldsymbol{\beta}^H = \begin{Bmatrix} \beta^H_{11} \\ \beta^H_{22} \\ \beta^H_{12} \end{Bmatrix}. \tag{2.92}$$

Using the matrix formulation on the equations 2.72 and 2.73, the homogenized elasticity matrix D^H and the homogenized thermal stress tensor can be calculated using the equations (Huang *et al.*, 2013; Zuo *et al.*, 2013; Yan *et al.*, 2014; Rodrigues and Fernandes, 1995)

$$\boldsymbol{D}^H = \frac{1}{|\boldsymbol{Y}|}\int_Y \boldsymbol{D}^m \left(I - \boldsymbol{B}^m \boldsymbol{U}^m\right) dy, \tag{2.93}$$

and

$$\boldsymbol{\beta}^H = \frac{1}{|\boldsymbol{Y}|}\int_Y \boldsymbol{D}^m \left(\boldsymbol{\alpha}^m - \boldsymbol{B}^m \boldsymbol{\varphi}^m\right) dy, \tag{2.94}$$

where $\boldsymbol{\alpha}^m$ is the thermal expansion coefficient in the micro-scale given by

$$\boldsymbol{\alpha}^m = (\boldsymbol{D}^m)^{-1}\boldsymbol{\beta}^m. \tag{2.95}$$

2.3.4 Boundary conditions for periodic materials

For two dimensional problems, the micro-scale model related to the equation 2.86 must be solved three times. While the problem stated in the equation 2.87 needs to be solved just one time, because of the isotropy of the local materials. The solution $\boldsymbol{U}^m$ of the equation 2.86, is a three column matrix where the values of the first and second column, correspond to the displacement induced by a unit initial strain in a horizontal and vertical direction, respectively; the third column correspond to the displacement induced by an initial shear strain. The solution $\boldsymbol{\varphi}^m$, of the equation 2.87, is the displacement induced by a thermal strain due to a temperature change equal to one ($\Delta T = 1$).

It is necessary to define the boundary conditions to solve the micro-scale boundary value problems. Considering a base cell with Y-dimensions on the local level y as shown in the figure

2.4, using the main hypothesis of the homogenization method: the periodicity (see equation 2.32) and being the microscopic displacement the Y-periodic solution, it is obtained expression

$$\boldsymbol{U}^m(\boldsymbol{y}) = \boldsymbol{U}^m(\boldsymbol{y} + \boldsymbol{Y}). \tag{2.96}$$

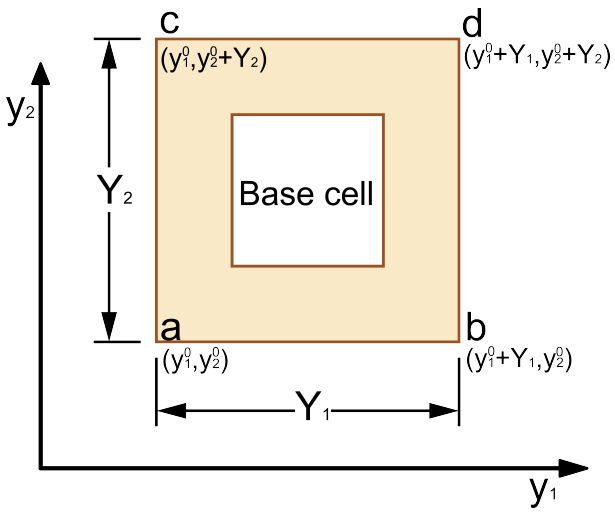

Figure 2.4: Periodic base cell model.

For rectangular base cell as the presented on figure 2.4, with $\boldsymbol{U}_1^m$ and $\boldsymbol{U}_2^m$ being the components of the displacement field $\boldsymbol{U}^m$ in the y_1 and y_2 directions, the periodic displacement boundary conditions can be expressed as

$$\boldsymbol{U}_1^m(y_1^0, y_2) = \boldsymbol{U}_1^m(y_1^0 + Y_1, y_2), \tag{2.97}$$

$$\boldsymbol{U}_2^m(y_1^0, y_2) = \boldsymbol{U}_2^m(y_1^0 + Y_1, y_2), \tag{2.98}$$

$$\boldsymbol{U}_1^m(y_1, y_2^0) = \boldsymbol{U}_1^m(y_1, y_2^0 + Y_2), \tag{2.99}$$

and

$$\boldsymbol{U}_2^m(y_1, y_2^0) = \boldsymbol{U}_2^m(y_1, y_2^0 + Y_2), \tag{2.100}$$

where the equations 2.97 and 2.98 indicate the vertical and horizontal displacement of the sides $\overline{ac}$ and $\overline{bd}$ are the same. Similarly, the equations 2.99 and 2.100 indicate that the vertical and horizontal displacement of the sides $\overline{ab}$ and $\overline{cd}$ are the same.

When the base cell is symmetric, these boundary conditions lead to the symmetric boundary conditions presented in Hassani (1996) and Hassani and Hinton (1998b). For a non-symmetric base cell, the periodic boundary conditions are imposed as multi-point constraints (Yang and Becker, 2004).

This multi-point constraint can be formulated as coordinate transformation using a transformation matrix $\boldsymbol{T}$ (Cook *et al.*, 2001). The matrix $\boldsymbol{T}$, also called condensation matrix, allows the condensation of the degrees of freedom associated to the sides $\overline{cd}$ and $\overline{bd}$ on the degrees of freedom related to the sides $\overline{ab}$ and $\overline{ac}$, respectively.

Due to the condensation, the condensed global system has less degrees of freedom than the initial global system. The condensation matrix is a $N_{GL}x(N_{GL} - N_{ER})$ rectangular matrix , where N_{GL} are the degrees of freedom of the global system and N_{ER} is the number of restriction equations.

It is considered the base cell of the figure 2.4, in order to clarify the condensation matrix construction, where the degrees of freedom associated to the side $\overline{cd}$ (5, 6, 7 and 8) are going to be condensed on the d.o.f related to the side $\overline{ab}$ (1, 2, 3 and 4).The degrees of freedom related to the nodes a, b, c and d are presented in the table 2.1.

Table 2.1: Degrees of freedom (d.o.f) associated to the nodes a, b, c and d.

Node	d.o.f
a	1, 2
b	3, 4
c	5, 6
d	7, 8

The condensation matrix of this problem is the $8x4$ rectangular matrix presented on the equation 2.101, because the number of d.o.f are eight ($N_{GL} = 8$) and the restriction equations are four ($N_{ER} = 4$).

$$\mathbf{T} = \begin{array}{c} \begin{matrix} 1 & 2 & 3 & 4 \end{matrix} \\ \begin{bmatrix} 1 & 0 & 0 & 0 \\ 0 & 1 & 0 & 0 \\ 0 & 0 & 1 & 0 \\ 0 & 0 & 0 & 1 \\ 1 & 0 & 0 & 0 \\ 0 & 1 & 0 & 0 \\ 0 & 0 & 1 & 0 \\ 0 & 0 & 0 & 1 \end{bmatrix} \end{array} \begin{matrix} 1 \\ 2 \\ 3 \\ 4 \\ 5 \\ 6 \\ 7 \\ 8 \end{matrix} \tag{2.101}$$

In the equation 2.101, it can be observed that the degrees of freedom 5, 6, 7 and 8 are condensed on the d.o.f 1, 2, 3 and 4.

The condensed micro-scale problems 2.88 and 2.87 can be estated using the condensation matrix as

$$\widetilde{\boldsymbol{K}^m}\widetilde{\boldsymbol{U}^m} = \widetilde{\boldsymbol{F}^m} \tag{2.102}$$

and

$$\widetilde{\boldsymbol{K}^m}\widetilde{\boldsymbol{\varphi}^m} = \widetilde{\boldsymbol{f}_t^m} \tag{2.103}$$

respectively, where $\widetilde{\boldsymbol{K}}^m$ is the condensed stiffness matrix, $\widetilde{\boldsymbol{F}^m}$ and $\widetilde{\boldsymbol{f}_t^m}$ are the condensed forces, and $\widetilde{\boldsymbol{U}^m}$ and $\widetilde{\boldsymbol{\varphi}^m}$ the condensed solutions, given by

$$\widetilde{\boldsymbol{K}^m} = \boldsymbol{T}^T\boldsymbol{K}^m\boldsymbol{T}, \tag{2.104}$$

$$\widetilde{\boldsymbol{F}^m} = \boldsymbol{T}^T\boldsymbol{F}^m, \tag{2.105}$$

and

$$\widetilde{\boldsymbol{f}_t^m} = \boldsymbol{T}^T\boldsymbol{f}_t^m. \tag{2.106}$$

The solution of the initial system can be calculated as follow:

$$\boldsymbol{U}^m = \boldsymbol{T}\widetilde{\boldsymbol{U}^m} \tag{2.107}$$

and

$$\boldsymbol{\varphi}^m = \boldsymbol{T}\widetilde{\boldsymbol{\varphi}^m}. \tag{2.108}$$

The calculation of the homogenized elasticity matrix ($\boldsymbol{D}^H$) and the homogenized thermal expansion coefficient ($\boldsymbol{\beta}^H$) were implemented considering a mesh of quadrilateral elements of four nodes, and the obtained results were validated from comparisons with benchmark problems of the literature

3 TOPOLOGY OPTIMIZATION FOR MULTI-MATERIAL THERMOELASTIC MULTI-SCALE PROBLEM

In this research, two kinds of optimization problems are studied, in order to get the stiffer structure and a desired property; the first is the topology optimization of a thermo-mechanical structure, the second one a concurrent design of a thermo-mechanical structure, and the third one is the topology optimization of a base cell material. In this chapter is presented the formulation of the optimization problems, the material interpolation schemes used, the sensitivity analysis and the topology optimization method used.

3.1 Thermo-mechanical structure project formulation

The thermo-mechanical structural design problem can be stated as a topology optimization problem. The topology optimization problem consist in find the stiffer structure with a given volume of the M materials, when thermal and mechanical loads occur simultaneously in the structure, where M is the number of material allowed on the design domain. The thermal loads are considered design-dependent body loads, in other words, the thermal loads are dependent on the shape and topology of the structure.

The mean compliance is minimized, in order to get the maximum stiffness, then the optimization problem, with the volume constraint on the M materials phases can be stated as follow:

$$\begin{aligned}
find: \quad & \boldsymbol{X}^M \\
minimize: \quad & C^M = \frac{1}{2}(\boldsymbol{p}^M)^T \boldsymbol{u}^M = \frac{1}{2}\left(\boldsymbol{f}^{M,mec} + \boldsymbol{f}^{M,ter}\right)^T \boldsymbol{u}^M \\
subject \quad to: \quad & V_j^{M,*} - \sum_{i=1}^{N} V_i^M X_{ij}^M - \sum_{i=1}^{j-1} V_i^{M,*} = 0 \quad j = 1, 2, ..., M-1 \\
& \boldsymbol{K}^M \boldsymbol{u}^M = \boldsymbol{f}^{M,mec} + \boldsymbol{f}^{M,ter} \\
& X_{ij}^M = x_{min} \quad \vee \quad 1
\end{aligned} \tag{3.1}$$

where $\boldsymbol{c}^M$ is the mean compliance, $\boldsymbol{p}^M$ the force applied on the structure, $\boldsymbol{f}^{M,mec}$ the mechanical load, $\boldsymbol{f}^{M,ter}$ the thermal load, $\boldsymbol{u}^M$ the displacement vector on macro-scale, M the number of material phases, $V_j^{M,*}$ the prescribed volume for each material j, N is the number of elements, $\boldsymbol{X}^M$ the design variable for the i^{th} element and j^{th} material, and the superscript M indicates that the matrices and vectors are related to the macro-scale.

Using the thermo-mechanical structural design formulation it is possible to find in the macro-scale domain, using two phases (void and material) or M-phase materials configuration, the structural topologies that respect the problem stated in the equation 3.1.

3.2 Formulation of the material design problem (micro-scale design)

It can be stated a topology optimization problem, in order to get a material (micro-structure domain) with a desired thermal expansion when the structure (macro-structure domain) is heating uniformly. In this case, the topology optimization problem consist in find the distribution of the m materials phases on the micro-structural design domain, that maximize or minimize a function of the homogenized vector of the thermal expansion coefficients ($\boldsymbol{\alpha}^H$), using the model of the heterogeneous material described on the chapter 2. In this work the function of the homogenized thermal expansion coefficient chosen was the following:

$$f(\boldsymbol{\alpha}^H) = \alpha_{11}^H + \alpha_{22}^H + \alpha_{12}^H \tag{3.2}$$

Then, the topology optimization problem, for the material design problem, can be stated as follow:

$$\begin{aligned}
find: \quad & \boldsymbol{X}^m \\
minimize: \quad & f(\boldsymbol{\alpha}^H) = \alpha_{11}^H + \alpha_{22}^H + \alpha_{12}^H \\
subject \quad to: \quad & V_l^{m,*} - \sum_{k=1}^{n} V_k^m X_{kl}^M - \sum_{k=1}^{l-1} V_k^{m,*} = 0 \quad l = 1, 2, ..., m-1 \\
& \boldsymbol{K}^m \boldsymbol{U}^m = \boldsymbol{F}^m \\
& \boldsymbol{K}^m \boldsymbol{\varphi}^m = \boldsymbol{f}_t^m \\
& X_{kl}^m = x_{min} \quad \vee \quad 1
\end{aligned} \tag{3.3}$$

where X_{kl}^m is the design variable for the k^{th} element and l^{th} material in the micro-structure (base cell), $V_l^{m,*}$ the prescribed volume for each material l, n the number of elements in the base cell mesh, and the superscript m indicates that the matrices and vectors are related to the micro-scale.

The homogenized vector of the thermal expansion coefficients $\boldsymbol{\alpha}^H$ is given by the relation between the homogenized elasticity matrix ($\boldsymbol{D}^H$) and the homogenized thermal stress vector ($\boldsymbol{\beta}^H$), as

$$\boldsymbol{\alpha}^H = (\boldsymbol{D}^H)^{-1} \boldsymbol{\beta}^H. \tag{3.4}$$

In two dimensional elastic problem, the vector of the thermal expansion coefficients $\boldsymbol{\alpha}^H$ can be written as

$$\boldsymbol{\alpha}^H = \left\{ \begin{array}{c} \alpha_{11} \\ \alpha_{22} \\ \alpha_{12} \end{array} \right\}, \tag{3.5}$$

where α_{11} and α_{22} are the equivalent thermal expansion coefficient of the macro-structural problem in the horizontal and vertical directions, respectively.

3.3 Material interpolation for multiple materials

It is convenient to interpolate the elasticity matrix and the thermal expansion coefficient using the design variables $\boldsymbol{X}^M$ or $\boldsymbol{X}^m$, due to the desired topology is composed of two materials and void. In this sections is presented two different material interpolations based on the solid isotropic material with penalization model (SIMP) (Bendsøe and Sigmund, 1999), the first one considered only two materials and void, and the second one is valid for M or m materials, being M and m the number of desired materials on the macro-scale and micro-scale design domain, respectively.

3.3.1 Material interpolation among two material phases and void

This interpolation used a simple artificial mixture assumption (Sigmund and Torquato, 1997; Luo *et al.*, 2010; Gao and Zhang, 2011; Wang *et al.*, 2016b), where the elasticity matrix D and the vector of the thermal expansion coefficients α for an i^{th} element can be written in terms of the design variables $\boldsymbol{X}^m$ as

$$\boldsymbol{D}_i = (X_{i1}^m)^{p1} \left[(X_{i2}^m)^{p2} \boldsymbol{D}_1 + \left\{ 1 - (X_{i2}^m)^{p2} \right\} \boldsymbol{D}_2 \right], \tag{3.6}$$

and

$$\boldsymbol{\alpha}_i = \left[(X_{i2}^m)^q \boldsymbol{\alpha}_1 + \left\{ 1 - (X_{i2}^m)^q \right\} \boldsymbol{\alpha}_2 \right], \tag{3.7}$$

where the subscripts 1 and 2 indicates that the property are related to the material 1 and material 2, respectively; $p1$, $p2$ and q are the penalization factors. The design variable $X_{i1}^m = x_{min}$ indicate that the element i is void, $X_{i1}^m = 1$ mean that the element i is solid material. If the element i is a solid material, it can be material 1, with $X_{i2}^m = 1$ or material 2 with $X_{i2}^m = x_{min}$.

It can be observed that the thermal expansion coefficient does not depend on the design variable X_{i1}^m, this phenomenon is presented due to once it is chosen the mixture of the materials

phases (X_{i2}^m), the value of the thermal expansion coefficient does not depend on the volume of solid material (Deng *et al.*, 2013).

The material model presented in equations 3.6 and 3.7 can be used directly on micro-scale and in macro-scale models, using $\boldsymbol{X}^m$ for micro-scale and $\boldsymbol{X}^M$ for macro-scale.

3.3.2 Material interpolation for m materials

Huang and Xie (2008) proposed to do the interpolation between two neighboring phases, in order to get a general interpolation, valid for multiple materials. Assuming that the properties of the element i can vary only between the properties of the material phases j and $j+1$, the interpolation can be stated as

$$\boldsymbol{D}_i = (X_{ij}^m)^{pj}\boldsymbol{D}_j + \left\{1-(X_{ij}^m)^{pj}\right\}\boldsymbol{D}_{j+1} \qquad j = 1, 2, ..., m, \tag{3.8}$$

and

$$\boldsymbol{\alpha}_i = (X_{ij}^m)^{qj}\boldsymbol{\alpha}_j + \left\{(1-(X_{ij}^m)^{qj}\right\}\boldsymbol{\alpha}_{j+1} \qquad j = 1, 2, ..., m, \tag{3.9}$$

where m is the number of material phases, $X_{ij}^m = 1$ and $X_{ij}^m = x_{min}$ indicates that the element i^{th} is made of the material j^{th} or material $j+1^{th}$, respectively.

To use this interpolation for the M material phases of the macro-scale model, it is necessary to use the design variable of the macro-scale ($\boldsymbol{X}_{ij}^M$) instead of the micro-scale design variable ($\boldsymbol{X}_{ij}^m$)

3.4 Bi-directional Evolutionary Topology Optimization method

The Bi-directional Evolutionary Structural Optimization (BESO) is the numerical method used in this work to solve the topology optimization problem described above. The BESO method is an evolutionary design method that allows the material to be added as well as to be removed to modify the topology (Yang *et al.*, 1999).

The criterion of addition and remotion of material is based on the sensitivity analysis. The sensitivity analysis is an estimative of the structural response when the design variables are modified, this estimative is based on the calculation of the derivatives (Paris *et al.*, 2010). In this section is presented the sensitivity analysis for the topology optimization problems, a brief description of the BESO method procedure and the used parameters.

3.4.1 Sensitivity numbers analysis for multi-scale thermo-elasticity problems

In the BESO method, the sensitivity number, $\boldsymbol{SN}^M$ for macro-scale and $\boldsymbol{sn}^m$ for micro-scale, denote a relative ranking of the elemental sensitivities, and it is used to update the design variables. In this section is presented the sensitivity number for the two thermo-elastic design problems presented in this work.

- **Sensitivity number for the thermo-mechanical structure design problem (macro-scale design)** For the thermo-mechanical structure design problem, the sensitivity number can be found by the gradient of the objective function $\boldsymbol{c}$, given by the equation 3.1, with respect to the design variables X_{ij}^M in the macro-scale (Gao and Zhang, 2010), as

$$SN_{ij}^M = \frac{\partial C^M}{\partial X_{ij}^M}. \tag{3.10}$$

It is necessary to use the adjoint variable method, In order to calculate the sensitivity number given by the equation 3.10. Then the sensitivity number can be calculated as

$$SN_{ij}^M = \frac{\partial}{\partial X_{ij}^M}\left(-\frac{1}{2}\left(\boldsymbol{p}^M\right)^T \boldsymbol{u}^M\right) + \boldsymbol{\lambda}^T \frac{\partial}{\partial X_{ij}^M}\left(\boldsymbol{K}^M \boldsymbol{u}^M - \boldsymbol{p}^M\right). \tag{3.11}$$

Deriving with respect to the design variable on the macro-scale X_{ij}^M, the equation 3.11 yields

$$\begin{aligned} SN_{ij}^M = &-\frac{1}{2}\left(\frac{\partial \boldsymbol{p}^M}{\partial X_{ij}^M}\right)^T \boldsymbol{u}^M - \frac{1}{2}\left(\frac{\partial \boldsymbol{u}^M}{\partial X_{ij}^M}\right)^T \boldsymbol{p}^M + \\ &\boldsymbol{\lambda}^T \frac{\partial \boldsymbol{K}^M}{\partial X_{ij}^M}\boldsymbol{u}^M + \left(\frac{\partial \boldsymbol{u}^M}{\partial X_{ij}^M}\right)^T \boldsymbol{K}^M \boldsymbol{\lambda} + \boldsymbol{\lambda}^T \frac{\partial \boldsymbol{p}^M}{\partial X_{ij}^M}, \end{aligned} \tag{3.12}$$

where the derivative of the total force $\boldsymbol{p}^M$ is given by

$$\frac{\partial \boldsymbol{p}^M}{\partial X_{ij}^M} = \frac{\partial \boldsymbol{f}^{M,ter}}{\partial X_{ij}^M} + \frac{\partial \boldsymbol{f}^{M,mec}}{\partial X_{ij}^M}, \tag{3.13}$$

and due to the mechanical load $\boldsymbol{f}^M$ does not have any dependence on the design variable X_{ij}^M, it can be stated that

$$\frac{\partial \boldsymbol{f}^M}{\partial X_{ij}^M} = 0. \tag{3.14}$$

Substituting the equation 3.14 into equation 3.13, equation 3.13 into 3.12 and reorganized

the terms, yields

$$SN_{ij}^{M} = -\frac{1}{2}\left(\frac{\partial \boldsymbol{f}^{M,ter}}{\partial X_{ij}^{M}}\right)^{T}\boldsymbol{u}^{M} + \left(\frac{\partial \boldsymbol{u}^{M}}{\partial X_{ij}^{M}}\right)^{T}\left(-\frac{1}{2}\boldsymbol{p}^{M} + \boldsymbol{K}^{M}\boldsymbol{\lambda}\right) + \boldsymbol{\lambda}^{T}\frac{\partial \boldsymbol{K}^{M}}{\partial X_{ij}^{M}}\boldsymbol{u}^{M} - \boldsymbol{\lambda}^{T}\frac{\partial \boldsymbol{f}^{M,ter}}{\partial X_{ij}^{M}}. \tag{3.15}$$

The following equation must be satisfied, in order to avoid the calculation of the derivative of the displacement field on the macro-scale ($\boldsymbol{u}^{M}$), with respect to the design variable X_{ij}^{M}

$$-\frac{1}{2}\boldsymbol{p}^{M} + \boldsymbol{K}^{M}\boldsymbol{\lambda} = 0. \tag{3.16}$$

Comparing the equation 3.16 with the equilibrium equation on macro-scale 2.29, it can be stated that

$$\boldsymbol{\lambda} = \frac{1}{2}\boldsymbol{u}^{M}. \tag{3.17}$$

Substituting the equation 3.17 into 3.15, it is obtained the sensitivity number for the thermo-mechanical structure design problem, as

$$SN_{ij}^{M} = -\left(\frac{\partial \boldsymbol{f}^{M,ter}}{\partial X_{ij}^{M}}\right)^{T}\boldsymbol{u}^{M} + \frac{1}{2}\left(\boldsymbol{u}^{M}\right)^{T}\frac{\partial \boldsymbol{K}^{M}}{\partial X_{ij}^{M}}\boldsymbol{u}^{M}, \tag{3.18}$$

where $\boldsymbol{K}^{M}$ is the stiffness matrix given by the equation 2.30, $\boldsymbol{f}^{M,ter}$ is the thermal force given by the equation 2.31 and $\boldsymbol{u}^{M}$ is the displacement vector. Then, the derivative of the stiffness matrix and the thermal force are given by equations 3.19 and 3.20, respectively.

$$\frac{\partial \boldsymbol{K}^{M}}{\partial X_{ij}^{M}} = \int_{\Omega}(\boldsymbol{B}^{M})^{T}\frac{\partial \boldsymbol{D}^{M}}{\partial X_{ij}^{M}}\boldsymbol{B}^{M}d\Omega. \tag{3.19}$$

$$\frac{\partial \boldsymbol{f}^{M,ter}}{\partial X_{ij}^{M}} = \int_{\Omega}(\boldsymbol{B}^{M})^{T}\left(\frac{\partial \boldsymbol{D}^{M}}{\partial X_{ij}^{M}}\boldsymbol{\alpha}^{M} + \boldsymbol{D}^{M}\frac{\partial \boldsymbol{\alpha}^{M}}{\partial X_{ij}^{M}}\right)\Delta T d\Omega. \tag{3.20}$$

Using plane stress assumption and the general material interpolation described in chapter 3.3.2, the therms $\boldsymbol{D}^{M}$ and $\boldsymbol{\alpha}^{M}$ for each element i, in the macro-scale domain, are given by the following equations:

$$\boldsymbol{D}^{M} = (X_{ij}^{M})^{P_j}\boldsymbol{D}_{j}^{H} + \left\{1 - (X_{ij}^{M})^{P_j}\right\}\boldsymbol{D}_{j+1}^{H} \qquad j = 1, 2, ..., M \tag{3.21}$$

$$\boldsymbol{\alpha}^{M} = (X_{ij}^{M})^{Q_j}\boldsymbol{\alpha}_{j}^{H} + \left\{1 - (X_{ij}^{M})^{Q_j}\right\}\boldsymbol{\alpha}_{j+1}^{H} \qquad j = 1, 2, ..., M \tag{3.22}$$

where P_j and Q_j are the penalization factors for the material model in macro-scale do-

main.

Equation 3.23 and equation 3.24 are the derivatives with respect to the design variable X_{ij}^{M} of the equation 3.21 and equation 3.22, respectively.

$$\frac{\partial \boldsymbol{D}^{M}}{\partial X_{ij}^{M}} = P_j (X_{ij}^{M})^{(P_j-1)} (\boldsymbol{D}_j^{H} - \boldsymbol{D}_{j+1}^{H}) \quad j = 1, 2, ..., M. \tag{3.23}$$

$$\frac{\partial \boldsymbol{\alpha}^{M}}{\partial X_{ij}^{M}} = Q_j (X_{ij}^{M})^{(Q_j-1)} (\boldsymbol{\alpha}_j^{H} - \boldsymbol{\alpha}_{j+1}^{H}) \quad j = 1, 2, ..., M. \tag{3.24}$$

Using equation 3.18 to equation 3.24, it is possible to calculate the sensitivity number for each element for the macro-scale problem. The calculated sensitivity number is ranked to evaluate which element will be removed and which will be added to the structure domain, using BESO procedure (Huang and Xie, 2010).

- **Material design problem (micro-scale design)**

For the material design, the derivative of the homogenized thermal expansion coefficient is necessary. The derivative of the the equation 3.4 with respect to the design variable in the micro-scale (X_{kl}^{m}), is

$$\frac{\partial \boldsymbol{\alpha}^{H}}{\partial X_{kl}^{m}} = (\boldsymbol{D}^{H})^{-1} \left(\frac{\partial \boldsymbol{\beta}^{H}}{\partial X_{kl}^{m}} - \frac{\partial \boldsymbol{D}^{H}}{\partial X_{kl}^{m}} \boldsymbol{\alpha}^{H} \right), \tag{3.25}$$

where the derivatives of the homogenized tensors $\frac{\partial \boldsymbol{D}^{H}}{\partial X_{kl}^{m}}$ and $\frac{\partial \boldsymbol{\beta}^{H}}{\partial X_{kl}^{m}}$, for any lth material phase, are calculated using the adjoint variable method (Huang *et al.*, 2013). The main advantage of this approach is the elimination of the required derivatives of the displacements $\boldsymbol{U}^{m}$ and $\boldsymbol{\varphi}$. The equations 2.86 and 2.87 can be rewritten as a residual equation as follow:

$$\boldsymbol{R}_U = \int_Y (\boldsymbol{B}^{m})^T \boldsymbol{D}^{m} dy - \boldsymbol{K}^{m} \boldsymbol{U}^{m} = \frac{1}{|Y|} \int_Y (\boldsymbol{B}^{m})^T \boldsymbol{D}^{m} dy - \frac{1}{|Y|} \boldsymbol{K}^{m} \boldsymbol{U}^{m} = 0, \tag{3.26}$$

and

$$\boldsymbol{R}_\varphi = \int_Y (\boldsymbol{B}^{m})^T \boldsymbol{\beta}^{m} dy - \boldsymbol{K}^{m} \boldsymbol{\varphi}^{m} = \frac{1}{|Y|} \int_Y (\boldsymbol{B}^{m})^T \boldsymbol{D}^{m} \boldsymbol{\alpha}^{m} dy - \frac{1}{|Y|} \boldsymbol{K}^{m} \boldsymbol{\varphi}^{m} = 0, \tag{3.27}$$

where $|Y|$ is the base cell volume and the superscript m indicates that the properties are related to the micro-scale. The derivatives of the equations 3.26 and 3.27 with respect to de design variable are

$$\frac{\partial \boldsymbol{R}_U}{\partial X_{kl}^{m}} = \frac{1}{|Y|} \int_Y (\boldsymbol{B}^{m})^T \frac{\partial \boldsymbol{D}^{m}}{\partial X_{kl}^{m}} dy - \frac{1}{|Y|} \frac{\partial K^{m}}{\partial X_{kl}^{m}} \boldsymbol{U}^{m} - \frac{1}{|Y|} \boldsymbol{K}^{m} \frac{\partial \boldsymbol{U}^{m}}{\partial X_{kl}^{m}} \tag{3.28}$$

and

$$\frac{\partial \boldsymbol{R}_{\varphi}}{\partial X_{kl}^{m}} = \frac{1}{|Y|}\int_{Y}(\boldsymbol{B}^{m})^{T}\frac{\partial \boldsymbol{D}^{m}}{\partial X_{kl}^{m}}\boldsymbol{\alpha}^{m}dy + \frac{1}{|Y|}\int_{Y}(\boldsymbol{B}^{m})^{T}\boldsymbol{D}^{m}\frac{\partial \boldsymbol{\alpha}^{m}}{\partial X_{kl}^{m}}dy - \frac{1}{|Y|}\frac{\partial \boldsymbol{K}^{m}}{\partial X_{kl}^{m}}\boldsymbol{\varphi}^{m} - \frac{1}{|Y|}\boldsymbol{K}^{m}\frac{\partial \boldsymbol{\varphi}^{m}}{\partial X_{kl}^{m}}. \tag{3.29}$$

Substituting the equation 2.88 into the equations 3.28 and 3.29, it is obtained

$$\frac{\partial \boldsymbol{R}_{U}}{\partial X_{kl}^{m}} = \frac{1}{|Y|}\int_{Y}(\boldsymbol{B}^{m})^{T}\frac{\partial \boldsymbol{D}^{m}}{\partial X_{kl}^{m}}(\boldsymbol{I} - \boldsymbol{B}^{m}\boldsymbol{U}^{m})dy - \frac{1}{|Y|}\int_{Y}(\boldsymbol{B}^{m})^{T}\boldsymbol{D}^{m}\boldsymbol{B}^{m}dy\frac{\partial \boldsymbol{U}^{m}}{\partial X_{kl}^{m}} \tag{3.30}$$

and

$$\frac{\partial \boldsymbol{R}_{\varphi}}{\partial X_{kl}^{m}} = \frac{1}{|Y|}\int_{Y}(\boldsymbol{B}^{m})^{T}\frac{\partial \boldsymbol{D}^{m}}{\partial X_{kl}^{m}}(\boldsymbol{\alpha}^{m} - \boldsymbol{B}^{m}\boldsymbol{\varphi}^{m})dy + \frac{1}{|Y|}\int_{Y}(\boldsymbol{B}^{m})^{T}\boldsymbol{D}^{m}\frac{\partial \alpha_{kl}^{m}}{\partial X_{kl}^{m}}dy - \frac{1}{|Y|}\int_{Y}(\boldsymbol{B}^{m})^{T}\boldsymbol{D}^{m}\boldsymbol{B}^{m}dy\frac{\partial \boldsymbol{\varphi}^{m}}{\partial X_{kl}^{m}}. \tag{3.31}$$

A matrix of Lagrange multipliers can be multiplied by the residual equation and added to the equations 2.72 and 2.94 without modifying the result as

$$\boldsymbol{D}^{H} = \frac{1}{|Y|}\int_{Y}\boldsymbol{D}^{m}(\boldsymbol{I} - \boldsymbol{B}^{m}\boldsymbol{U}^{m})dy + \boldsymbol{\lambda}^{T}\underbrace{\left(\frac{1}{|Y|}\int_{Y}(\boldsymbol{B}^{m})^{T}\boldsymbol{D}^{m}dy - \frac{1}{|Y|}\boldsymbol{K}^{m}\boldsymbol{U}^{m}\right)}_{\boldsymbol{R}_{U}} \tag{3.32}$$

and

$$\boldsymbol{\beta}^{H} = \frac{1}{|Y|}\int_{Y}\boldsymbol{D}^{m}(\boldsymbol{\alpha}^{m} - \boldsymbol{B}^{m}\boldsymbol{\varphi}^{m})dy + \boldsymbol{\lambda}^{T}\underbrace{\left(\frac{1}{|Y|}\int_{Y}(\boldsymbol{B}^{m})^{T}\boldsymbol{D}^{m}\boldsymbol{\alpha}^{m}dy - \frac{1}{|Y|}\boldsymbol{K}^{m}\boldsymbol{\varphi}^{m}\right)}_{\boldsymbol{R}_{\varphi}}. \tag{3.33}$$

Due to the residual equation is equal to zero, the equations 3.32 and 3.33 are true for any value of $\boldsymbol{\lambda}$.

Deriving the equations 3.32 and 3.33 with respect to the design variable $\boldsymbol{X}^{m}$, they are obtained the following equations

$$\frac{\partial \boldsymbol{D}^{H}}{\partial X_{kl}^{m}} = \frac{1}{|Y|}\int_{Y}\frac{\partial \boldsymbol{D}^{m}}{\partial X_{kl}^{m}}(\boldsymbol{I} - \boldsymbol{B}^{m}\boldsymbol{U}^{m})dy - \frac{1}{|Y|}\int_{Y}\boldsymbol{D}^{m}\boldsymbol{B}^{m}\frac{\partial \boldsymbol{U}^{m}}{\partial X_{kl}^{m}}dy + \boldsymbol{\lambda}^{T}\left(\frac{1}{|Y|}\int_{Y}(\boldsymbol{B}^{m})^{T}\frac{\partial \boldsymbol{D}^{m}}{\partial X_{kl}^{m}}(\boldsymbol{I} - \boldsymbol{B}^{m}\boldsymbol{U}^{m})dy - \frac{1}{|Y|}\int_{Y}(\boldsymbol{B}^{m})^{T}\boldsymbol{D}^{m}\boldsymbol{B}^{m}dy\frac{\partial \boldsymbol{U}^{m}}{\partial X_{kl}^{m}}\right) \tag{3.34}$$

and

$$\frac{\partial \boldsymbol{\beta}^H}{\partial X_{kl}^m} = \frac{1}{|Y|}\int_Y \frac{\partial \boldsymbol{D}^m}{\partial X_{kl}^m}(\boldsymbol{\alpha}^m - \boldsymbol{B}^m\boldsymbol{\varphi}^m)dy + \frac{1}{|Y|}\int_Y \boldsymbol{D}^m\frac{\partial \boldsymbol{\alpha}^m}{\partial X_{kl}^m}dy$$
$$-\frac{1}{|Y|}\int_Y \boldsymbol{D}^m\boldsymbol{B}^m\frac{\partial \boldsymbol{\varphi}^m}{\partial X_{kl}^m}dy + \boldsymbol{\lambda}^T\left(\frac{1}{|Y|}\int_Y (\boldsymbol{B}^m)^T\frac{\partial \boldsymbol{D}^m}{\partial X_{kl}^m}(\boldsymbol{\alpha}^m - \boldsymbol{B}^m\boldsymbol{\varphi}^m)dy\right) \quad (3.35)$$
$$+\boldsymbol{\lambda}^T\left(\frac{1}{|Y|}\int_Y (\boldsymbol{B}^m)^T\boldsymbol{D}^m\frac{\partial \boldsymbol{\alpha}^m}{\partial X_{kl}^m}dy - \frac{1}{|Y|}\int_Y (\boldsymbol{B}^m)^T\boldsymbol{D}^m\boldsymbol{B}^m dy\frac{\partial \boldsymbol{\varphi}^m}{\partial X_{kl}^m}\right),$$

reorganizing the therms on the equations 3.34 and 3.36, yields:

$$\frac{\partial \boldsymbol{D}^H}{\partial X_{kl}^m} = \frac{1}{|Y|}\int_Y (\boldsymbol{I} + \boldsymbol{B}^m\boldsymbol{\lambda})^T\frac{\partial \boldsymbol{D}^m}{\partial X_{kl}^m}(\boldsymbol{I} - \boldsymbol{B}^m\boldsymbol{U}^m)dy \quad (3.36)$$
$$-\frac{1}{|Y|}\left(\int_Y \boldsymbol{D}^m\boldsymbol{B}^m dy + \boldsymbol{\lambda}^T\int_Y (\boldsymbol{B}^m)^T\boldsymbol{D}^m\boldsymbol{B}^m dy\right)\frac{\partial \boldsymbol{U}^m}{\partial X_{kl}^m}$$

and

$$\frac{\partial \boldsymbol{\beta}^H}{\partial X_{kl}^m} = \frac{1}{|Y|}\int_Y (\boldsymbol{I} + \boldsymbol{\lambda}\boldsymbol{B}^m)^T\frac{\partial \boldsymbol{D}^m}{\partial X_{kl}^m}(\boldsymbol{\alpha}^m - \boldsymbol{B}^m\boldsymbol{\varphi}^m)dy +$$
$$\frac{1}{|Y|}\int_Y (\boldsymbol{I} + \boldsymbol{\lambda}\boldsymbol{B}^m)^T\boldsymbol{D}^m\frac{\partial \boldsymbol{\alpha}^m}{\partial X_{kl}^m}dy \quad (3.37)$$
$$-\frac{1}{|Y|}\left(\int_Y \boldsymbol{D}^m\boldsymbol{B}^m dy + \boldsymbol{\lambda}^T\int_Y (\boldsymbol{B}^m)^T\boldsymbol{D}^m\boldsymbol{B}dy\right)\frac{\partial \boldsymbol{\varphi}^m}{\partial X_{kl}^m}.$$

In order to eliminate the therms $\frac{\partial \boldsymbol{U}^m}{\partial X_{kl}^m}$ and $\frac{\partial \boldsymbol{\varphi}^m}{\partial X_{kl}^m}$, the Lagrange multipliers must be satisfy the following equality: Lagrange multipliers must be satisfy the following equality:

$$\int_Y \boldsymbol{D}^m b dy + \boldsymbol{\lambda}^T\int_Y (\boldsymbol{B}^m)^T\boldsymbol{D}^m\boldsymbol{B}^m dy = 0 \quad (3.38)$$

rearranging the terms, yields:

$$\int_Y (\boldsymbol{B}^m)^T\boldsymbol{D}^m\boldsymbol{B}^m dy\boldsymbol{\lambda} = -\int_Y \boldsymbol{D}^m\boldsymbol{B}^m dy, \quad (3.39)$$

and comparing the equation 3.39 with the equation 2.82 can be stated the follow:

$$\boldsymbol{\lambda} = -\boldsymbol{U}^m. \quad (3.40)$$

Substituting the value of $\boldsymbol{\lambda}$ on the equations 3.37 and 3.38, yields:

$$\frac{\partial \boldsymbol{D}^H}{\partial X_{kl}^m} = \frac{1}{|Y|}\int_Y (\boldsymbol{I} - \boldsymbol{B}^m\boldsymbol{U}^m)^T\frac{\partial \boldsymbol{D}^m}{\partial X_{kl}^m}(\boldsymbol{I} - \boldsymbol{B}^m\boldsymbol{U}^m)dy \quad (3.41)$$

and

$$\frac{\partial \boldsymbol{\beta}^H}{\partial X_{kl}^m} = \frac{1}{|Y|}\int_Y (\boldsymbol{I} - \boldsymbol{B}^m\boldsymbol{U}^m)^T \frac{\partial \boldsymbol{D}^m}{\partial X_{kl}^m}(\boldsymbol{\alpha}^m - \boldsymbol{B}^m\boldsymbol{\varphi}^m)dy + \frac{1}{|Y|}\int_Y (\boldsymbol{I} - \boldsymbol{B}^m\boldsymbol{U}^m)^T \boldsymbol{D}^m \frac{\partial \boldsymbol{\alpha}^m}{\partial X_{kl}^m} dy \tag{3.42}$$

Using the equations 3.41 and 3.42, it is possible to calculate the derivative of the homogenized thermal expansion coefficient $\frac{\partial \boldsymbol{\alpha}^H}{\partial X_{kl}^m}$ by the equation 3.25.

3.4.2 Validation of the derivatives of the homogenized properties

The derivative of the homogenized properties $\boldsymbol{D}^H$ and $\boldsymbol{\beta}^H$ is verified using the Taylor series check. The goal is to verify if the difference between the exact solution and the approximated solution presents the order of quadratic convergence.

$$\underbrace{\boldsymbol{D}^H(\boldsymbol{X} + \Delta\boldsymbol{X})}_{real \quad solution} = \underbrace{\boldsymbol{D}^H(\boldsymbol{X}) + \frac{\partial \boldsymbol{D}^H(\boldsymbol{X})}{\partial \boldsymbol{X}}\Delta\boldsymbol{X}}_{aproximate \quad solution} + \underbrace{\boldsymbol{C}\Delta\boldsymbol{X}^n}_{quadratic \quad order}, \tag{3.43}$$

where $\boldsymbol{X}$ is the design variable, and $\Delta\boldsymbol{X}$ a perturbation.

In order to clarify the calculation of the variable order of quadratic convergence n, the following quadratic manipulations are made:

$$\boldsymbol{D}^H(\boldsymbol{X} + \Delta\boldsymbol{X}) - \left[\boldsymbol{D}^H(\boldsymbol{X}) + \frac{\partial \boldsymbol{D}^H(\boldsymbol{X})}{\partial \boldsymbol{X}}\Delta\boldsymbol{X}\right] = \boldsymbol{C}\Delta\boldsymbol{X}^n \tag{3.44}$$

$$||\boldsymbol{D}^H(\boldsymbol{X} + \Delta\boldsymbol{X}) - \left[\boldsymbol{D}^H(\boldsymbol{X}) + \frac{\partial \boldsymbol{D}^H(\boldsymbol{X})}{\partial \boldsymbol{X}}\Delta\boldsymbol{X}\right]|| = |\boldsymbol{C}|||\Delta\boldsymbol{X}^n|| \tag{3.45}$$

$$log\left(||\boldsymbol{D}^H(\boldsymbol{X} + \Delta\boldsymbol{X}) - \left[\boldsymbol{D}^H(\boldsymbol{X}) + \frac{\partial \boldsymbol{D}^H(\boldsymbol{X})}{\partial \boldsymbol{X}}\Delta\boldsymbol{X}\right]||\right) = log\left(|\boldsymbol{C}|\right) + nlog(||\Delta\boldsymbol{X}||) \tag{3.46}$$

- for $\Delta\boldsymbol{X}_1$

$$log\left(||\boldsymbol{D}^H(\boldsymbol{X} + \Delta\boldsymbol{X}_1) - \left[\boldsymbol{D}^H(\boldsymbol{X}) + \frac{\partial \boldsymbol{D}^H(\boldsymbol{X})}{\partial \boldsymbol{X}}\Delta\boldsymbol{X}_1\right]||\right) = log\left(|\boldsymbol{C}|\right) + nlog(||\Delta\boldsymbol{X}_1||) \tag{3.47}$$

- for $\Delta \boldsymbol{X}_2$

$$log\left(||\boldsymbol{D}^H(\boldsymbol{X}+\Delta\boldsymbol{X}_2)-\left[\boldsymbol{D}^H(\boldsymbol{X})+\frac{\partial \boldsymbol{D}^H(\boldsymbol{X})}{\partial \boldsymbol{X}}\Delta\boldsymbol{X}_2\right]||\right)=log\left(|\boldsymbol{C}|\right)+nlog(||\Delta\boldsymbol{X}_2||). \tag{3.48}$$

The equation 3.47 is subtracting from the equation 3.48,in order to eliminate the therm $log\left(|\boldsymbol{C}|\right)$. Then the variable n can be obtained as:

$$a=log\left(||\boldsymbol{D}^H(\boldsymbol{X}+\Delta\boldsymbol{X}_2)-\left[\boldsymbol{D}^H(\boldsymbol{X})+\frac{\partial \boldsymbol{D}^H(\boldsymbol{X})}{\partial \boldsymbol{X}}\Delta\boldsymbol{X}_2\right]||\right) \tag{3.49}$$

$$b=log\left(||\boldsymbol{D}^H(\boldsymbol{X}+\Delta\boldsymbol{X}_1)-\left[\boldsymbol{D}^H(\boldsymbol{X})+\frac{\partial \boldsymbol{D}^H(\boldsymbol{X})}{\partial \boldsymbol{X}}\Delta\boldsymbol{X}_1\right]||\right) \tag{3.50}$$

$$c=log(\Delta\boldsymbol{X}_2)-log(\Delta\boldsymbol{X}_1) \tag{3.51}$$

$$n=\frac{a-b}{c} \tag{3.52}$$

The tables 3.1 and 3.2 present the quadratic convergence order for some design variables $\boldsymbol{X}^m$, validating the derivatives of the homogenized properties $\boldsymbol{D}^H$ and $\boldsymbol{\beta}^H$ using a mesh of 3×3 four node plane stress elements and perturbations $\Delta\boldsymbol{X}_1=1\times10^{-5}*\boldsymbol{X}^m$ and $\Delta\boldsymbol{X}_2=1\times10^{-6}*\boldsymbol{X}^m$

Table 3.1: Convergence test results for $\boldsymbol{D}^H$

Design variable	n
$(\boldsymbol{X}^m)^T=\begin{bmatrix}1&1&1&1&1&1&1&1&1\\1&1&1&1&1&1&1&1&1\end{bmatrix}$	2.0001
$(\boldsymbol{X}^m)^T=\begin{bmatrix}1&1&1&1&1&1&1&1&1\\1&x_{min}&x_{min}&x_{min}&x_{min}&x_{min}&x_{min}&x_{min}&x_{min}\end{bmatrix}$	2.0009

Table 3.2: Convergence test results for $\boldsymbol{\beta}^H$

Design variable	n
$(\boldsymbol{X}^m)^T=\begin{bmatrix}1&1&1&1&1&1&1&1&1\\1&1&1&1&1&1&1&1&1\end{bmatrix}$	2.0000
$(\boldsymbol{X}^m)^T=\begin{bmatrix}1&1&1&1&1&1&1&1&1\\1&x_{min}&x_{min}&x_{min}&x_{min}&x_{min}&x_{min}&x_{min}&x_{min}\end{bmatrix}$	1.9997

The Taylor check results presented on the tables 3.1 and 3.2 was made using a mesh of

3×3 plane stress elements, and between the material phase 1 ($X_{k1}^m = 1$ and $X_{k2}^m = 1$) and material phase 2 ($X_{k1}^m = 1$ and $X_{k2}^m = x_{min}$).

3.5 Description of the BESO method and used parameters

The multi-scale topology optimization method using multiple materials starts discretized the design domains (on the macro-scale, micro-scale or both). The optimization procedure uses an initial volume of 100% of the material 1 on macro-scale. It is necessary a discontinuity in the micro-scale,in order to get a displacement field that allows the calculation of the sensitivity number. This work uses a mesh of 100×100 bilinear isoparametric four node plane stress elements on the micro-scale, where the four central nodes of the whole design domain are the material phase 2 and the others are the material phase 1. The figure 3.1 is presented to illustrate the initial distribution of the material 1 and material 2 in the base cell for a mesh of 4×4 elements.

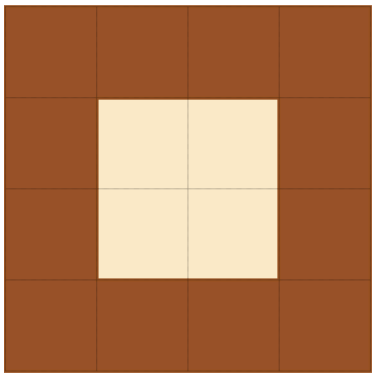

Figure 3.1: Initial distribution of the material in the base cell

Using the discretization it is solved the finite element equilibrium equations on macro-scale (equation 2.29) and on micro-scale (equations 2.86 and 2.87), obtaining the displacement field which is used to calculate the sensitivity numbers as presented on section 3.4.1.

3.5.1 Filter scheme for BESO method and stabilizing the evolutionary problem

A filtering scheme is introduced into the BESO method, in order to avoid the checkerboard patterns and the mesh-dependency problems. The procedure consists of two steps: calculate the sensitivity numbers of each node using the sensitivity number of the neighboring elements and convert this nodal sensitivity numbers into smoothed elemental sensitivity numbers, as

described in detail by Huang and Xie (2010).

The nodal sensitivity numbers SN^n do not have a real physical meaning and can be calculated by averaging the sensitivity numbers of the elements connected to each node as follow:

$$SN_j^n = \frac{\sum_{i=1}^{N_n} SN_i^e}{N_n}, \tag{3.53}$$

where N_n are the elements connected to the jth node. The equation 3.53 is valid only when all the elements on the design domain are equal. The figure 3.2(a) shows the nodes 1 and 2, it can be observed that the node 1 has four neighboring elements and the node 2 has only one, then the nodal sensitivity number of the node 2 is equal to the sum of the sensitivity numbers of the four neighboring elements divided by four, while the nodal sensitivity number for the node 1 is equal to the sensitivity number of the element 1.

It is necessary to identify the nodes that will influence the sensitivity number of an e^{th} element, to convert the nodal sensitivity number into smoothed elemental sensitivity numbers. As shown in figure 3.2(b), a circular sub-domain of radius r_{min} is projected from the center of the eth element. The nodal sensitivities of every node inside the circular domain are considered into the calculation of the smoothed sensitivity number of the eth element, and their contributions depend on the distance between the center of the element e and every node $j(r_{ej})$.

Using the distance r_{ej}, it is possible to define a weight factor ω_{ej} as

$$\omega_{ej} = \begin{cases} \frac{r_{ej}}{\sum_{k=1}^{L} r_{ek}} & r_{ej} \leq r_{min} \\ 0 & r_{ej} > r_{min} \end{cases}, \tag{3.54}$$

where L is the number of nodes inside the circular sub-domain or ratio r_{min}. Then, the smoothed sensitivity number can be calculated using

$$\widetilde{SN}^e = \frac{\sum_{j=1}^{k} \omega_{ej} SN_j^n}{\sum_{j=1}^{k} \omega_{ej}}, \tag{3.55}$$

where k is the total number of nodes in the circle of radius r_{min}.

The presented filter scheme solves the problems of mesh and checkerboard dependency; however, the objective function and the topology may not converge smoothly, this is because in the BESO method discrete project variables (x_{min} and 1) are used to indicate the remotion or addition of elements from the design domain. To reduce the variation of the objective function,

Huang and Xie (2007) proposed to make a historical average of the number of sensitive as

$$SN_e = \frac{SN_e^k + SN_e^{k-1}}{2}, \tag{3.56}$$

where k is the current iteration number.

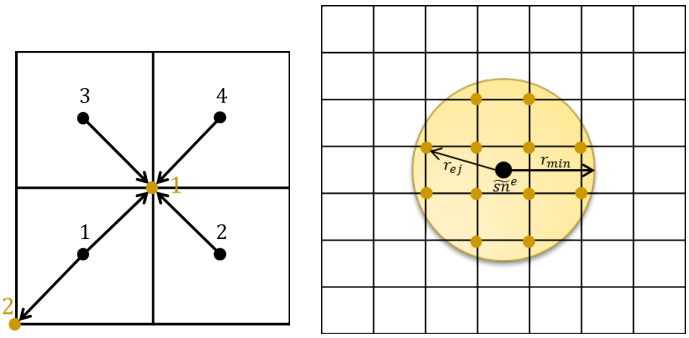

(a) (b)

Figure 3.2: Filter scheme (a) node connectivity; (b) filter radio.

3.5.2 Volume constraint and convergence criterion for BESO method

The BESO is an iterative procedure, where the volume of the materials change throughout the iteration until the desired volume V_f is reached. It is necessary the calculation of the volume for the next iteration $k+1$, due to the iteration procedure. To calculate this volume it is necessary to analyze three possible cases:

- **Case 1** If the volume of the current iteration k is greater than the prescribed volume V_f, an amount greater than ERV_k (see figure 3.3(a)), being ER the evolutionary ratio, which is defined as an input parameter of the optimization algorithm. The volume of the iteration $k+1$ is calculated as follows:

$$V_{k+1} = V_K(1 - ER) \tag{3.57}$$

- **Case 2** If the prescribed volume V_f is greater than the volume of the current iteration V_k, an amount equal o greater than ERV_k (see figure 3.3(b)). The volume of the iteration $k+1$ is calculated as follows:

$$V_{k+1} = V_f \tag{3.58}$$

The volume addition ratio AR, is an input parameter of the optimization procedure, introduced with the purpose of limiting the amount of material to be added to each iteration.

In order to verify the convergence of the evolutionary process, the stopped criterion shown in the equation 3.59 must be satisfied to finalize the optimization algorithm.

$$\frac{|\sum_{i=1}^{N} F_{k-i-1} - \sum_{i=1}^{N} F_{k-N-i-1}|}{\sum_{i=1}^{N} F_{k-i-1}} \leq \tau, \tag{3.59}$$

where k is the current iteration, F is the objective function, τ the convergence tolerance and N is an integer number defined as an input of the optimization algorithm. For the numerical results $N = 5$ is used as shown in the figure 3.4.

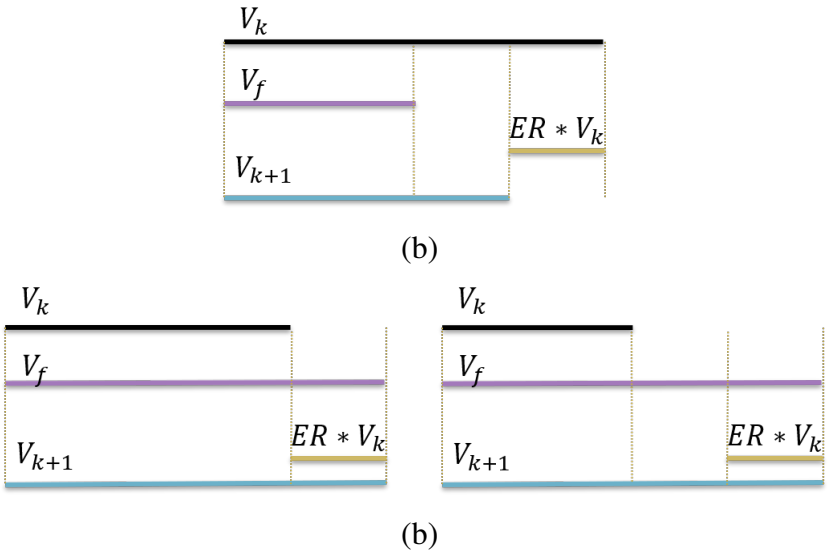

Figure 3.3: Volume constraint (a) Case 1; (b) Case 2

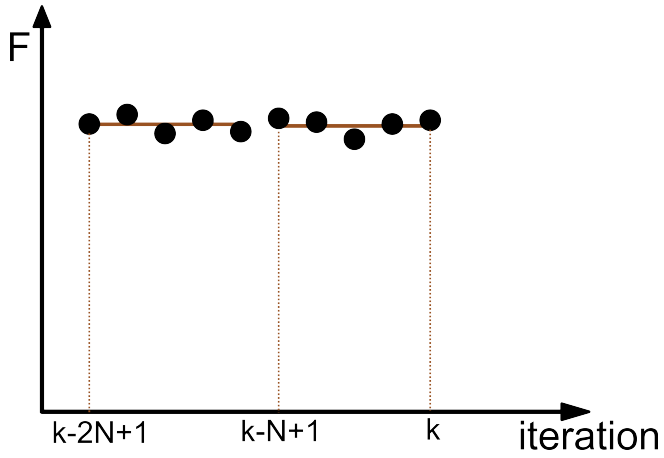

Figure 3.4: Objective function convergence criterion

The stopped criterion, evolutionary rates ER and AR, historical average and filter techniques used in this work are identical that proposed bu Huang and Xie (2010)

3.6 Multi-scale and multi-material BESO procedure

A flowchart of the algorithm of the evolutionary iteration procedure of the multi-scale and multi-material BESO method is presented in the figure 3.5. The BESO parameters are presented in the table 3.3. The algorithm allows m material phases on micro-scale and M materials on macro-scale, that resulting in $m-1$ and $M-1$ sensitivity number and design variable for each element on macro and micro-scale, respectively.

The BESO algorithm starts with the entire design domain of material 1 on macro-scale, the material 2 gradually increases until the volume constraint for material 2 is satisfied, then the volume of material 2 remains constant, and the volume of material 3 gradually increases until the volume constraint for material 3 is satisfied. This process is carried out until the volume constraint for material M is satisfied. The same process is carried out for the m materials phases on micro-scale, if the multi-scale problem is solved.

Table 3.3: BESO parameters.

Variable	Description
V_{fM}	Final volume fraction of the M materials on macro-scale
v_{fm}	Final volume fraction of the m materials on micro-scale
ER	Evolutionary ratio for macro-scale
er	Evolutionary ratio for micro-scale
AR_{max}	Volume addition ratio for macro-scale
ar_{max}	Volume addition ratio for micro-scale
R_{min}	Filter ratio for macro-scale
r_{min}	Filter ratio for for micro-scale
τ	Convergence tolerance
N	Convergence parameter

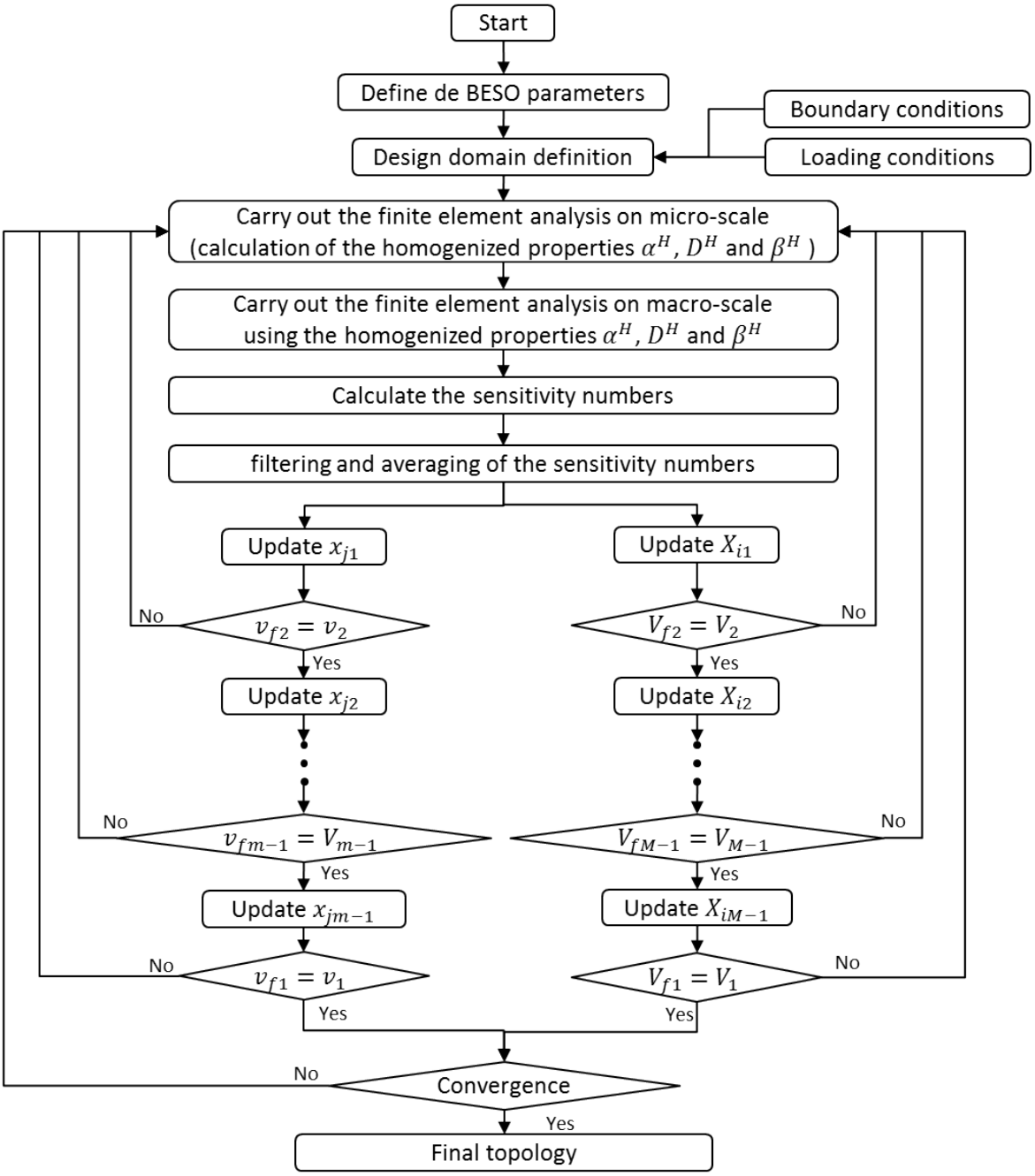

Figure 3.5: Flowchart of the multi-scale and multi-material BESO.

4 NUMERICAL EXAMPLES AND DISCUSSION

This chapter presents the numerical results obtained in this research. The studied Bi-directional Evolutionary Structural Optimization (BESO) method is used. In some examples, the results are compared with classical problems found in the literature to validate the algorithm.

4.1 Topology optimization of a short cantilever beam - Validation problem

A cantilever beam stiffness optimization is a classical problem used to validate a topology optimization procedure. The topology optimization problem can be stated as

$$\begin{array}{lll} Find & \boldsymbol{X}^M & \\ that \quad minimize & C^M = \frac{1}{2}(\boldsymbol{f}^{M,mec})^T \boldsymbol{u}^M & \\ subject \quad to & V^{M,*} - \sum_{i=1}^{N} V_i^M X_i^M = 0 & (4.1) \\ & \boldsymbol{K}^M \boldsymbol{u}^M = \boldsymbol{f}^{M,mec} & \\ & X_i^M = x_{min} \quad \vee \quad 1 & \end{array}$$

where $\boldsymbol{X}^M$ is the design variable in the macro-scale, C^M is the mean compliance, that is the inverse measure of the overall stiffness of a structure (Huang and Xie, 2010), $\boldsymbol{f}^{M,mec}$ is the force vector, $\boldsymbol{u}^m$ is the displacement vector, $V^{M,*}$ is the prescribed volume of the solid material, N is the total number of elements in the system, $\boldsymbol{K}^m$ the global stiffness matrix, and x_{min} is a small value(e.g. 0.001), which indicates that no element is allowed to be completely removed from the design domain (Huang and Xie, 2010). As shown in the figure 4.1, the design domain is 80 mm in length and 50 mm in height. A 100 N force is applied in the middle of the free end. Young's modulus $E = 100$ GPa and Poisson's ratio $\nu = 0.3$ are considered. The design domain is meshed using 160×80 bilinear isoparametric four node plane stress elements. The BESO parameters considered in this example can be seen in table 4.1.

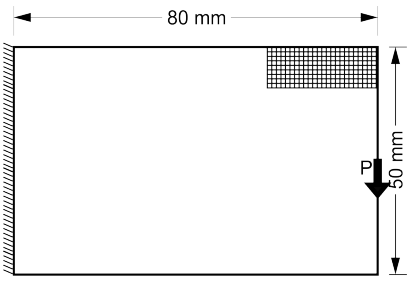

Figure 4.1: Design domain of a short cantilever beam.

Table 4.1: BESO parameters for a stiffness minimization of a cantilever beam

Variable	Description	Value
V_f^M	Final volume fraction	0.5
ER^M	Evolutionary ratio	1%
AR_{max}^M	Volume addition ratio	5%
r_{min}^M	Filter ratio	$3mm$
τ	Convergence tolerance	0.1%
N	Convergence parameter	5

The figure 4.2 shows the results obtained by Huang and Xie (2007) using the SIMP method and the results obtained in this work using the BESO method implemented. It can be observed that the result obtained using the BESO algorithm implemented in this work, is similar to the result using the SIMP algorithm. The main difference are the gray elements which denote intermediate density in the SIMP topology.

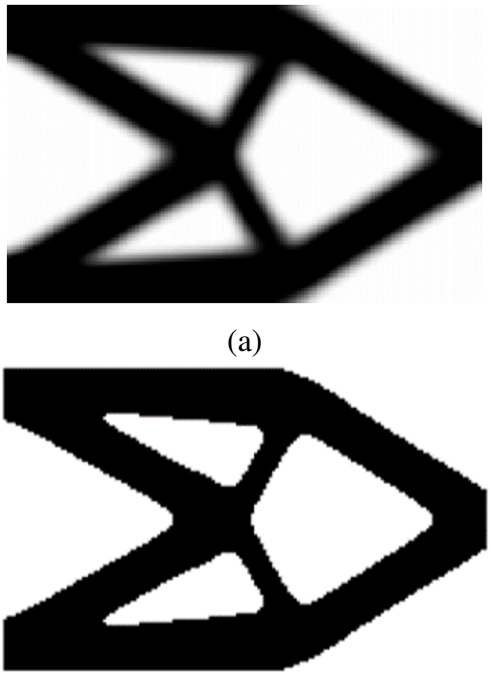

(a)

(b)

Figure 4.2: Topology optimization for a short cantilever beam (a) SIMP method (Huang and Xie, 2007); (b) BESO method.

The results showed in the figure 4.2 demonstrate that the present implementation for compliance minimization agrees with the benchmark results presented in the literature.

4.2 Topology optimization with multiple materials - Validation problem

It is known that extreme thermo-mechanical properties can be achieved by combining more than two materials phases with conventional materials (Sigmund and Torquato, 1996). For this reason, it is necessary that the topology optimization method allows more than two materials phases in the design domain. In this example, a multi-material BESO is presented for the two different material interpolations referred to in section 3.3.

The topology optimization problem is to find the distribution of the two materials in the design domain, that minimize the compliance of the structure, subject to a volume constraint in both phases. The topology optimization problem can be stated as

$$\begin{array}{lll} Find & \boldsymbol{X}^M & \\ that \quad minimize & C^M = \frac{1}{2}(\boldsymbol{f}^{M,mec})^T \boldsymbol{u}^M & \\ subject \quad to & V_j^{M,*} - \sum_{i=1}^{N} V_i^M X_{ij}^M - \sum_{i=1}^{j-1} V_i^{M,*} = 0 \quad j = 1,2 & (4.2) \\ & \boldsymbol{K}^M \boldsymbol{u}^M = \boldsymbol{f}^{M,mec} & \\ & X_{ij}^M = x_{min} \quad \vee \quad 1; \quad j = 1,2 & \end{array}$$

where $V_j^{M,*}$ is the prescribed volume for each jth material phase.

It is considered the beam shown in the figure 4.3. A 10 N downward force is applied at the bottom middle. For symmetry, is considered only the right half of the domain, which is discretized using a mesh of 120×40 bilinear isoparametric four node plane stress elements with a 5N downward force. It is allowed void as well as two materials with Young's moduli $E_1 = 1$ GPa and $E_2 = 0.1$GPa and Poisson's ratio $\nu_1 = \nu_2 = 0.3$. The BESO parameters using in this example can be seen in table 4.2.

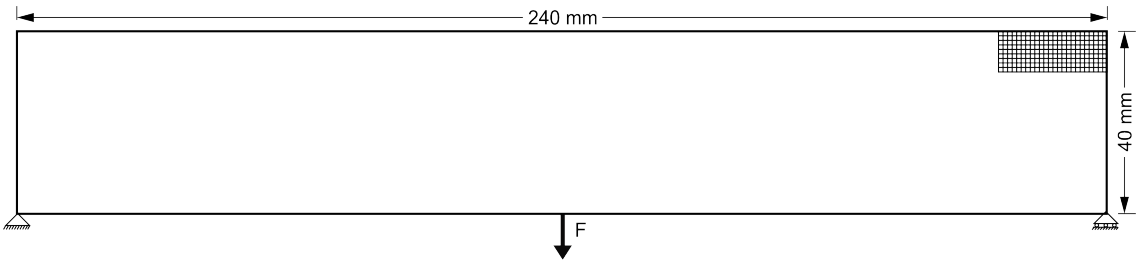

Figure 4.3: Design domain of a MBB beam.

Table 4.2: BESO parameters for a multi-material stiffness minimization of a MBB beam

Variable	Description	Value
V_{f1}^{M}	Final volume fraction of the material 1 for both interpolations	0.15
V_{f2}^{M}	Final volume fraction of the material 2 for both interpolations	0.25
ER^{M}	Evolutionary ratio for interpolation 1	3%
ER^{M}	Evolutionary ratio for interpolation 2	4%
AR_{max}^{M}	Volume addition ratio for interpolation 1	2%
AR_{max}^{M}	Volume addition ratio for interpolation 2	1%
r_{min}^{M}	Filter ratio for interpolation 1	$3.5mm$
r_{min}^{M}	Filter ratio for interpolation 2	$3.3mm$
τ	Convergence tolerance for both interpolations	0.01%
N	Convergence parameter for both interpolations	5

The figure 4.4 shows the comparison of the obtained results by Huang and Xie (2008) and the obtained results using both interpolations of materials studied in this work. It can be seen that the final topologies are similar, this correspondence validate the BESO method implemented when multiple materials are allowed in the design domain.

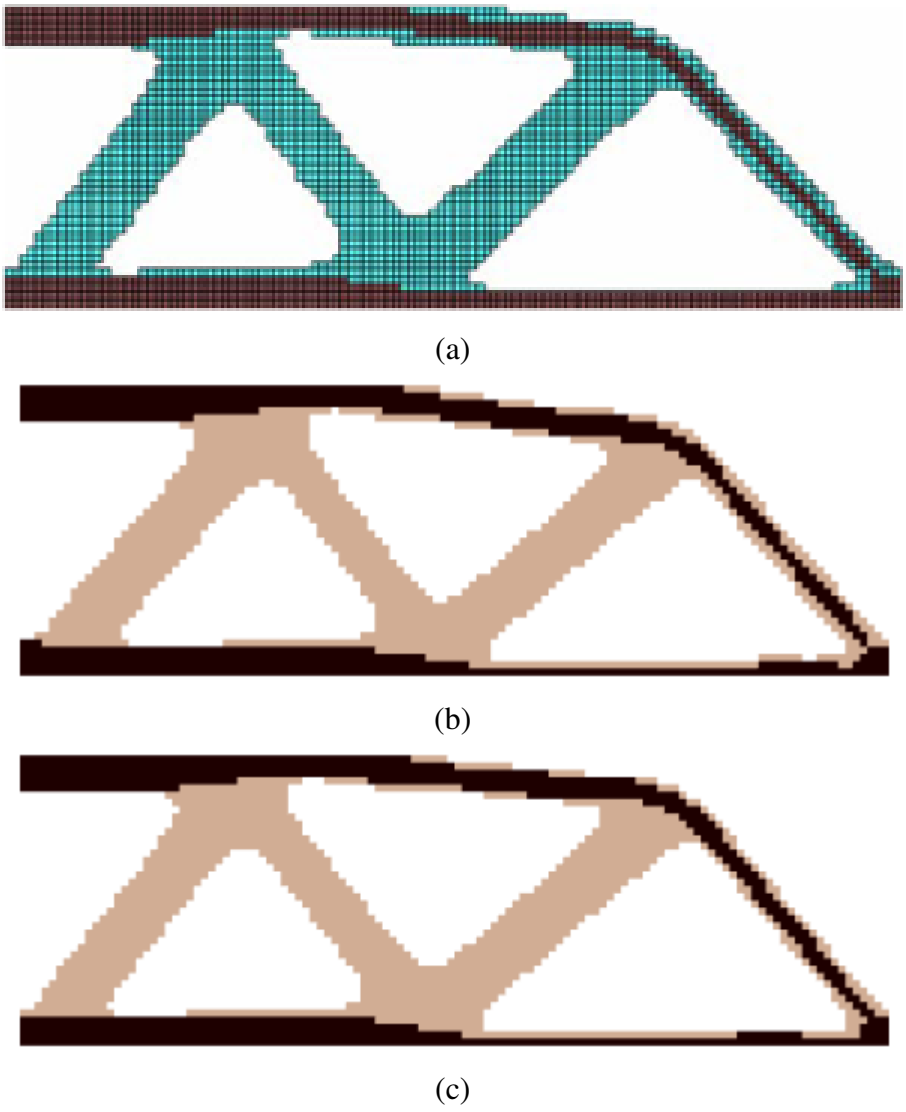

(a)

(b)

(c)

Figure 4.4: BESO final topology for a three-phase structure (a) Topology found by Huang and Xie (2008); (b) Topology found using the material interpolation 1 (see section 3.3.1); (c) Topology found using the material interpolation 2 (see section 3.3.2).

4.3 Topology optimization of a thermo-mechanical continuum structure - Validation problem

This example is presented to validate the implemented BESO method when thermal and mechanical loads occur simultaneously. The topology optimization problem, in this case, is to minimize the compliance of the structure when thermal and mechanical loads are applied. In this example it is allowed in the design domain only one material and void, then the topology

optimization problem can be stated as

$$\begin{array}{lll} Find & \boldsymbol{X}^M & \\ that \quad minimize & C^M = \frac{1}{2}(\boldsymbol{p}^M)^T\boldsymbol{u}^M = \frac{1}{2}(\boldsymbol{f}^{M,ter} + \boldsymbol{f}^{M,mec})^T\boldsymbol{u}^M & \\ subject \quad to & V^{M,*} - \sum_{i=1}^{N} V_i^M X_i^M = 0 & \\ & \boldsymbol{K}^M\boldsymbol{u}^M = \boldsymbol{p}^M & \\ & X_i^M = x_{min} \quad \vee \quad 1 & \end{array} \tag{4.3}$$

where P is the total force applied on the structure, that is the sum of the mechanical and thermal force.

In this example it is considered a cantilever beam as shown in figure 4.5 with $L = 6$mm and $H = 3$mm. The structure is subjected to a concentrated force $F = 1000$ N and a temperature change $\Delta T = 100$ °C. The structure is meshed using 60×30 bilinear isoparametric four node plane stress elements. The material has Young's modulus $E = 210$ GPa and Poisson's ratio $\nu = 0.3$. The BESO parameters are presented in table 4.3

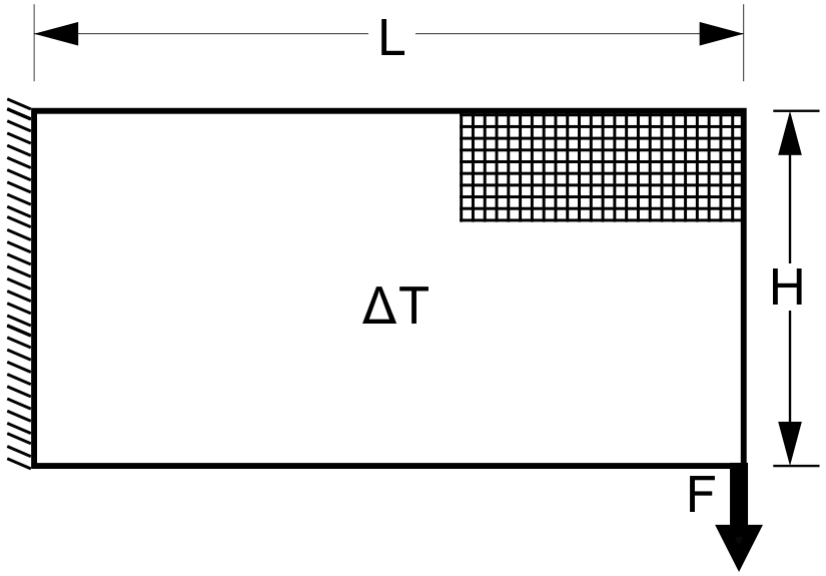

Figure 4.5: Cantilever beam.

Table 4.3: BESO parameters for a thermo-mechanical stiffness minimization of a cantilever beam

Variable	Description	Value
V_f^M	Final volume fraction	0.4
ER^M	Evolutionary ratio	1.1%
AR_{max}^M	Volume addition ratio	2%
r_{min}^M	Filter ratio	$0.17mm$
τ	Convergence tolerance	0.1%
N	Convergence parameter	5

The figure 4.6 shows the results obtained by Li *et al.* (2010) using the moving asymptotes method (MMA) and by the BESO method implemented in this work. It can be observed that the results obtained using the BESO algorithm implemented are similar to the result using the moving asymptotes method. The topology obtained using the BESO algorithm does not present intermediate density (grayscale elements) as can be observed on the topology obtained using the MMA. The agreement between both results is quite good.

(a)

(b)

Figure 4.6: Topology optimization for a thermo-mechanical beam for a $\Delta T = 100$ °C: (a) Method of Moving Asymptotes (MMA) (Li *et al.*, 2010); (b) BESO method.

4.4 Multi-scale and multi-material BESO - Validation problem

A numerical example presented by Xu *et al.* (2016) is reproduced, to validate the implemented multi-scale and multi-material algorithm. In this example, the topology optimization problem is to find the distribution of the two phase material in the microscale, and the distribution of the composite material in the macroscale, that maximize the stiffness of the structure. The topology optimization problems can be stated as

$$\begin{array}{lll} Find & \boldsymbol{X}^m, \quad \boldsymbol{X}^M & \\ that \quad minimize & C^M = \frac{1}{2}(\boldsymbol{f}^{M,mec})^T \boldsymbol{u}^M & \\ subject \quad to & V_l^{m,*} - \sum_{k=1}^{n} V_k^m X_{kl}^m - \sum_{k=1}^{l-1} V_k^{m,*} = 0 \quad l = 1,2 & \\ & V^{M,*} - \sum_{i=1}^{N} V_i^M X_i^M = 0 & \\ & \boldsymbol{K}^m \boldsymbol{U}^m = \boldsymbol{F}^m & \\ & \boldsymbol{K}^M \boldsymbol{u}^M = \boldsymbol{f}^{M,mec} & \\ & X_{kl}^m = x_{min} \quad \vee \quad 1; \quad l = 1,2 & \\ & X_i^M = x_{min} \quad \vee \quad 1 & \end{array} \tag{4.4}$$

where the uppercase and lowercase letters indicate that the variables are related to the macroscale and the microscale domain, respectively. The thermal excitations are not considered in this case.

Xu *et al.* (2016) analyzed the beam shown in the figure 4.8 with $0.5m$ in length and $0.2m$ in height. A 50KN downward force is applied at the bottom middle. It is allowed void as well as two materials with Young's moduli $E_1 = 210GPa$ and $E_2 = 70GPa$, and Poisson's ratio $\nu_1 = \nu_2 = 0.3$. The macro-scale and the micro-scale are meshed using 150×60 and 100×100 bilinear isoparametric four node plane stress elements, respectively. The BESO parameters using in this example can be seen in table 4.4

The figure 4.7 shows the topologies obtained by Xu *et al.* (2016) and by using the BESO method implemented. In this work is used the same material interpolation (based on the material interpolation scheme of the solid isotropic material with penalization - SIMP) for the macro-scale and micro-scale. The procedure implemented by Xu *et al.* (2016) use a SIMP interpolation different than the one considers in this work for the micro-scale and for the macro-scale an alternative interpolation scheme proposed by Stolpe and Svanberg (2001). It was compared only the final topology for the elastic case because the derivative of the homogenized thermal stress tensor $\boldsymbol{\beta}^H$ presented by Xu *et al.* (2016) is different than the one derived in this work and due to this the final topologies for the thermo-elastic design are different.

In the macro-scale, both topologies present four bars at the center of the structure, with the

difference, that in the topology obtained by Xu *et al.* (2016) (4.7(a)) can be observed a smaller separation between these bars than the separation between the bars of the topology obtained using the implemented algorithm.

Analyzing the topologies shown in the figures 4.7(c) and 4.7(d), it can be found some differences between them. The magnitude of the difference between the both topologies is quite small, presenting a difference of 1.4% for the homogenized elasticity matrix ($\boldsymbol{D}^H$) and 0.28% for the homogenized thermal expansion coefficient ($\boldsymbol{\alpha}^H$). This correspondence validate the multi-scale and multi-material BESO procedure implemented, for the structural uncoupled case.

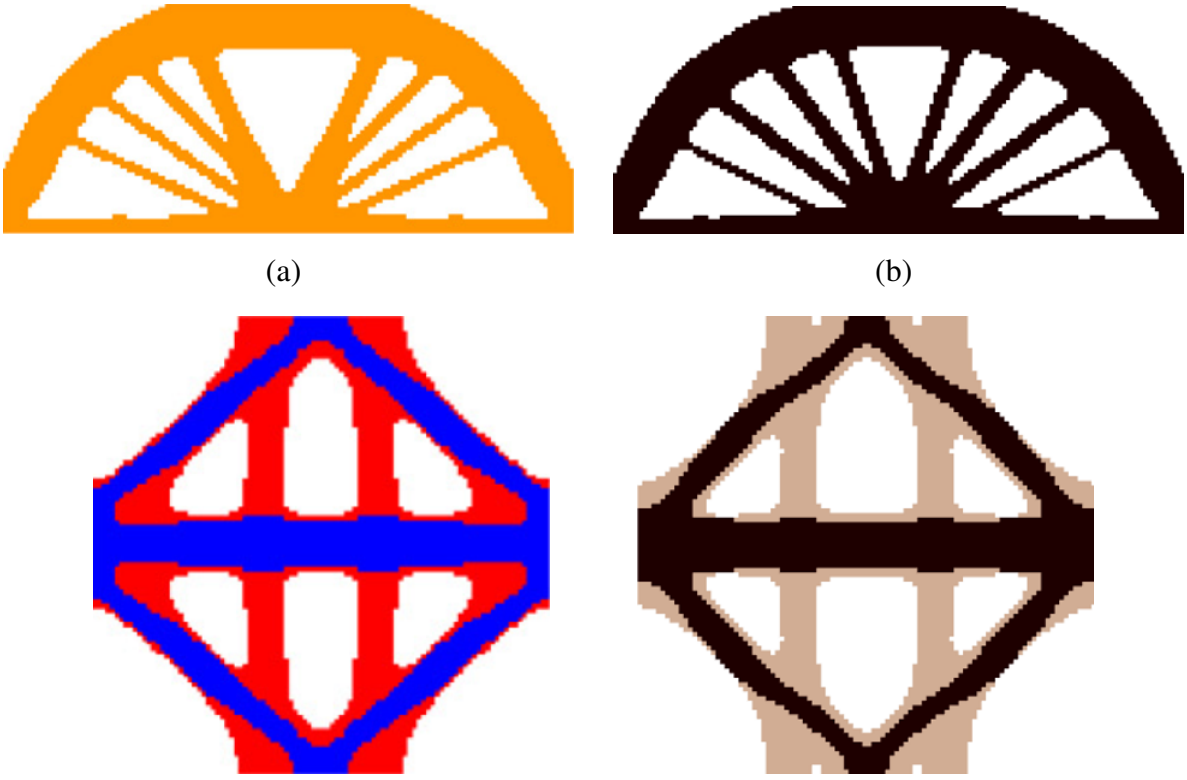

(a) (b)

$$\boldsymbol{D}_1^H = \begin{bmatrix} 4.0217 & 1.2673 & 0 \\ 1.2673 & 2.8301 & 0 \\ 0 & 0 & 1.2974 \end{bmatrix} \qquad \boldsymbol{D}_2^H = \begin{bmatrix} 3.9998 & 1.2040 & 0 \\ 1.2040 & 2.8370 & 0 \\ 0 & 0 & 1.2974 \end{bmatrix}$$

$$\boldsymbol{\alpha}_1^H = \begin{bmatrix} 0.1235 \\ 0.1899 \\ 0 \end{bmatrix} \qquad \boldsymbol{\alpha}_2^H = \begin{bmatrix} 0.1241 \\ 0.1896 \\ 0 \end{bmatrix}$$

(c) (d)

Figure 4.7: Multi-scale and multi-material topology optimization of a roller-supported beam (a) Final topology on macro-scale found by (Xu *et al.*, 2016); (b) Final topology on macro-scale found using the implemented algorithm; (c) Final topology and homogenized properties on micro-scale found by (Xu *et al.*, 2016); (d) Final topology and homogenized properties on micro-scale found using the implemented algorithm

Table 4.4: BESO parameters for a multi-material and multi-scale stiffness minimization of a roller-supported beam

Variable	Description	Value
V_f^M	Final volume fraction of the composite material on macro-scale	0.5
V_{f1}^m	Final volume fraction of the material 1 on micro-scale	0.25
V_{f2}^m	Final volume fraction of the material 2 on micro-scale	0.25
ER^M	Evolutionary ratio for macro-scale	3%
ER^m	Evolutionary ratio for micro-scale	3%
AR_{max}^M	Volume addition for macro-scale	1%
AR_{max}^m	Volume addition ratio for micro-scale	1%
r_{min}^M	Filter ratio for macro-scale	3 elements
r_{min}^m	Filter ratio for micro-scale	5 elements
τ	Convergence tolerance	1%
N	Convergence parameter for	5

4.5 Thermo-mechanical structure design examples

Two examples are presented in order to show the effectiveness of the BESO method implemented when multiples materials are allowed on the topology optimization of thermo-mechanical structures. In these examples only the macroscale is considered. The mean compliance is minimized, and the influence of the temperature changes and the mechanical load on the obtained topologies are analyzed.

In these examples the topology optimization problem is to find the material distribution of the two materials and void in the design domain, that minimize the mean compliance (or maximize the total stiffness of the structure) only in the macroscale, subject to a volume constraint in each material. The topology optimization problem can be stated as follow:

$$\begin{array}{lll} Find & \boldsymbol{X}^M & \\ that \quad minimize & C^M = \frac{1}{2}(\boldsymbol{p}^M)^T\boldsymbol{u}^M = \frac{1}{2}(\boldsymbol{f}^{M,ter} + \boldsymbol{f}^{M,mec})^T\boldsymbol{u}^M & \\ subject \quad to & V_j^{M,*} - \sum_{i=1}^{N} V_i^M X_{ij}^M - \sum_{i=1}^{j-1} V_i^{M,*} = 0 \quad j = 1,2 & (4.5) \\ & \boldsymbol{K}^M\boldsymbol{u}^M = \boldsymbol{p}^M & \\ & X_{ij}^M = x_{min} \quad \vee \quad 1; \quad j = 1,2 & \end{array}$$

The design domain of the first example, illustrated in figure 4.8, is a roller-supported beam submitted to a constant temperature change ΔT and subjected to a concentrated load $F =$

$1000\ N$. The structure is meshed using 160×60 bilinear isoparametric four node plane stress elements, and it is heated uniformly considering different values of the temperature change ΔT: 0, 25, 50 and 100 °C. The proposed multi-material algorithm is used and the properties of the two materials considered are presented in the table 4.5.

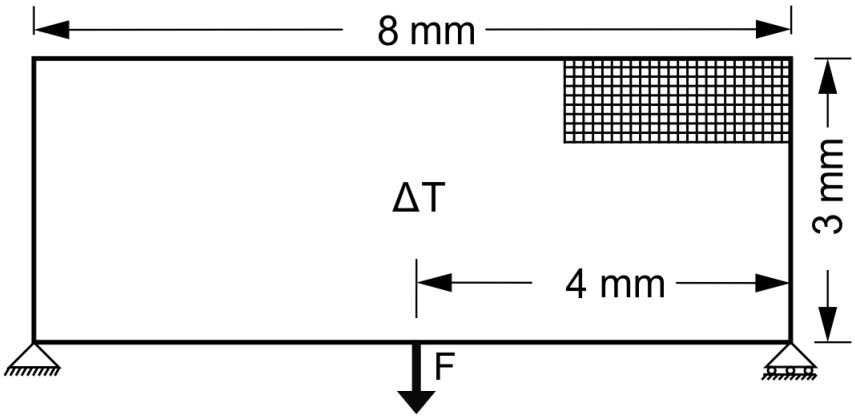

Figure 4.8: Design domain of a roller-supported beam: one concentrated load.

Table 4.5: Materials properties of the two materials considered for the thermo-mechanical structure design examples

Material 1	Young's modulus	$210\ GPa$
	Thermal expansion coefficient	1.2×10^{-5}°C^{-1}
	Poisson's ratio	0.30
Material 2	Young's modulus	$70\ GPa$
	Thermal expansion coefficient	2.3×10^{-5} °C^{-1}
	Poisson's ratio	0.30

The soft-kill BESO method is applied using penalties exponents $p = 3$ and $q = 3$. The table 4.6 summarize the BESO parameters considered. The figure 4.9 shows the final topologies, where the black and the pink (or gray) elements represent the material 1 and material 2, respectively and The figure 4.9 also shows the the evolutionary histories of the mean compliance and evolutionary histories of the volume fraction of both materials.

Table 4.6: BESO parameters for a multi-material stiffness minimization of a thermo-mechanical structure

Variable	Description	Value
V_{f1}^{M}	Final volume fraction of the material 1	0.15
V_{f2}^{M}	Final volume fraction of the material 2	0.25
ER^{M}	Evolutionary ratio	2%
AR_{max}^{M}	Volume addition ratio	1%
r_{min}^{M}	Filter ratio	$0.17mm$
τ	Convergence tolerance	0.01%
N	Convergence parameters	5

In the evolutionary histories presented in the figure 4.9, the compliance varies smoothly on the iterative process, and with the increase of the temperature change the final value of the compliance increases. The final topologies vary with the value of the temperature change ΔT, it can be observed that for high values of ΔT, the algorithm concentrated the material 1 at the center of the structure creating different topologies.

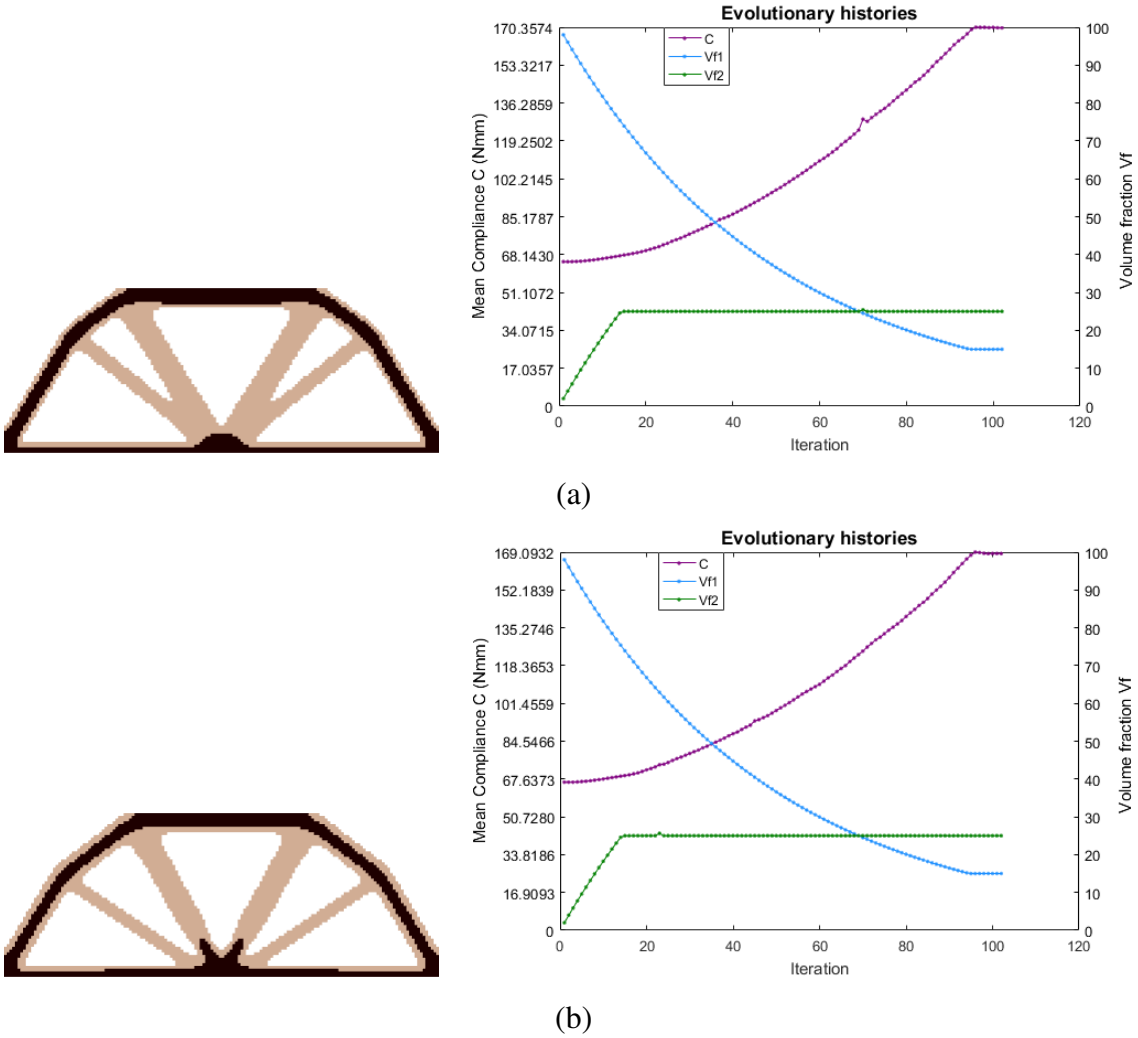

Figure 4.9: The optimal topologies and the evolutionary histories for the one concentrated load. (a) Δ T = 0 °C; (b) ΔT = 25 °C; (c) ΔT = 50 °C; (d) Δ T =100 °C

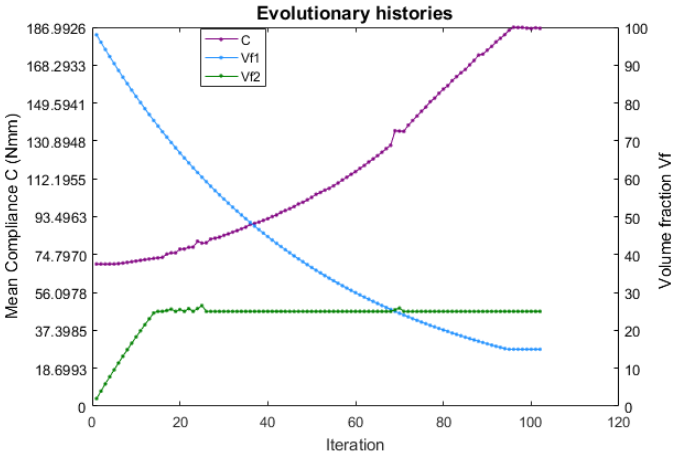

(c)

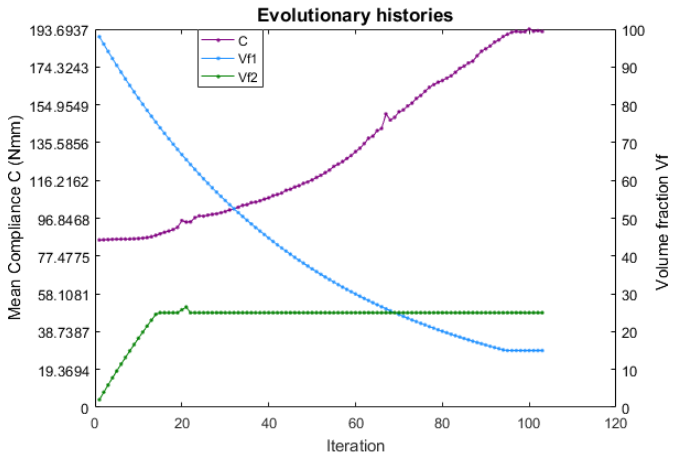

(d)

Figure 4.9: The optimal topologies and the evolutionary histories for the one concentrated load. (a) Δ T = 0 °C; (b) ΔT = 25 °C; (c) ΔT = 50 °C; (d) Δ T =100 °C

In the second example, the mechanical load is modified in order to analyze the influence of the load condition in the final topology, three concentrated mechanical loads are considered as can be illustrated in the figure 4.10. Using the same materials properties (see table 4.5) and algorithm parameters (see table 4.6) of the load case 1, the final topologies, the evolutionary histories of the mean compliance and the evolutionary histories of the volume fraction of both material phases are presented in the figure 4.11.

The variation of the compliance value along the iteration is also smooth, and its final value increases with the increase of the temperature changes, as can be observed in the figure 4.11. The final topology depends on the magnitude of the temperature change. In the figure 4.11 can be observed that inasmuch as the temperature change increases, the algorithm concentrated the material 1 on the bottom of the structure where the loads are applied.

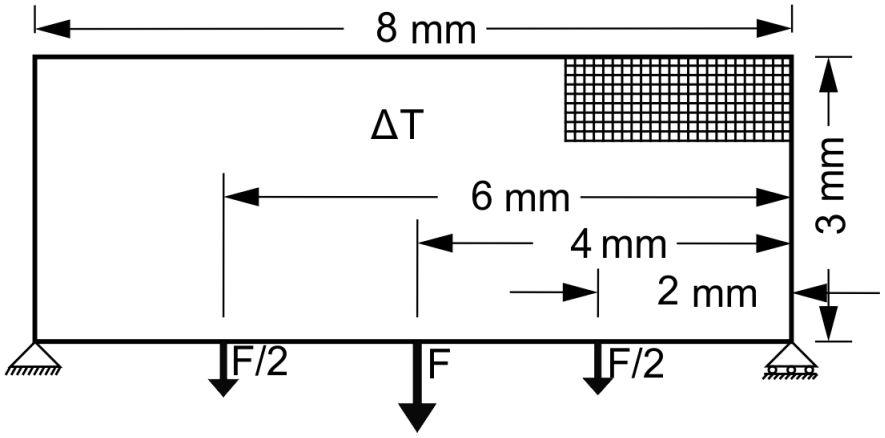

Figure 4.10: Design domain of a roller-supported beam: three concentrated loads.

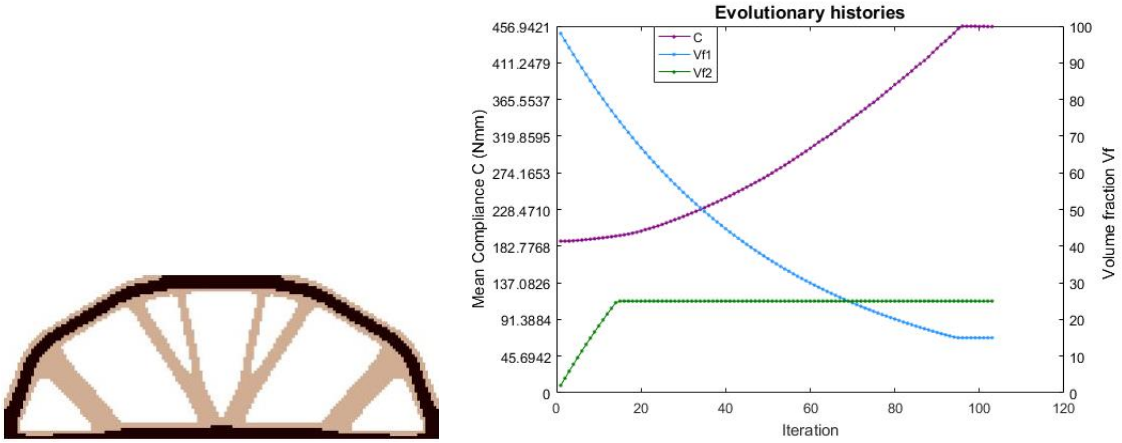

(a)

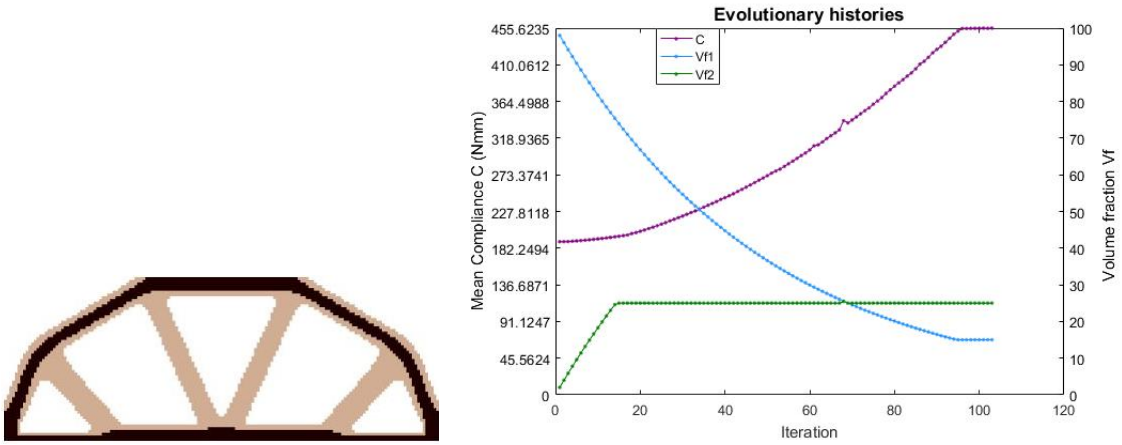

(b)

Figure 4.11: The optimal topologies and the evolutionary histories for the three concentrated loads. (a) Δ T = 0 °C; (b) ΔT = 25 °C; (c) ΔT = 50 °C; (d) Δ T =100 °C

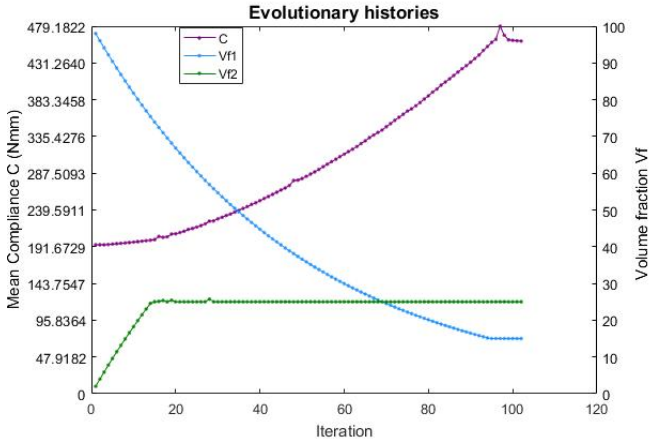

(c)

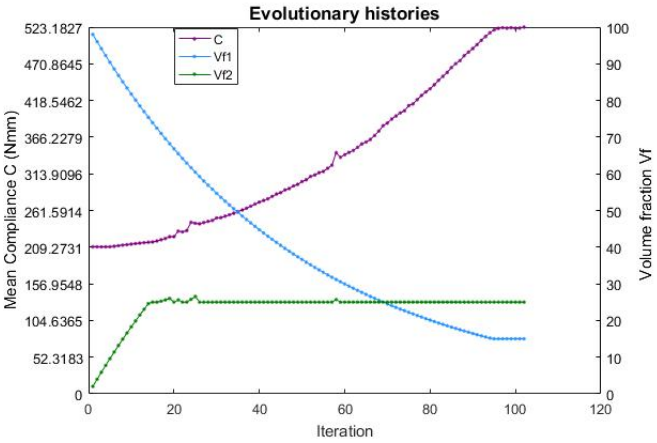

(d)

Figure 4.11: The optimal topologies and the evolutionary histories for the three concentrated loads. (a) Δ T = 0 °C; (b) ΔT = 25 °C; (c) ΔT = 50 °C; (d) Δ T =100 °C

4.6 Material design examples

These examples are presented to show the effectiveness of the BESO method implemented, in the topology optimization of a base cell in order to find a new composite material with a specific property. The topology optimization problem, considered in these examples, is to find the distribution of the two material phases and void, in the base cell that minimize an objective function, that is the sum of the components of the homogenized thermal expansion coefficient α^H, subject to a volume constraint in each material. In this example, they are specified two geometrical symmetry axis in order to get an orthotropic material. The topology optimization problem can be stated as follow

$$
\begin{array}{lll}
Find & \boldsymbol{X}^m & \\
that \quad minimize & \alpha_{11}^H + \alpha_{22}^H + \alpha_{21}^H & \\
subject \quad to & V_l^{m,*} - \sum_{k=1}^{n} V_k^m V_{kl}^m - \sum_{k=1}^{l-1} V_k^{m,*} = 0 \quad l = 1,2 & \\
& \boldsymbol{K}^m \boldsymbol{U}^m = \boldsymbol{F}^m & \\
& \boldsymbol{K}^m \boldsymbol{\varphi}^m = \boldsymbol{f}_t^m & \\
& X_{kl}^m = x_{min} \quad \vee \quad 1; \quad l = 1,2 &
\end{array}
\tag{4.6}
$$

where α_{11}^H, α_{22}^H and, α_{12}^H are the three components of the homogenized thermal expansion coefficient. The design domain is a unit base cell, that is meshed using 100×100 bilinear isoparametric four node plane stress elements. The proposed multi-material algorithm is used, considering hypothetical materials with the properties presented in the table 4.7.

Table 4.7: Materials properties of the hypothetical materials

Material 1	Young's modulus	1
	Thermal expansion coefficient	10
	Poisson's ratio	0.30
Material 2	Young's modulus	1
	Thermal expansion coefficient	1
	Poisson's ratio	0.30

The soft-kill BESO method is applied using a $x_{min} = 0.001$. The table 4.8 summarize the BESO parameters considered. The figure 4.12(a) shows the final topology obtained for the base cell, where the black and the pink elements represent the material 1 and material 2, respectively. An array of 3×3 base cells is presented in the figure 4.12(b), to illustrate the periodic microstructure of a material made using the obtained base cell. The figure 4.12(c) presents the evolutionary histories of the objective function and the volume fraction of each material. The homogenized thermal expansion coefficient of the final topology is the follow:

$$
\boldsymbol{\alpha}^H = \left\{ \begin{array}{c} 0.0612 \\ 3.7040 \\ 0.0000 \end{array} \right\} \tag{4.7}
$$

In the figure 4.12(c) it can be observed that the objective function is smooth on the iterative process.The algorithm concentrates the material 1 (that is the material with a greater thermal expansion coefficient) on the sides of the base cell, this affect the value of the thermal expansion coefficient α_{22}, in other words, if the algorithm concentrated the material 1 at the top and bottom of the base cell, the value of the coefficient α_{11} would be greater than the value of the coefficient

α_{22}.

The value of the homogenized thermal expansion coefficient of the obtained base cell indicates that the structure made of the base cell presented in the figure 4.12(a) will be present a horizontal thermal expansion of 6.12% of the thermal expansion of an structure made of material 2.

Table 4.8: BESO parameters for a thermal expansion minimization of the base cell

Variable	Description	Value
p_1	Penalty exponent for the interpolation between D_1 and D_2	3
p_2	Penalty exponent for the interpolation between D_2 and D_3	3
q_1	Penalty exponent for the interpolation between α_1 and α_2	3
q_2	Penalty exponent for the interpolation between α_2 and α_3	0
V_{f1}^m	Final volume fraction of the material 1	0.1
V_{f2}^m	Final volume fraction of the material 2	0.4
ER^m	Evolutionary ratio	4%
AR_{max1}^m	Volume addition ratio for the design variable 1	0.01%
AR_{max2}^m	Volume addition ratio for the design variable 2	0.001%
$frac$	Volume fraction of the removed material 1 that will be converted into material 2 in each iteration	0.5%
r_{min}^m	Filter ratio	0.25
τ	Convergence tolerance	0.1%
N	Convergence parameters	5

The variable $frac$ is a BESO parameter that indicates how much of the removed material 1 will become material 2 in each iteration. For example, if the value of $frac$ is 0.5, fifty percent of the removed material 1 will become material 2 and the other fifty percent will turn void.

The figure 4.13 is presented in order to illustrate the influence of the parameter $frac$ in the final topology. They are presented the final topology, an array of 3x3 base cell, and the evolutionary histories for four values of $fraf$, 1.0, 0.9, 0.6, and 0.5.

As can be observed in the figure 4.13 the final topologies are similar for all the values of $frac$ presented in this example. The main difference is found in the evolutionary histories, where the value of the objective function becomes smoother along the iterations, with the decrease of the $frac$ value. For the example presented in the figure 4.12 was used a $frac$ value of 0.5 in order to have the smoother convergence possible between the analyzed $frac$ values.

In the figure 4.14 are presented the final topologies, the array of 3x3 base cells and the evolutionary histories for four values of the evolutionary ratio er: 0.02, 0.03, 0.04 and, 0.05. The final topologies obtained for the different values of er are similar, with a difference in the orientation; As can be observed in the figure 4.14 for er values of 0.02 and 0.05 the base cell has the minimal thermal expansion in the vertical direction, while for er values of 0.03 and 0.04 has the minimal thermal expansion in the horizontal direction. This phenomenon can be presented due to no constraint of isotropy are imposed and because two lines of symmetry are considered.

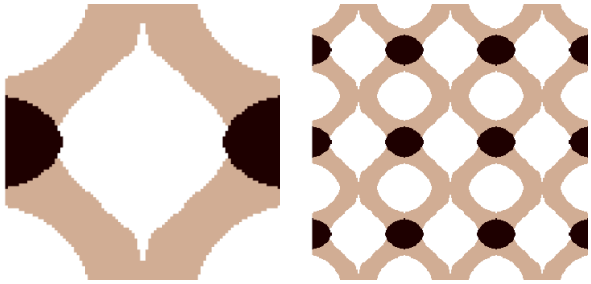

(a) (b)

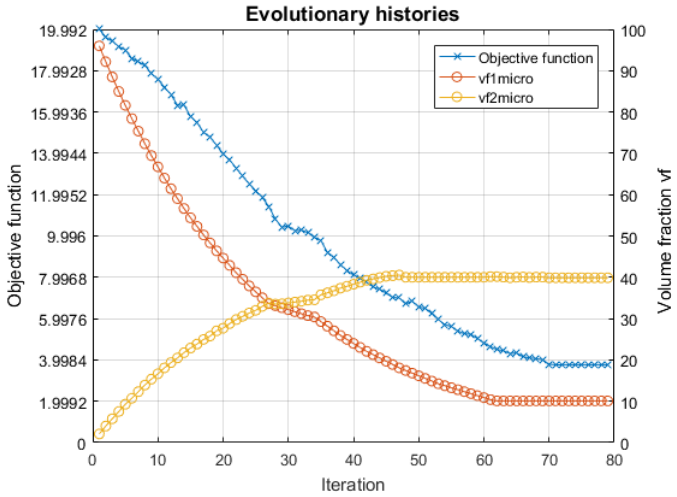

(c)

Figure 4.12: Results for the minimization of the sum of the thermal expansion coefficients: (a) final topology of the base cell; (b) 3x3 array; (c)the evolutionary histories of the objective function and the volume fractions

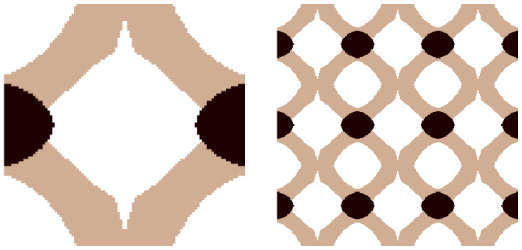

$$\alpha^H = \begin{bmatrix} 0.4455 \\ 3.5113 \\ 0 \end{bmatrix}$$

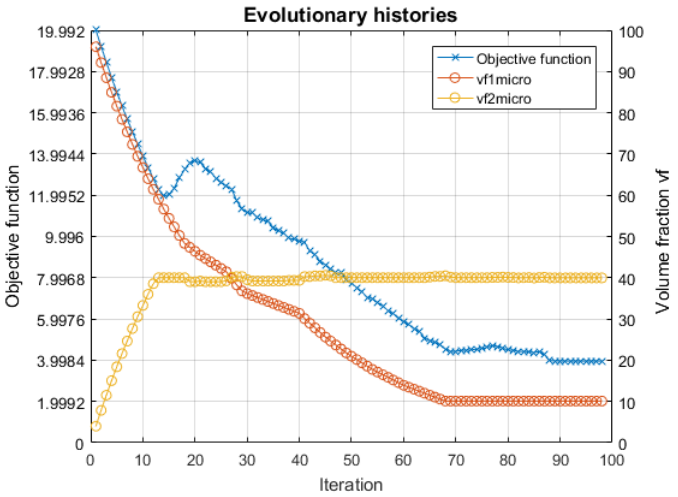

(a)

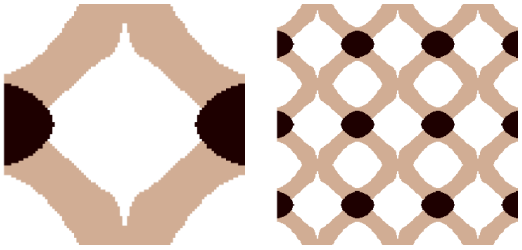

$$\alpha^H = \begin{bmatrix} 0.4225 \\ 3.5430 \\ 0 \end{bmatrix}$$

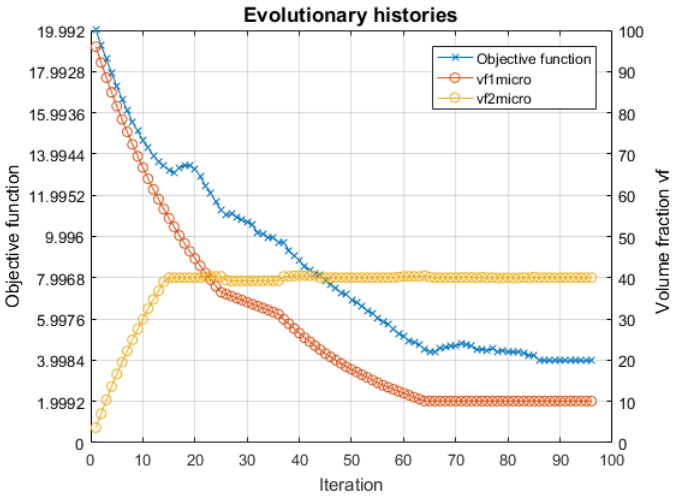

(b)

Figure 4.13: The optimal topologies and the evolutionary histories for the minimization of the thermal expansion coefficients for different values of $frac$:(a) $frac$ = 1.0; (b)$frac$ = 0.9; (c) $frac$ = 0.6; (d) $frac$ =0.5

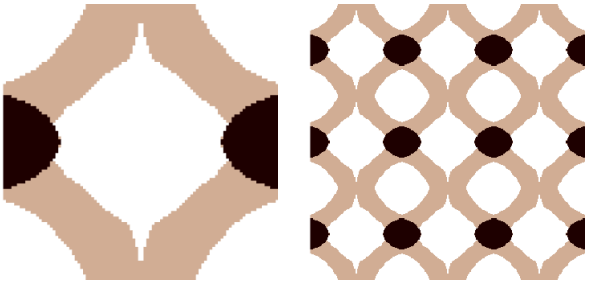

$$\alpha^H = \begin{bmatrix} 0.3295 \\ 3.6014 \\ 0 \end{bmatrix}$$

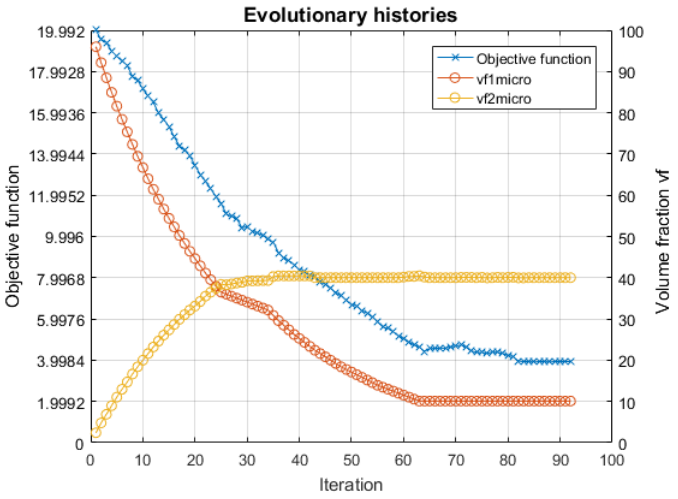

(c)

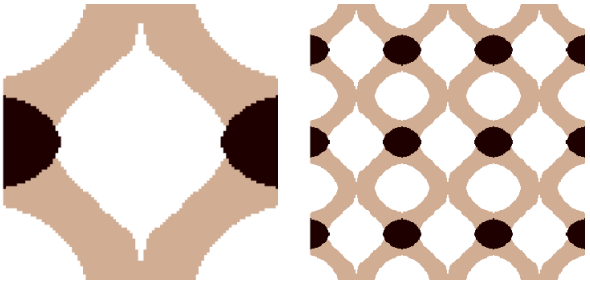

$$\alpha^H = \begin{bmatrix} 0.0612 \\ 3.7040 \\ 0 \end{bmatrix}$$

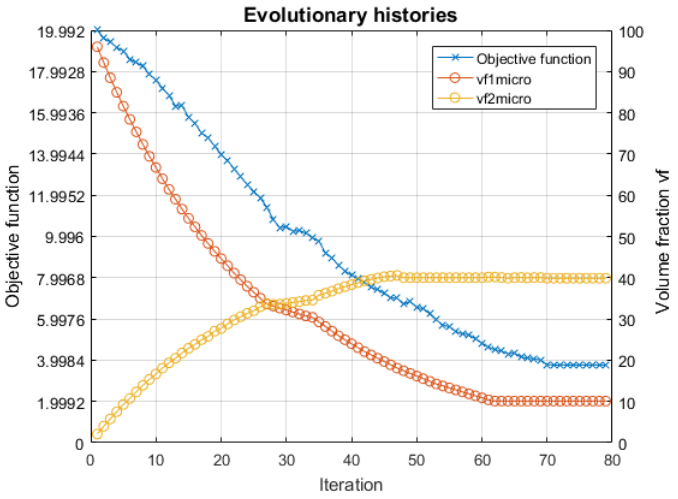

(d)

Figure 4.13: The optimal topologies and the evolutionary histories for the minimization of the thermal expansion coefficients for different values of $frac$:(a) $frac$ = 1.0; (b)$frac$ = 0.9; (c) $frac$ = 0.6; (d) $frac$ =0.5

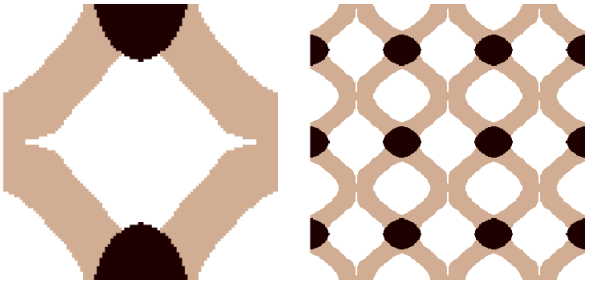

$$\alpha^H = \begin{bmatrix} 3.7692 \\ 0.2437 \\ 0 \end{bmatrix}$$

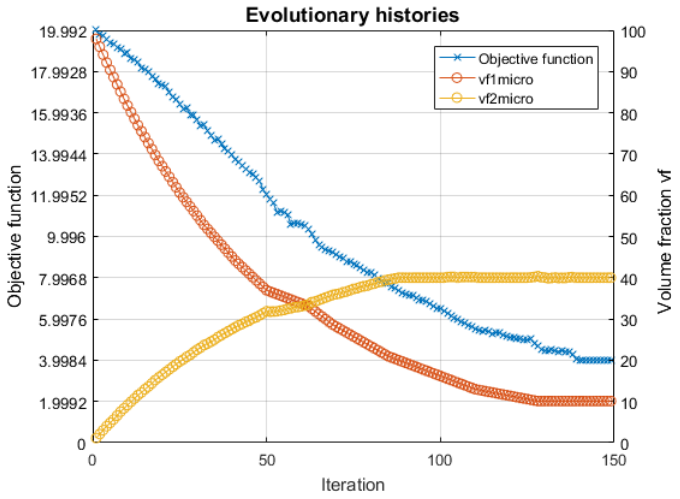

(a)

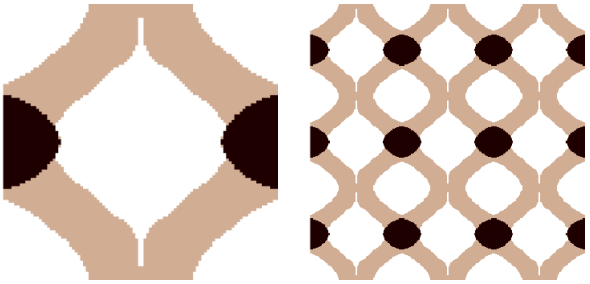

$$\alpha^H = \begin{bmatrix} 0.4885 \\ 3.3979 \\ 0 \end{bmatrix}$$

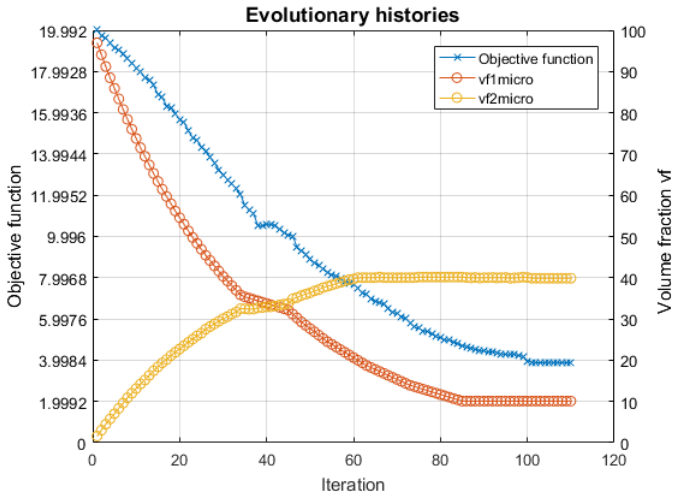

(b)

Figure 4.14: The optimal topologies and the evolutionary histories for the minimization of the thermal expansion coefficients for different values of er: (a) er = 0.02; (b) er = 0.03; (c) er = 0.04; (d) er =0.05

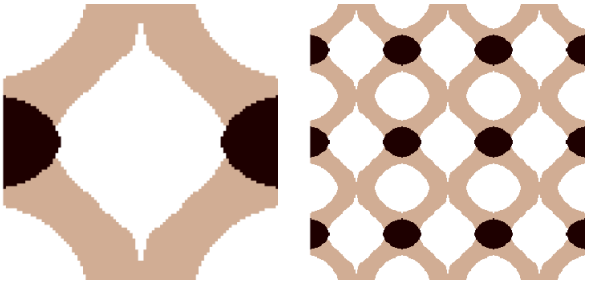

$$\alpha^H = \begin{bmatrix} 0.0612 \\ 3.7040 \\ 0 \end{bmatrix}$$

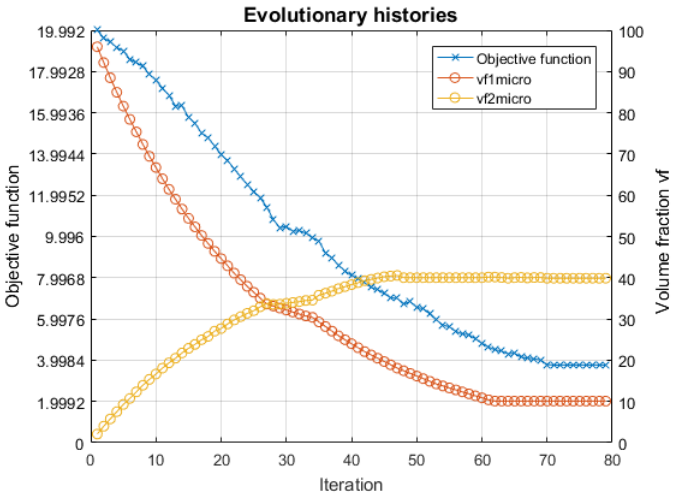

(c)

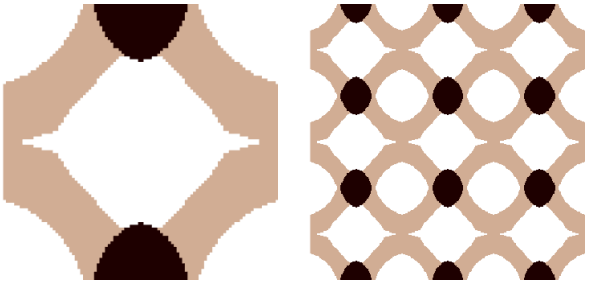

$$\alpha^H = \begin{bmatrix} 3.2880 \\ 0.5809 \\ 0 \end{bmatrix}$$

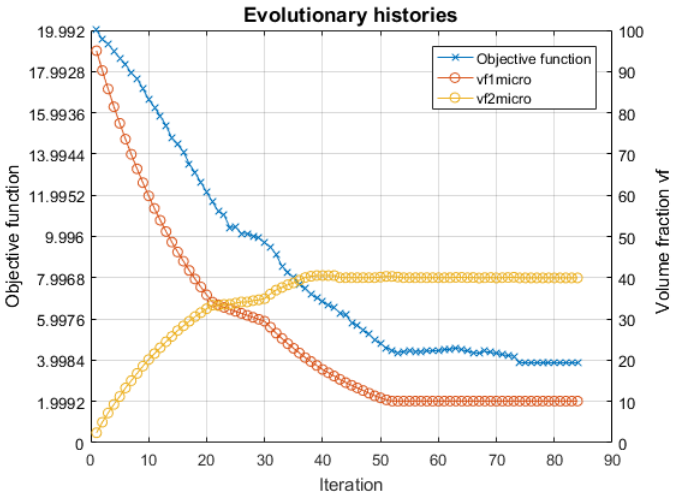

(d)

Figure 4.14: The optimal topologies and the evolutionary histories for the minimization of the thermal expansion coefficients for different values of er: (a) er = 0.02; (b) er = 0.03; (c) er = 0.04; (d) er =0.05

5 CONCLUSIONS AND SUGGESTED FUTURE WORKS

This chapter present the analysis and conclusions related to the development of this work. The main objective was the implementation of an multi-scale and multi-material algorithm using the Bi-Evolutionary Structural Optimization method (BESO). The algorithm was proposed to solve topology optimization problems related with the maximization of the mean compliance of a thermo-elastic structure and the minimization of a thermal expansion coefficient of a composite material. At the end of this chapter, suggestions for future work are made, in order to enhance this work.

5.1 Conclusions

This work presented a study of multi-scale and multi-material evolutionary topology optimization. The implementation and validation of the results obtained for the problem of minimization of the mean compliance considering thermo-mechanical loads and multiple materials are presented. In addition, the presented methodology was applied in the minimization of the thermal expansion coefficient of a base cell.

Two different material interpolations based on the material interpolation scheme with penalization was implemented and the final topology obtained using the both interpolation are similar.

The homogenization theory was studied and applied to model the thermo-elasticity problem. Using the finite element analysis in the periodic cell, the fields of nodal displacements due to an initial strain and initial thermal strain could be calculated. From the displacement fields in the unit base cell, it was possible to obtain the structural behavior (the homogenized elasticity matrix and the homogenized thermal expansion coefficient).

The application of the thermo-elastic topological optimization was done using the Bi-Evolutionary Structural Optimization method (BESO). The multi-scale and multi-material algorithm implemented was used to study two different projects, the first one is the minimization of the mean compliance on a thermoelastic structure using multiple materials, and the second one is the minimization of the thermal expansion coefficient in a base cell using multiple materials. Some considerations about each project are discussed below:

Thermo-mechanical structure design

- The implemented algorithm was applied in the design of thermo-mechanical structures with multiple materials. The interpolation of the elastic matrix and the thermal expansion coefficient has been done, using the material interpolation scheme with penalization. The sensitive of the mean compliance with respect to the design variables is derived.
- Two numerical examples are presented to show the effectiveness of the proposed procedure to design thermo-mechanical structures with multiple materials. The final topologies present a sandwich of material 2 over a core of material 1. The evolutionary histories indicate that the final value of the objective function increases with the increase of the temperature change.
- The final topologies depend on the temperature changes as well as on the load condition. As the temperature increases, the algorithm places the material 1 (which is the stiffer material) between the supports and the concentrated loads.
- The evolutionary history of the mean compliance and of the volume fraction of both material are smooth along the iterations.

Material design

- The implemented algorithm proved to be a computational tool suitable for material design. A material was design, with a horizontal thermal expansion coefficient less than 10% of the thermal expansion of the material 2 (which is the material with the less thermal expansion coefficient). The algorithm creates an ellipse of material one that is positioned in the opposite horizontal vertices of a diamond made of material 2.
- The influence of the evolutionary ration er and, the volume fraction of the removed material 1 that will be converted into material 2 in each iteration $frac$, on the final topology was analyzed. The final topologies are similar for values of $frac$ of 1.0, 0.9, 0.6 and 0.5. The influence of the parameter $frac$ can be observed on the evolutionary history of the objective function, that become smoother when the value of $frac$ decreases. The er parameter has influence on the orientation of the base cell, and on the number of iterations until convergence. This phenomenon can be presented due to no isotropic restriction on the topology optimization process are imposed.

The implemented algorithm can be used to study thermo-elastic project on the macro-scale, micro-scale or in a concurrent approach. In this work the thermo-mechanical structure project considers only the macro-scale, the material project considers only the micro-scale,

and it is presented an example to show the effectiveness of the implemented algorithm in a concurrent design.

5.2 Suggestions for future research

Some suggestions for future works to continue the study presented are summarized in the list below:

- Addition of isotropic restrictions in the minimization of the coefficient of thermal expansion
- Study other objective function in order to obtain a desired property (thermal expansion coefficient, Poisson's ratio or elasticity matrix).
- Implement a bi-objective function in order to minimize two different properties at the same time, such as the thermal expansion coefficient and the Poisson's ratio.
- Algorithm implementation for tri-dimensional thermo-elastic problems using the BESO method
- Application of the homogenization theory and multi-scale optimization for heat conduction problems, considering the presence of thermo-mechanical loads.

References

AZEVEDO, F.M. **Bi-directional Evolutionary Acoustic Topology Optimization for Muffler Design**. 2017. Master Thesis. Universidade Estadual de Campinas.

BABUSKA, I. Homogenization approach in engineering. **Computing Methods in Applied Sciences and Engineering**, v. 134, 137–153, 1976.

BENDSøE, M.P. and KIKUCHI, N. Generating optimal topologies in structural design using a homogenization method. **Computer Methods in Applied Mechanics and Engineering**, v. 71, n. 2, 197 – 224, 1988.

BENDSøE, M.P. and SIGMUND, O. Material interpolation schemes in topology optimization. **Archive of Applied Mechanics**, v. 69, n. 9, 635–654, Nov 1999.

BENDSøE, M.P. and SIGMUND, O. **Topology Optimization - Theory, Methods and Applications**. Springer, 2nd ed., 2003.

CALIXTO, T.K.L. **Otimização Topológica Evolucionária Multiescala Aplicada a Problemas de Elasticidade Linear**. 2015. Master Thesis. Universidade Estadual de Campinas.

CHENG, C.H. **Modeling of the thermal elasto-plastic behaviour for composite materials using the homogenization method**. 1992. PhD Thesis. University of Michigan.

COOK, R.D.; MALKUS, D.S. and PLESHA, M.E. **Concepts and applications of finite element analysis**. Jihn Wiley & Sons. Inc, 2001.

DEATON, J.D. and GRANDHI, R.V. Stress-based topology optimization of thermal structures. In **10th World Congress on Structural and Multidisciplinary Optimization**. 2013.

DEATON, J.D. and GRANDHI, R.V. Stress-based design of thermal structures via topology optimization. **Structural and Multidisciplinary Optimization**, v. 53, 253–270, 2016.

DENG, J.; YAN, J. and CHENG, G. Multi-objective concurrent topology optimization of thermoelastic structures composed of homogeneous porous material. **Structural and Multidisciplinary Optimization**, v. 47, n. 4, 583–597, 2013.

DESMORAT, B. Structural rigidity optimization with an initial design dependent stress field. application to thermo-elastic stress loads. **European Journal of Mechanics - A/Solids**, v. 37, 150 – 159, 2013.

DU, Y.; LUOB, Z.; TIANA, Q. and CHEN, L. Topology optimization for thermo-mechanical compliant actuators using mesh-free methods. **Engineering Optimization**, v. 41, n. 8, 753–772, 2009.

GAO, T. and ZHANG, W. Topology optimization involving thermo-elastic stress load. **Structural and Multidisciplinary Optimization**, v. 42, n. 5, 725–738, 2010.

GAO, T. and ZHANG, W. A mass constraint formulation for structural topology optimization with multiphase materials. **International Journal for Numerical Methods in Engineering**, v. 88, n. 8, 774–796, 2011.

GUEDES, J.M. and KIKUCHI, N. Preprocessing and postprocessing for materials based on the homogenization methos with adaptative finite element methods. **Computer methods in applied mechanics and engineering**, v. 83, 143–198, 1990.

HASSANI, B. A direct method to derive the boundary conditions of the homogenization equation for symmetric cells. **Communications in Numerical Methods in Engineering**, v. 12, n. 3, 185–196, 1996.

HASSANI, B. and HINTON, E. A review of homogenization and topology optimization i–homogenization theory for media with periodic structure. **Computers and Structures**, v. 69, 707–717, 1998a.

HASSANI, B. and HINTON, E. A review of homogenization and topology optimization iii-topology optimization using optimality criteria. **Computers and Structures**, v. 69, 739–756, 1998b.

HOU, J.; ZHU, J.H. and LI, Q. On the topology optimization of elastic supporting structures

under thermomechanical loads. **International Journal of Aerospace Engineering**, v. 2016, 12, 2016.

HUANG, X. and XIE, Y. Convergent and mesh-independent solutions for the bi-directional evolutionary structural optimization method. **Finite Elements in Analysis and Design**, v. 43, n. 14, 1039 – 1049, 2007.

HUANG, X. and XIE, Y. **Evolutionary Topology Optimization of Continuum Structures**. John Wiley & Sons Ltd., 2010.

HUANG, X. and XIE, Y.M. Bi-directional evolutionary topology optimization of continuum structures with one or multiple materials. **Computational Mechanics**, v. 43, n. 3, 393, Jul 2008.

HUANG, X.; ZHOU, S.; XIE, Y. and LI, Q. Topology optimization of microstructures of cellular materials and composites for macrostructures. **Computational Materials Science**, v. 67, 397–407, 2013.

HUGHES, T.J. **The Finite Element Method**. Dover publications, INC, 2000.

JOG, C. Distributed-parameter optimization and topology design for non-linear thermoelasticity. **Computer Methods in Applied Mechanics and Engineering**, v. 132, n. 1, 117 – 134, 1996.

LI, D.; ZHANG, X.; GUAN, Y. and ZHAN, J. Topology optimization of thermo-mechanical continuum structure. In **IEEE/ASME International Conference on Advanced Intelligent Mechatronics**. 2010.

LI, Q.; STEVEN, G. and XIE, Y. A simple checkerboard suppression algorithm for evolutionary structural optimization. **Structural and Multidisciplinary Optimization**, v. 22, n. 3, 230–239, Oct 2001a.

LI, Q.; STEVEN, G.P.; QUERIN, O.M. and XIE, Y. Shape and topology design for heat conduction by evolutionary structural optimization. **International Journal of Heat and Mass Transfer**, v. 42, n. 17, 3361 – 3371, 1999.

LI, Q.; STEVEN, G.P. and XIE, Y.M. Thermoelastic topology optimization for problems with varying temperature fields. **Journal of Thermal Stresses**, v. 24, n. 4, 347–366, 2001b.

LUO, Z.; GAO, W. and SONG, C. Design of multi-phase piezoelectric actuators. **Journal of Intelligent Material Systems and Structures**, v. 21, n. 18, 1851–1865, 2010.

LUO, Z.; TONG, L. and MA, H. Shape and topology optimization for electrothermomechanical microactuators using level set methods. **Journal of Computational Physics**, v. 228, 3173–3181, 2009.

MADRID, C.M.P. **Bi-directional Evolutionary Topology Optimization of Compliant Mechanisms Design using a Multi-criteria Approach**. 2016. Master Thesis. Universidade estadual de Campinas.

MASLEN, E.H. and SCHWEITZER, G. **Magnetic Bearings Theory, Design, and Application to Rotating Machinery**. Springer, Berlin, Heidelberg, 2009.

NETO, J.A.O. **Otimização topológica de estruturas termoelásticas tridimensionais**. 2011. Master Thesis. Universidade Federal do Rio Grande do Norte.

NISHIWAKI, S.; FRECKER, M.I.; MIN, S. and KIKUCHI, N. Topology optimization of compliant mechanisms using the homogenization method. **International journal for numerical methods in engineering.**, v. 42, 535–559, 1998.

PARIS, J.; NAVARRINA, F.; COLOMINAS, I. and CASTELEIRO, M. Stress constraints sensitivity analysis in structural topology optimization. **Computer Methods in Applied Mechanics and Engineering**, v. 199, n. 33, 2110 – 2122, 2010.

PEDERSEN, P. and PEDERSEN, N.L. Strength optimized designs of thermoelastic structures. **Structural and Multidisciplinary Optimization**, v. 42, n. 5, 681–691, Nov 2010.

PICELLI, R. **Otimizaçao evolucionária usando malhas hexagonais**. 2011. Master Thesis. Universidade Estadual de Campinas.

PICELLI, R.; VICENTE, W.; PAVANELLO, R. and XIE, Y. Evolutionary topology optimization for natural frequency maximization problems considering acoustic-structure interaction.

Finite Elements in Analysis and Design, v. 106, 56 – 64, 2015.

PORTO, E.C.B. **Método da homogeneização aplicado à otimização estrutural topológica**. 2006. Master Thesis. Universidade Estadual de Campinas.

PORTO, E.C.B. and PAVANELLO, R. Influência dos parâmetros de homogeneização sobre a solução estrutural topoloógica ótima. In **8 Congreso Iberoamericano de Ingenieria Mecanica**, v. 1, pp. 1–9. Cusco-Peru, 2007.

RODRÍGUEZ, S.Q. **Otimização Topológica Multiobjetivo de Estruturas submetidas a carregamentos Termo-Mecânicos**. 2015. Master Thesis. Universidade Estadual de Campinas.

RODRIGUES, H. and FERNANDES, P. A material based model for topology optimization of thermoelastic structures. **International journal for numerical methods in engineering**, v. 38, 1951–1965, 1995.

RODRIGUEZ, S.Q. and PAVANELLO, R. Bidirectional evolutionary optimization considering design-dependent thermo-mechanical loads. In **Ibero-Latin American Congress on Computational Methods in Engineering - CILAMCE. 2014.** 2014.

RODRIGUEZ, S.Q. and PAVANELLO, R. Thermo-mechanical multi-objective bidirectional evolutionary structural optimization using weighted sum method for mean compliance and heat conduction problem. In **1st Pan-American Congress on Computational Mechanics - PANACM 2015 XI Argentine Congress on Computational Mechanics - MECOM 2015**. 2015.

SEDGEWICK, R. and FLAJOLET, P. **An introduction to the analysis of algorithms**. Pearson Education, 2013.

SIGMUND, O. Design of multiphysics actuators using topology optimization - part i: One-material structures. **Computer Methods in Applied Mechanics and Engineering**, v. 190, n. 49, 6577 – 6604, 2001.

SIGMUND, O. and TORQUATO, S. Composites with extremal thermal expansion coefficients. **Applied Physics Letters**, v. 69, n. 21, 3203–3205, 1996.

SIGMUND, O. and TORQUATO, S. Design of materials with extreme thermal expansion using a three-phase topology optimization method. **Journal of the Mechanics and Physics of Solids**, v. 45, n. 6, 1037–1067, 1997.

SIGMUND, O. and TORQUATO, S. Design of smart composite materials using topology optimization. **Smart Mater. Struct.**, v. 8, 365–379, 1999.

SILVA, F.I. **Síntese Computacional de Absorvedores Acústicos Poroelásticos**. 2007. PhD Thesis. Universidade Estadual de Campinas.

SILVA, F.I. and PAVANELLO, R. OtimizaÇÃo paramÉtrica de sistemas de isolaÇÃo acÚstica. In **VI Congresso Nacional de Engenharia mecânica**, v. 1, pp. 1–8. Campina Grande, 2010a.

SILVA, F.I. and PAVANELLO, R. Synthesis of porous-acoustic absorbing systems by an evolutionary optimization method. **Engineering Optimization**, v. 42, n. 10, 887–905, 2010b.

STOLPE, M. and SVANBERG, K. An alternative interpolation scheme for minimum compliance topology optimization. **Structural and Multidisciplinary Optimization**, v. 22, n. 2, 116–124, 2001.

VICENTE, W.; PICELLI, R.; PAVANELLO, R. and XIE, Y. Topology optimization of frequency responses of fluido-structure interaction systems. **Finite Elements in Analysis and Design**, v. 98, 1 – 13, 2015.

VICENTE, W.; ZUO, Z.; PAVANELLO, R.; CALIXTO, T.; PICELLI, R. and XIE, Y. Concurrent topology optimization for minimizing frequency responses of two-level hierarchical structures. **Computer Methods in Applied Mechanics and Engineering**, v. 301, 116 – 136, 2016.

VICENTE, W.M. **Otimização Topológica Evolucionária Aplicada a Sistemas Elasto-Acústicos**. 2013. PhD Thesis. Universidade Estadual de Campinas.

WANG, M.Y.; WANG, X. and GUO, D. A level set method for structural topology optimization. **Computer Methods in Applied Mechanics and Engineering**, v. 192, n. 1, 227 – 246, 2003.

WANG, Y.; GAO, J.; LUO, Z.; BROWN, T. and ZHANG, N. Level-set topology optimization

for multimaterial and multifunctional mechanical metamaterials. **Engineering Optimization**, v. 49, n. 1, 22–42, 2016a.

WANG, Y.; LUO, Z.; ZHANG, N. and WU, T. Topological design for mechanical metamaterials using a multiphase level set method. **Structural and Multidisciplinary Optimization**, v. 54, 937–954, 2016b.

XIA, Q. and WANG, M.Y. Topology optimization of thermoelastic structures using level set method. **Computational Mechanics**, v. 42, 837–857, 2008.

XIE, Y.M. and STEVEN, G.P. A simple evolutionary procedure for structural optimization. **Computers and Structures**, v. 49, n. 5, 885–896, 1993.

XU, B.; HUANG, X.; ZHOU, S. and XIE, Y. Concurrent topological design of composite thermoelastic macrostructure and microstructure with multi-phase material for maximum stiffness. **Composite Structures**, v. 150, 84–102, 2016.

YAN, X.; HUANG, X.; ZHA, Y. and XIE, Y. Concurrent topology optimization of structures and their composite microstructures. **Computers & Structures**, v. 133, n. Supplement C, 103 – 110, 2014.

YANG, Q.S. and BECKER, W. Numerical investigation for stress, strain and energy homogenization of orthotropic composite with periodic microstructure and non-symmetric inclusions. **Computational Materials Science**, v. 31, n. 1, 169 – 180, 2004.

YANG, X.Y.; XEI, Y.M.; STEVEN, G.P. and QUERIN, O.M. Bidirectional evolutionary method for stiffness optimization. **AIAA Journal**, v. 37, n. 11, 1483–1488, 1999.

ZHANG, H.; BAEYENS, J.; DEGRÈVE, J. and CACÈRES, G. Concentrated solar power plants: Review and design methodology. **Renewable and Sustainable Energy Reviews**, v. 22, n. Supplement C, 466 – 481, 2013.

ZUO, Z.H.; HUANG, X.; RONG, J.H. and XIE, Y.M. Multi-scale design of composite materials and structures for maximum natural frequencies. **Materials & Design**, v. 51, n. Supplement C, 1023 – 1034, 2013.

APPENDIX A – Formulation and sensitivity analysis for the concurrent design of a thermo-mechanical problem

The multi-scale thermo-mechanical design problem can be made considering a concurrent design, in other words, the topology optimization problem consider the macro-scale and micro-scale at the same time. Similar to the previous problem, the topology optimization problem consist in find the stiffer structure with a given volume of the M materials in the macro-scale and m materials in the micro-scale, when thermal and mechanical loads occur simultaneously in the structure.

The mean compliance is minimized, in order to get the maximum stiffness, then the optimization problem, with the volume constraint on the M materials in macro-scale and m materials in micro-scale, can be stated as

$$
\begin{aligned}
find: \quad & \boldsymbol{X}^M, \quad \boldsymbol{X}^m \\
minimize: \quad & C^M = \frac{1}{2}(\boldsymbol{p}^M)^T \boldsymbol{u}^m = \frac{1}{2}\left(\boldsymbol{f}^{M,mec} + \boldsymbol{f}^{M,ter}\right)^T \boldsymbol{u}^M \\
subject \quad to: \quad & V_j^{M,*} - \sum_{i=1}^{N} V_i^M X_{ij}^M - \sum_{i=1}^{j-1} V_i^{M,*} = 0 \quad j = 1,2,...,M-1 \\
& V_l^{m,*} - \sum_{k=1}^{n} V_k^m X_{kl}^m - \sum_{k=1}^{l-1} V_k^{m,*} = 0 \quad l = 1,2,...,m-1 \\
& \boldsymbol{K}^M \boldsymbol{u}^M = \boldsymbol{f}^{M,mec} + \boldsymbol{f}^{M,ter} \\
& \boldsymbol{K}^m \boldsymbol{U}^m = \boldsymbol{F}^m \\
& \boldsymbol{K}^m \boldsymbol{\varphi}^m = \boldsymbol{f}_t^m \\
& X_{ij}^M = x_{min} \quad \vee \quad 1 \\
& X_{kl}^m = x_{min} \quad \vee \quad 1
\end{aligned}
\tag{A.1}
$$

where C^M is the mean compliance, $\boldsymbol{p}^M$ the force applied on the structure, $\boldsymbol{f}^{M,mec}$ the mechanical load, $\boldsymbol{f}^{M,ter}$ the thermal load, $\boldsymbol{u}^M$ the displacement vector on macro-scale, M the number of material in macro-scale, m the number of materials in micro-scale, $V_j^{M,*}$ the prescribed volume for each material j in macro-scale, $V_l^{m,*}$ the prescribed volume for each material l in micro-scale, N is the number of elements in macro-scale, n is the number of elements in micro-scale, X_{ij}^M the design variable for the i^{th} element and j^{th} material in macro-scale and X_{kl}^m the design variable for the k^{th} element and l^{th} material in micro-scale.

Using the multi-scale thermo-mechanical structural design problem it is possible to find in the macro-scale and the micro-scale domain the topologies that respect the problem stated

in the equation A.1, using M-phase materials in the macro-scale and m-phase materials in the micro-scale.

A.1 Sensitivity analysis for concurrent design of a thermo-mechanical problem

In this case, two sensitivity numbers must be calculated, the first one ($\boldsymbol{SN}^M$) is found by the gradient of the objective function C^M with respect to the design variables in macro-scale ($\boldsymbol{X}^M$), and the second one ($\boldsymbol{SN}^m$) is found by the gradient of the objective function C^M with respect to the design variables in microscale ($\boldsymbol{X}^m$).

The gradient of the objective function with respect to the design variable in macro-scale is calculated as in the section 3.4.1, using equation **??** to equation 3.24.

The remotion of an element in the base cell is relevant for all elements in the macro-structure that contains this type of material, due to this condition the sensitivity for this case is equal to the sum of the derivative of the compliance of all the elements of the micro-structure that contains this base cell. Thus, the sensitivity number in micro-scale is calculated as

$$SN_{kl}^m = -\sum_{i=1}^{N_j} \frac{\partial C^M}{\partial X_{kl}^m} = \sum_{i=1}^{N_j} \frac{1}{2} (\boldsymbol{u}^M)^T \frac{\partial \boldsymbol{K}^M}{\partial X_{kl}^m} \boldsymbol{u}^M - \sum_{i=1}^{N_j} \left(\frac{\partial \boldsymbol{f}^{M,ter}}{\partial X_{kl}^m} \right)^T \boldsymbol{u}^M \tag{A.2}$$

where N_j is the total number of elements in the macro-structural model whose micro-structure contains the base cell analyzed, $\boldsymbol{K}^M$ is the elemental stiffness matrix, in macro-scale, given by the equation 2.30 and $\boldsymbol{f}^{M,ter}$ is the elemental thermal force, in macro-scale, given by the equation 2.31. Then, the derivative of the stiffness matrix and the thermal force with respect to the design variable in micro-scale are given by equations A.3 and A.4, respectively.

$$\frac{\partial \boldsymbol{K}^M}{\partial X_{kl}^m} = \int_\Omega (\boldsymbol{B}^M)^T \frac{\partial \boldsymbol{D}^M}{\partial X_{kl}^m} \boldsymbol{B}^M d\Omega \tag{A.3}$$

$$\frac{\partial \boldsymbol{f}^{M,ter}}{\partial X_{kl}^m} = \int_\Omega (\boldsymbol{B}^M)^T \left(\frac{\partial \boldsymbol{D}^M}{\partial X_{kl}^m} \boldsymbol{\alpha}^M + \boldsymbol{D}^M \frac{\partial \boldsymbol{\alpha}^M}{\partial X_{kl}^m} \right) \Delta T d\Omega \tag{A.4}$$

Equation A.5 and equation A.6 are the derivatives with respect to the design variable $\boldsymbol{X}^m$ of the equation 3.21 and equation 3.22, respectively.

$$\frac{\partial \boldsymbol{D}^M}{\partial X_{kl}^m} = (X_{ij}^M)^{P_j} \frac{\partial D_j^H}{\partial X_{kl}^m} + \left\{ 1 - (X_{ij}^M)^{P_j} \right\} \frac{\partial D_{j+1}^H}{\partial X_{kl}^m} \qquad j = 1, 2, ..., M \tag{A.5}$$

$$\frac{\partial \boldsymbol{\alpha}^M}{\partial X_{kl}^m} = (X_{ij}^M)^{Q_j} \frac{\partial \boldsymbol{\alpha}_j^H}{\partial X_{kl}^m} + \left\{1 - (X_{ij}^M)^{Q_j}\right\} \frac{\partial \boldsymbol{\alpha}_{j+1}^H}{\partial X_{kl}^m} \qquad j = 1, 2, ..., M \tag{A.6}$$

The derivative of the homogenized thermal expansion coefficient $\frac{\partial \boldsymbol{\alpha}^H}{\partial \boldsymbol{X}^m}$, the homogenized elasticity matrix $\frac{\partial \boldsymbol{D}^H}{\partial \boldsymbol{X}^m}$ and of the homogenized thermal stress vector $\frac{\partial \boldsymbol{\beta}^H}{\partial \boldsymbol{X}^m}$ are calculated using the equations 3.25, 3.41 and 3.42 from the section 3.4.1.